MICROCOPY RESOLUTION TEST CHART
NATIONAL BUREAU OF STANDARDS-1963-A

SCATTERING OF AN ELECTROMAGNETIC PLANE WAVE
FROM A PERFECTLY ELECTRICALLY CONDUCTING
HALF-PLANE IN THE PROXIMITY OF PLANAR
MEDIA DISCONTINUITIES

By

Robert Dawson Coblin
and
L. Wilson Pearson

Department of Electrical Engineering
University of Mississippi
University, MS   38677

February, 1983

DTIC
ELECTE
MAR 1 3 1984

E

i

REPORT DOCUMENTATION PAGE		READ INSTRUCTIONS BEFORE COMPLETING FORM
1. REPORT NUMBER N/A	2. GOVT ACCESSION NO. AD.A138968	3. RECIPIENT'S CATALOG NUMBER
4. TITLE (and Subtitle) Scattering of an Electromagnetic Plane Wave From A Perfectly Electrically Conducting Half-Plane In The Proximity of Planar Media Discontinuities		5. TYPE OF REPORT & PERIOD COVERED Final Technical Report 1 Jan 1980 – 1 Jan 1983
		6. PERFORMING ORG. REPORT NUMBER N/A
7. AUTHOR(s) Robert Dawson Coblin and L. Wilson Pearson		8. CONTRACT OR GRANT NUMBER(s) N00014-81-K-0256 ~~N00014-77-K-0362~~
9. PERFORMING ORGANIZATION NAME AND ADDRESS Department of Electrical Engineering University of Mississippi University, MS 38677		10. PROGRAM ELEMENT, PROJECT, TASK AREA & WORK UNIT NUMBERS N/A
11. CONTROLLING OFFICE NAME AND ADDRESS ONR Resident Representative Georgia Institute of Technology Atlanta, GA 30332		12. REPORT DATE February 1983
		13. NUMBER OF PAGES 226
14. MONITORING AGENCY NAME & ADDRESS(if different from Controlling Office) ONR Western Regional Office 1030 East Green Street Pasadena, CA 91106		15. SECURITY CLASS. (of this report) UNCLASSIFIED
		15a. DECLASSIFICATION/DOWNGRADING SCHEDULE N/A

16. DISTRIBUTION STATEMENT (of this Report)

Distribution Unlimited

17. DISTRIBUTION STATEMENT (of the abstract entered in Block 20, if different from Report)

Distribution Unlimited

18. SUPPLEMENTARY NOTES

19. KEY WORDS (Continue on reverse side if necessary and identify by block number)

Diffraction, Scattering, Dielectric Interface

20. ABSTRACT (Continue on reverse side if necessary and identify by block number)

The problem of scattering of electromagnetic waves form a perfectly electrically conducting (PEC) half-plane is a classical problem in the field of electromagnetics and is the basis of the GTD (geometrical theory of diffraction). The application of this theory to modern aerospace structures is hampered due to the presence of media discontinuities which alter the scattering behavior. Therefore, the study of diffraction in the presence of such discontinuities is an important prerequisite to applying the GTD to practical problems. Two related problems are considered in this study

Cont. on back

DD FORM 1473 EDITION OF 1 NOV 65 IS OBSOLETE
1 JAN 73

Cont. #20

which involve planar media discontinuities. The first configuration concerns
a planar interface between two semi-infinite, homogeneous media with a PEC
half-plane covering half of the interface. The second configuration concerns
a dielectric slab embedded in a contrasting medium. On the upper surface of
the slab resides a PEC half-plane. Both structures are assumed to be excited
by a transverse magnetic plane wave.

The boundary value problems are structured as integral equations involving
the electric field which is tangential to the interface. The integral equations
are Fourier transformed to create Wiener-Hopf equations which are then solved.
The process of factorization is performed using a formal integral factorization
which is converted into a form that is amenable to numerical evaluation. The
solution is structured as a radiation integral and is evaluated asymptotically
to arrive at the far field ray-optic contributors.

Data is presented for the interface problem to exhibit distinctive properties
of the solution. Sample cases of practical interest are given. The data
is considered in the light of present theory concerning wave structure about a
dielectric interface and an analysis of the significant features of the data is
conducted.

ABSTRACT

The problem of scattering of electromagnetic waves from a perfectly electrically conducting (PEC) half-plane is a classical problem in the field of electromagnetics and is the basis of the GTD (geometrical theory of diffraction). The application of this theory to modern aerospace structures is hampered due to the presence of media discontinuities which alter the scattering behavior. Therefore, the study of diffraction in the presence of such discontinuities is an important prerequisite to applying the GTD to practical problems. Two related problems are considered in this study which involve planar media discontinuities. The first configuration concerns a planar interface between two semi-infinite, homogeneous media with a PEC half-plane covering half of the interface. The second configuration concerns a dielectric slab embedded in a contrasting medium. On the upper surface of the slab resides a PEC half-plane. Both structures are assumed to be excited by a transverse magnetic plane wave.

The boundary value problems are structured as integral equations involving the electric field which is tangential to the interface. The integral equations are Fourier transformed to create Wiener-Hopf equations which are then solved. The process of factorization is performed using a formal integral factorization which is converted into a form that is amenable to numerical evaluation. The solution is structured as a radiation integral and is evaluated asymptotically to arrive at the far field ray-optic contributors.

Data is presented for the interface problem to exhibit distinctive properties of the solution. Sample cases of practical interest are given. The data is considered in the light of present theory concerning wave structure about a dielectric interface and an analysis of the significant features of the data is conducted.

iii

TABLE OF CONTENTS

iv

LIST OF TABLES

LIST OF FIGURES

Figure   Page

Figure   Page

CHAPTER I

INTRODUCTION

The objective of this study is the solution of two related problems concerning the diffraction of time-harmonic, electromagnetic, plane waves. The first problem deals with the geometry given in Figure 1.1 and is henceforth referred to as the interface problem. As seen in the figure, two half-spaces are separated by a planar interface which is coincident with the x'-z' plane. On the interface is a perfectly electrically conducting (PEC), infinitely thin half-plane. The half-plane lies in the plane $y' = 0$ and extends along the positive x' direction from an edge which is coincident with the z' axis. An incident plane wave propagating strictly in the x'-y' plane in medium 1 (characterized by constitutive parameters (μ_1', ϵ_1')) impinges on the half-plane. There is assumed to be no variation of fields in the z' direction, hence the problem is two-dimensional.

The second problem, referred to as the slab problem, consists of the above half-plane residing on a dielectric slab characterized by (μ_0', ϵ_2') which is in turn imbedded in another medium (μ_0', ϵ_1') as shown in Figure 1.2.

Aside from the academic interest of studying such configurations, they resemble or model junctions involving composite materials such as

1
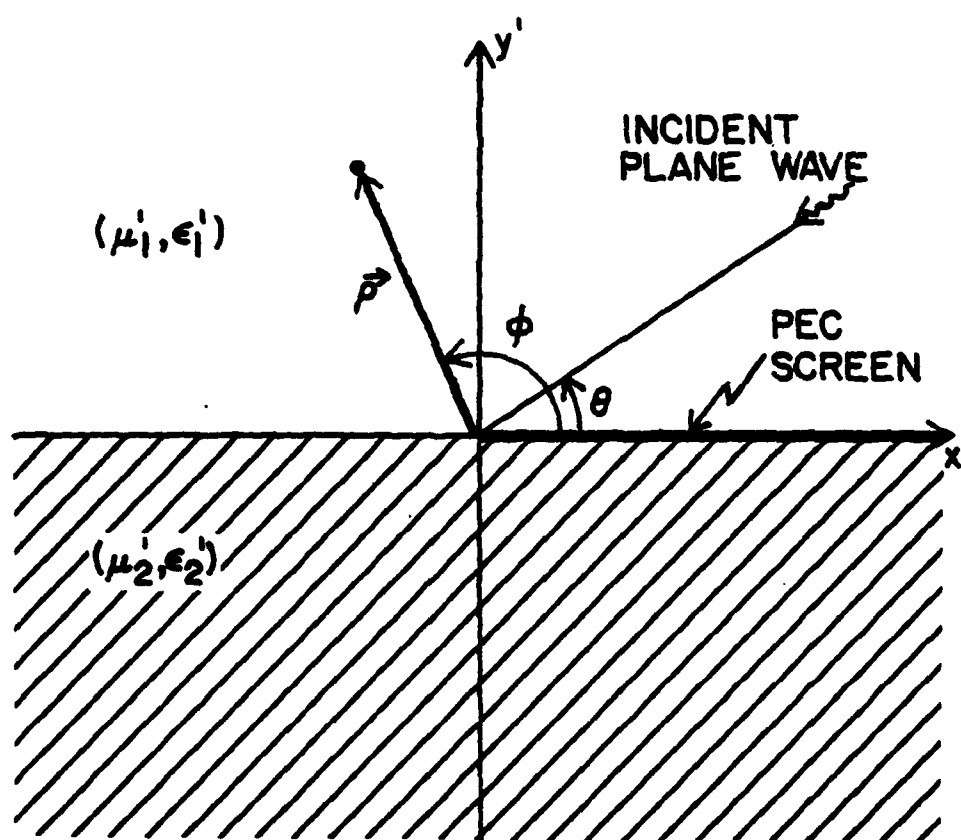
Figure 1.1.   Geometry of the interface problem.
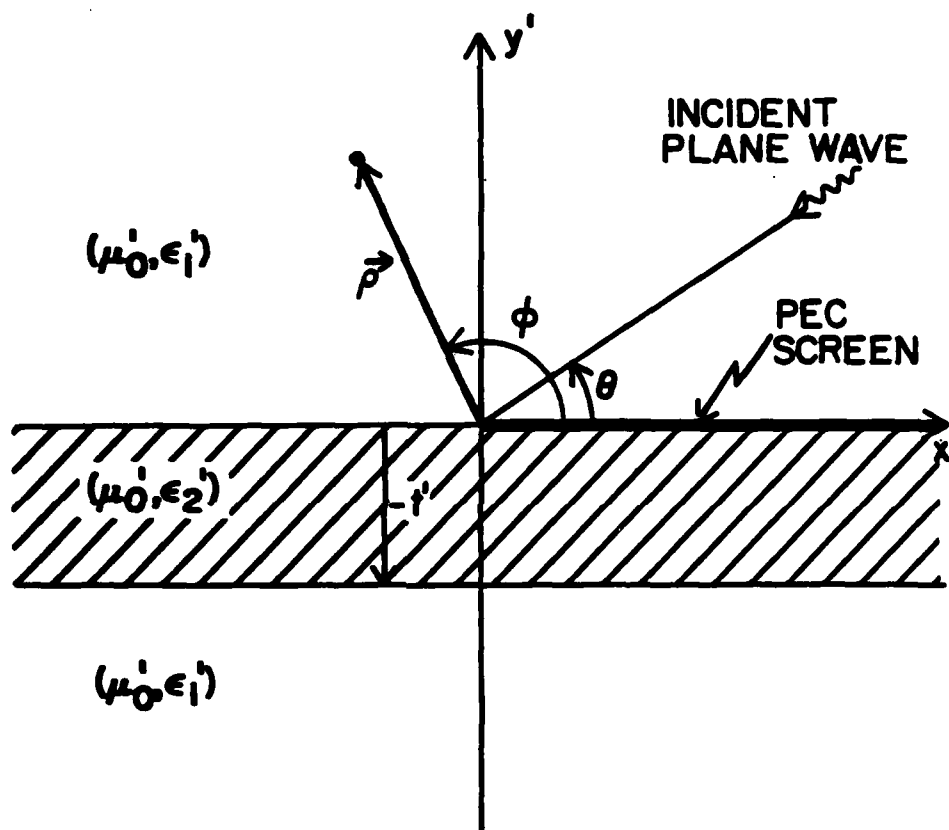
Figure 1.2. Geometry of the slab problem.

occur in modern aerospace structures. Therefore diffraction from such
planar composite structures is of practical interest. The first prob-
lem is a fundamental building block toward solving and interpreting more
complicated diffraction problems involving media interfaces. The second
structure serves as a canonical problem modeling a lapped-junction between
a metallic and a composite sheet. It is desirable to be able to ana-
lyze these structures using the geometrical theory of diffraction (GTD),
but no diffraction coefficients are available for either of them. As a
result, scattering problems involving these canonical structures cannot
be modeled using the GTD at present. One purpose of this study is to
solve these problems in an asymptotic limit and extract the ray consti-
tuents of the solution in order to derive the correct diffraction coef-
ficients for GTD modeling of composite/metal junctions.

The scope of study of the problem geometries is as follows. For
the interface problem the equations are formulated for four separate
cases: a TM (transverse magnetic) polarized incident plane wave with the
integral equations formulated first over the PEC screen and then over the
remaining (aperture) portion of the interface plane and a TE (transverse
electric) polarized incident wave again formulated over each half of the
interface plane. The case of the TM wave formulated over the aperture is
developed in full detail from the integral equation formulation to the
asymptotic analysis of the resulting radiation integrals. The other cases
can be developed in a like manner and the similarity of the analysis is
indicated. The interface problem is handled in full generality with the

constitutive parameters of the media allowed to be independent and lossy (though constrained to be passive). In the slab problem, only the TM incident wave is considered with the integral equation formulated over the PEC screen. The media are assumed to be lossless with the permeabilities equal and the permittivity of the slab greater than that of the surrounding medium.

The solution of diffraction from a half-plane can be traced back to the problem of scattering from a half-plane in a homogeneous medium which was solved by Sommerfeld (1896). Over the years this problem has been treated from a number of points of view. The application of the Wiener-Hopf technique to the half-plane problem is described in Noble (1958). The Wiener-Hopf approach was developed to deal with a class of integral equations on a semi-infinite domain and is a special case of the Riemann-Hilbert problem (Carrier, Krook and Pearson (1966)). It was applied to diffraction problems by J. Schwinger and E. T. Copson. Application of the Wiener-Hopf technique has been the principal subject of several books (Noble (1958), Mittra and Lee (1971), Weinstein (1969)). In the Sommerfeld half-plane problem, the diffracted fields are couched in the form of a Fourier inversion integral which can be computed as Fresnel integrals or approximated asymptotically as rays. This ray-optic result was utilized by Keller (1957,1962) to formulate a high frequency electromagnetic scattering theory which he called the geometrical theory of diffraction (GTD). The GTD has been extensively developed by others (see Hansen (1981) for a survey). The solutions of various canonical problems are

collected in the GTD and one subsequently models scattering from complex structures by isolating effects (localization) and synthesizing an approximate response from the canonical building blocks. Each new solution extends the capability of the theory, and the solutions presented here are intended to add two new canonical structures to those available for such ray solutions.

The Wiener-Hopf technique is used in this research since it is applicable to a planar geometry which leads to an integral equation on a semi-infinite domain, and it yields exact results. The difficulty in Wiener-Hopf analysis arises in performing the required factorization and decomposition steps. Therefore, any new factorization is of interest as it increases the collection of known factorizations. The interface problem has been addressed by several authors and the required factorization was not found to be available. A reduced form of the interface problem involving wave propagation across a seashore was solved by Clemmow (1966), Bazar and Karp (1962), Heins and Feshbach (1954), and others. Recognizing that a formal factorization integral exists in certain cases, several authors have performed an analysis of problems closely related to the interface problem. An analysis by Heitman and van den Berg (1975) resulted in a numerical evaluation of the factorization integral and did not attempt to examine the asymptotic field behavior. A recent analysis by Sunahara and Sekiguchi (1981) considered a closely related problem. However, their solution breaks down as the geometry limits into the interface problem. Part of the purpose of this study is to develop an efficient integral

factorization which yields all the analytical properties of the factor-
ization and is easy to evaluate numerically. This represents a natural
extention of the application of the Wiener-Hopf procedure from problems
where the analytical steps required can be performed and the results given
in terms of known functions to problems which do not yield such closed
form or determinate solutions.

CHAPTER II

ANALYTICAL PRELIMINARIES

2.1 Notation

The purpose of this chapter is to summarize the fundamental mathematical tools required for the solution of the problems of interest. It is intended as a reference for the remainder of this work. Notation and conventions are established in this chapter for the rest of the volume. All configurations are assumed to be strictly two-dimensional (no variation along the z direction). The fundamental time convention used is $e^{j\omega t}$, which is suppressed. As a result, Maxwell's equations take the form:

$$\vec{\nabla} \cdot \vec{e} = q/\epsilon \tag{2.1.1.a}$$

$$\vec{\nabla} \times \vec{e} = -\vec{m} - j\omega\mu\vec{h} \tag{2.1.1.b}$$

$$\vec{\nabla} \cdot (\mu\vec{h}) = 0 \tag{2.1.1.c}$$

$$\vec{\nabla} \times \vec{h} = \vec{j} + j\omega\epsilon\vec{e} \tag{2.1.1.d}$$

where $\vec{e}$ is the electric field, $\vec{h}$ is the magnetic field, q is the electric charge density, $\vec{j}$ is the electric current density and $\vec{m}$ is the magnetic current density.

The media to be considered are passive and, in general, lossy. They

9

can be characterized by complex constitutive parameters (μ, ε) which are complex numbers in the fourth quadrant (positive real part and nonpositive imaginary part). Also, the complex wave numbers are written as:

$k = k_r - jk_i$, where $k_r > 0$ and $k_i \geq 0$.

Wiener-Hopf analysis, which is used in the solution of the problems to be considered, is performed in the generalized Fourier transform (spectral) domain. For this analysis we choose the following Fourier transform pair:[1]

$$F(k_x) = F\{f(x)\} = \frac{1}{\sqrt{2\pi}} \int_{x_0 = -\infty}^{\infty} f(x_0)\, e^{+jk_x x_0}\, dx_0 \qquad (2.1.2.a)$$

$$f(x) = F^{-1}\{F(k_x)\} = \frac{1}{\sqrt{2\pi}} \int_{k_x = -\infty + jc}^{\infty + jc} F(k_x)\, e^{-jk_x x}\, dk_x \qquad (2.1.2.b)$$

Here the transform variable is allowed to be complex. The constant c is suitably chosen for convergence of the Fourier inversion integral in analogy to the Bromwich contour of the Laplace transform (Mittra and Lee (1971a)).

Various methods are available for arriving at the Wiener-Hopf equation for a problem. Because of the pervasiveness of the integral equation formulation for electromagnetic problems, we choose to use this type of equation as the starting point in formulating the Wiener-Hopf

[1] Throughout this work we use capitalized function names to denote the spectral (Fourier transform) domain image of a spatial domain function.

equation. The integral involved will be a convolution of a desired unknown in the problem with an appropriate Green's function, which, for two-dimensional problems, is of the form $H_0^{(2)}(k\,|x-x_0|)$. When the integral equation is Fourier transformed with respect to x, according to the convolution theorem, the integral is reduced to the product of the transform of the unknown times the transform of the Green's function. For the Green's function in free space, we have (Jones (1964)):

$$F\{g(\vec{\rho})\} = F\left\{-\frac{1}{4}\,H_0^{(2)}(k|\vec{\rho}|)\right\} = -\frac{1}{4}\left(\sqrt{\frac{2}{\pi}}\ \frac{e^{-j\beta|y|}}{\beta}\right) \qquad (2.1.3)$$

where $\beta = \sqrt{k^2-k_x^2}$ (the details of the definition of β are given below) and $\vec{\rho} = (x)\hat{x} + (y)\hat{y}$.

2.2 Specification of the Value of $\beta = \sqrt{k^2 - k_x^2}$

The two dimensional Green's function is the solution to the inhomogeneous wave equation with a line source at $\vec{\rho} = 0$ where we require waves emanating from the line source to be outgoing and decaying. This means that all the components in the spectral domain along the Fourier inversion path must also have these characteristics. Observe that in the inversion integral of (2.1.3) for $g(\vec{\rho})$, we must have $\text{Im}(\beta) \leq 0$ to give rise to decay along the y axis.

Clearly all physical waves will have $\text{Re}(\beta) \geq 0$ to provide outgoing wave behavior from $y = 0$ and will satisfy $\text{Im}(\beta) \leq 0$ so that the outgoing waves decay (consistent with the passiveness of the medium). Hence any

physical wave will lie in the region characterized by $Im(\beta) \leq 0$, so the boundary of the allowed region is $Im(\beta) = 0$, that is, β is purely real. In the β plane this is the real axis and in the β^2 plane this is the positive real axis so

$$\beta^2 = [(k_r^2 - k_i^2) - (\sigma^2 - \tau^2)] - 2j[k_r k_i + \sigma\tau] \qquad (2.2.1.a)$$

where

$$k = k_r - jk_i \text{ and } k_x = \sigma + j\tau \quad .$$

So in the β^2 plane, the boundary is given by

$$Im\,\beta^2 = -2(k_r k_i + \sigma\tau) = 0 \qquad (2.2.1.b)$$

and

$$Re\,\beta^2 = [(k_r^2 - k_i^2) - (\sigma^2 - \tau^2)] \geq 0 \quad , \qquad (2.2.1.c)$$

Figure 2.1 which depicts the lines specified above in the $k_x = \sigma + j\tau$ plane. We observe that the condition $Im(\beta) = 0$ implies $Im(\beta^2) = 0$ and $Re(\beta^2) \geq 0$. The equality obviously gives a pair of hyperbolas in the second and fourth quadrants. The branch cuts for the allowable region of k_x (top sheet of β) will run from $\pm k$ to infinity along these hyperbolas. To decide which part of the hyperbolas contain the branch cuts of β, we observe that the cuts force $Im(\beta) \leq 0$ on the top sheet which implies that they lie along $Im(\beta) = 0$ and therefore $Re(\beta^2) \geq 0$. So the branch cuts lie along the lines shown in Figure 2.1. These are the conventional hyperbolic branch cuts and preserve decay at infinity. Since our analysis will take us off the real axis in the spectral domain, it is
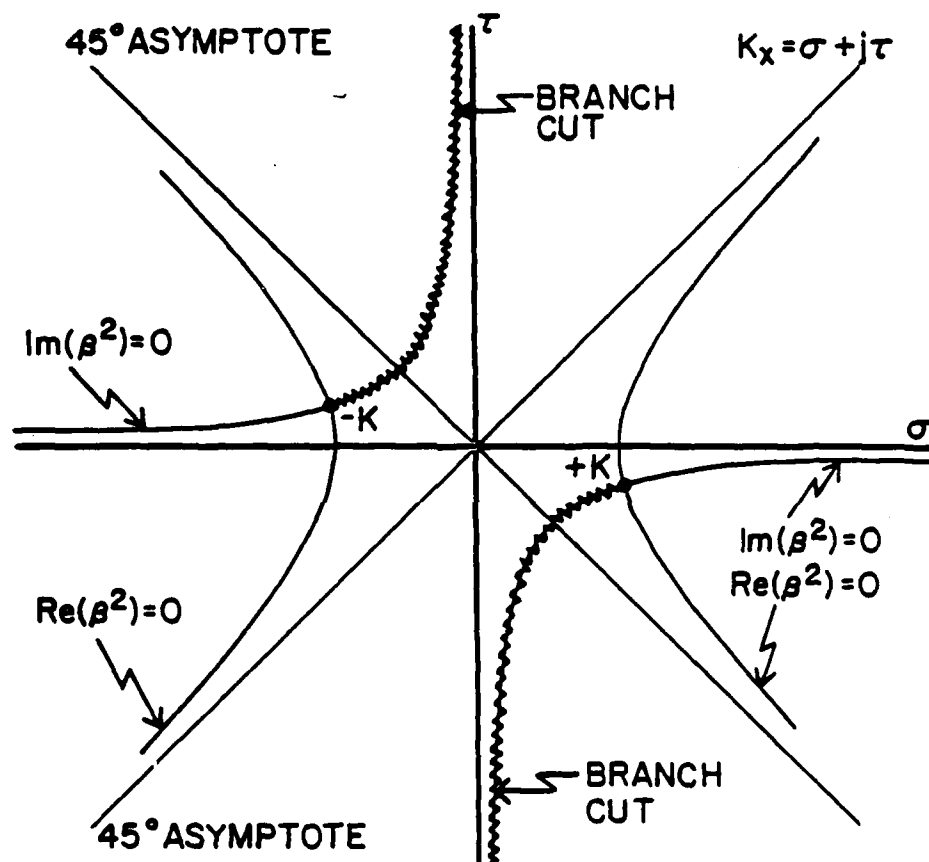
Figure 2.1. Domain of $\beta = \sqrt{k^2 - k_x^2}$.

important to understand where these cuts lie and to recognize that moving them may cause problems in closing an integration contour at infinity. We need a top sheet where the outgoing wave conditions stated above are satisfied on the Fourier transform path (the real axis) and which allows us to perform any semi-circular closures that we may need later. The k_x domain in Figure 2.2 shows the sign of $Re(\beta)$ for points in the k_x domain.

One other related issue must be dealt with before we leave the subject of the definition of β. In some situations subsequently, we evaluate the factors of $\beta = \sqrt{k^2 - k_x^2} = \sqrt{k + k_x} \cdot \sqrt{k - k_x}$ separately and must impose the above conditions in so doing. The complex number $(k - k_x)$ can be represented by a vector pointing from $+k_x$ to k. The modulus and argument of the number are taken as the length of the vector and angle with respect to a line running from $+k_x$ parallel to the positive real axis toward infinity as shown in Figure 2.3. The complex vector representation for $(k + k_x) = k_x - (-k)$ points from $-k$ to k_x and we utilize a similar definition for its argument as shown in Figure 2.3. As a result

$$\beta = \sqrt{k^2 - k_x^2} = [(k + k_x) \cdot (k - k_x)]^{\frac{1}{2}} = |k^2 - k_x^2|^{\frac{1}{2}} e^{j\left(\frac{\theta_1 + \theta_2}{2}\right)} \quad (2.2.2)$$

is found to obey our branch definition of β and so we have a simple rule for establishing the arguments of $\sqrt{k + k_x}$ and $\sqrt{k - k_x}$ which is consistent with the definition of β.

Finally, a point of terminology needs to be established. It will prove useful to consider branch definitions of β which have branch cuts
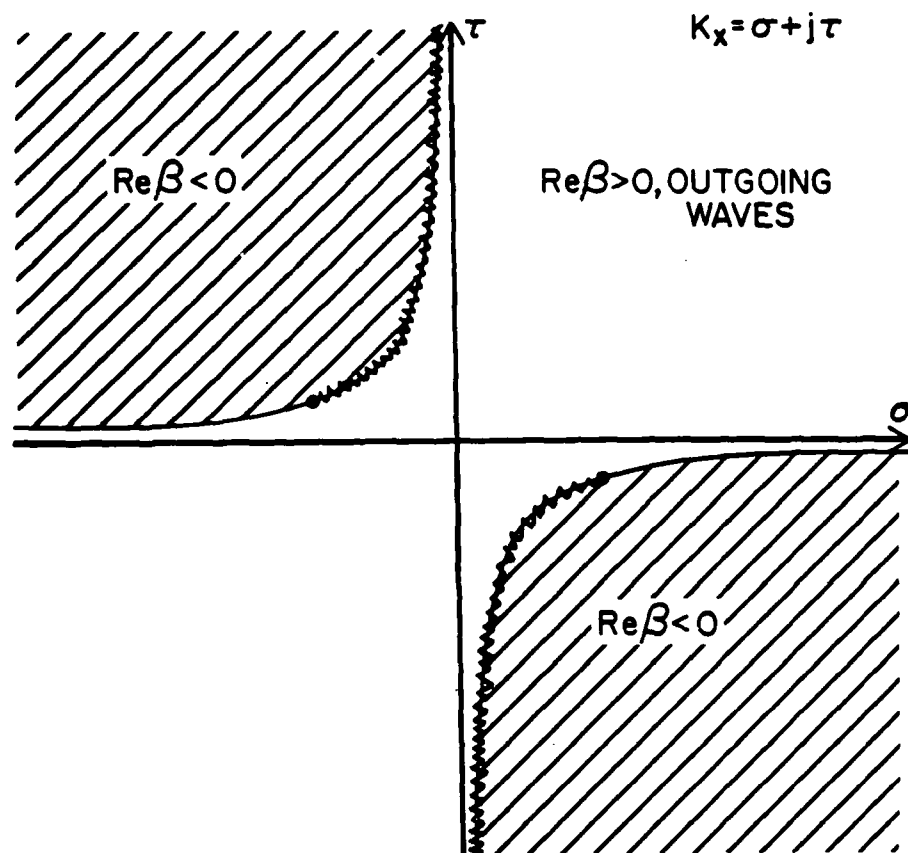
Figure 2.2.   Upper sheet values of β.
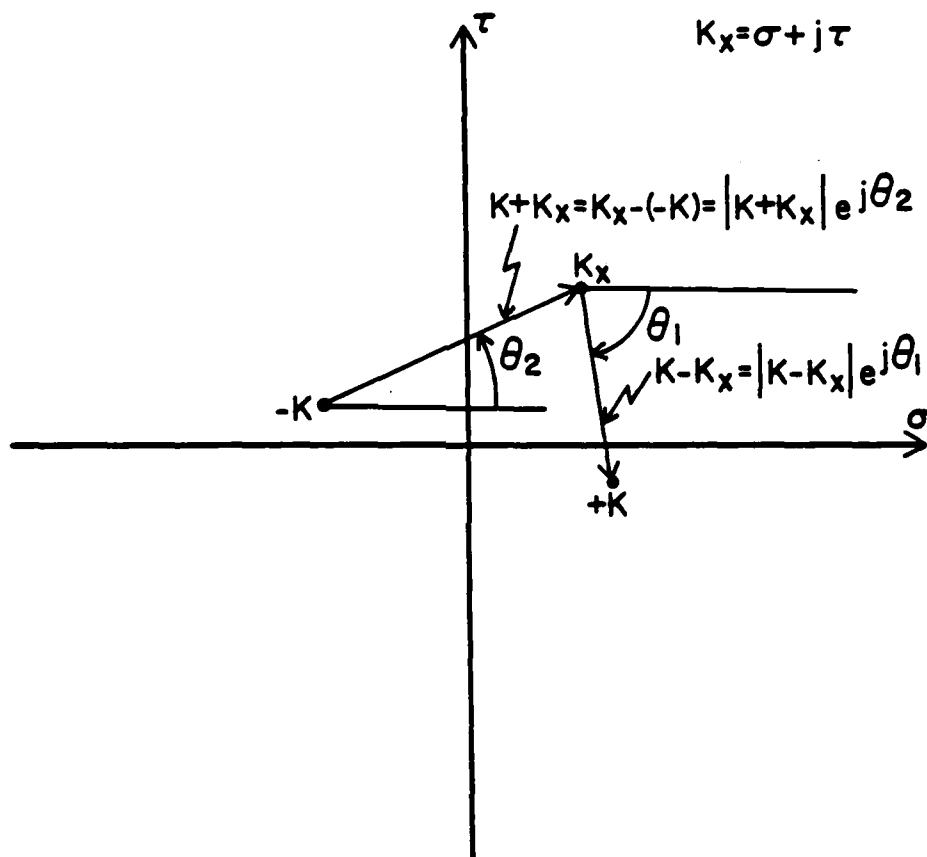
Figure 2.3. Vector interpretation of $(k+k_x)$ and $(k-k_x)$.

that are different than the hyperbolic branch cuts used in this section.
These alternative branches of β are arrived at by analytic continuation
of the function from the original branch definition. These new branch
definitions are described as analytic continuations of the function, β,
arising from the movement of the hyperbolic branch cuts of β. This
language is used to preserve the intuitive sense of connection between
successive branch definitions and an apology is made here to the precise
mathematician for the use of this phraseology.

2.3 Edge Condition

In order to uniquely specify the field solution for diffraction
from a surface which contains a discontinuity of the surface normal
vector, it is necessary to specify field behavior in the vicinity of the
edge since unbounded fields arise. This problem was dealt with by J.
Meixner (1954). He required that a satisfactory representation for the
fields in a small volume including the edge must be limited to a finite
amount of energy. For a problem involving scattering from a wedge in
the presence of different media, Mittra and Lee (1971b) have given the
general solution for three media. The asymptotic behavior of the fields
as the edge of the half-plane is approached from large distances is given
below for the problems to be considered in this study:

$$\begin{array}{cccc}
\text{E transverse} & \text{H transverse} & \text{Ez,Hz} & \\
0(\rho^{-\frac{1}{2}}) & 0(\rho^{-\frac{1}{2}}) & 0(\rho^{\frac{1}{2}}) & . \qquad (2.3.1)
\end{array}$$

2.4 Wiener-Hopf Technique

The Wiener-Hopf technique applies to problems formulated on a semi-infinite domain in a separable coordinate system and its use is ubiquitous throughout mathematical physics (see Noble (1958)). For example, in a two-dimensional boundary value problem where the boundary values are specified along a line so that along one semi-infinite ray a Dirichlet condition holds and along the remainder of the line a Neumann condition holds, a simple solution involving the Fourier transform of the differential equation and the boundary conditions cannot be effected since the boundary conditions do not hold along the entire domain of the transform. We do not repeat the development leading to the Wiener-Hopf solution since that is available in numerous references (see Mittra and Lee (1971a)). We simply state the results of the development. For the convenience of the reader, we follow the notation of Mittra and Lee.

An integral equation amenable to the Wiener-Hopf procedure is of the form

$$\frac{1}{\sqrt{2\pi}} \int_{x'=-\infty}^{0} f(x') \ g(x,x')dx' = h(x), \ x \in (-\infty,0) \quad , \quad (2.4.1)$$

The semi-infinite domain involved in this integral equation precludes Fourier transformation of the equation as it stands. In order to transform (2.4.1), it is necessary to extend the equation by introducing the definitions

$$\phi_-(x) = \begin{cases} 0, & x > 0 \\ \\ f(x), & x < 0 \end{cases} \qquad (2.4.2)$$

and

$$a_-(x) = \begin{cases} 0, & x > 0 \\ \\ h(x), & x < 0 \end{cases} \qquad (2.4.3)$$

With these definitions the integral equation may be rewritten as

$$\frac{1}{\sqrt{2\pi}} \int_{-\infty}^{\infty} \phi_-(x) \, g(x-x')dx' = a_-(x) + b_+(x), \quad x \in (-\infty,\infty) \ , \ (2.4.4)$$

where $b_+(x)$ is an unknown function which has support for x in $(0,\infty)$ and which must be introduced in order that the range of applicability of the original equation (2.4.1) may be formally extended to a doubly-infinite domain. Since $b_+(x)$ is not a part of the original problem pre-scription, it is a new unknown which should be recoverable in the solution process.

The form (2.4.4) is amenable to Fourier transformation. With an ap-peal to the convolution theorem of Fourier transforms, the equation be-comes

$$\Phi_-(k_x) \cdot G(k_x) = A_-(k_x) + B_+(k_x) \ . \qquad (2.4.5)$$

The constraints on the imaginary part of k_x are dictated by the exis-tence of the Fourier transforms of the functions in a particular problem.

The Wiener-Hopf procedure leads to a solution for the unknown

functions $\Phi_+(k_x)$ and $B_-(k_x)$ which are constructed as follows:

$$\Phi_-(k_x) = \frac{S_-(k_x)}{G_-(k_x)} \tag{2.4.6}$$

$$B_+(k_x) = - S_+(k_x) \cdot G_+(k_x) \tag{2.4.7}$$

The functions $G_+(k_x)$ and $G_-(k_x)$ are defined through the factorization of the transform of the kernel, $G(k_x)$, as follows:

$$G(k_x) = G_+(k_x) \cdot G_-(k_x) \tag{2.4.8}$$

where

$\quad G_+(k_x)$ is regular and non-zero for $\text{Im}(k_x) > \tau_-$,

and

$\quad G_-(k_x)$ is regular and non-zero for $\text{Im}(k_x) < \tau_+$.

The pair of functions $S_+(k_x)$ and $S_-(k_x)$ are defined through the decomposition of a function into two functions which are each individually regular over respective halves of the complex plane as given below:

$$\frac{A_-(k_x)}{G_+(k_x)} = S_+(k_x) + S_-(k_x) \tag{2.4.9}$$

where

$\quad S_+(k_x)$ is regular for $\text{Im}(k_x) \geq \tau_-$,

and

$\quad S_-(k_x)$ is regular for $\text{Im}(k_x) \leq \tau_+$.

Thus, in summary, we can recover the original unknown function, $f(x)$, through its transform as computed in (2.4.6). The other unknown,

which is introduced in (2.4.4), is also recovered. To construct $f(x)$, we must find functions which are regular and non-zero over respective halves of the complex k_x plane according to the factorization definition (2.4.8) and the decomposition definition (2.4.9). It is on these two steps that attention is focused in the Wiener-Hopf solution process.

2.5 Normalization

Throughout the body of this study, a normalization has been used to bring the scale of the variables to a consistent and convenient level. Unnormalized variables in the initial problem formulations are primed. So μ_1' refers to the actual complex permeability of medium 1 (physical property) and k_2' refers to the wave number of medium 2. Hence $k_1' = \omega \sqrt{\mu_1' \cdot \epsilon_1'}$. The normalization used is reflected in the following equations where the unprimed variable is the normalized variable and (μ_0, ϵ_0) are the constitutive parameters for free space:

$$k_1' = k_1 \cdot (\omega \sqrt{\mu_0 \cdot \epsilon_0}), \ \mu_1' = \mu_1 \cdot \mu_0, \ \epsilon_1' = \epsilon_1 \cdot \epsilon_0 .$$

The effect of this normalization is to reference values of any variable to the value which holds for free space at the frequency of interest.

Because the transform variable, k_x, is normalized to the free space wavenumber, $k_0 = \omega \sqrt{\mu_0 \cdot \epsilon_0}$, it is necessary to normalize distance to the free space wavelength:

$$x = k_0 \cdot x' = (2\pi \cdot (\text{distance in wavelengths}))$$

where x' is the unnormalized distance. This ensures that $k \cdot x = k' \cdot x'$, where the unprimed quantities are normalized and the primed ones are not.

CHAPTER III

WIENER-HOPF ANALYSIS OF THE INTERFACE PROBLEM

3.1 Statement of the Problem

The diffracting geometry to be considered is shown in Figure 3.1.
The half spaces for $y' > 0$ and $y' < 0$ contain media characterized by
(μ_1', ϵ_1') and (μ_2', ϵ_2') respectively and their interface coincides with the
x'-z' plane. The media are general and characterized by constitutive
parameters which are complex numbers having real part greater than zero
and imaginary part less than or equal to zero. An infinitely thin, per-
fectly electrically conducting (PEC) screen lies on the interface for
$x' > 0$. A plane wave is incident from medium 1 at an angle θ to the PEC
screen ($0 < \theta < \pi$). The incident wave may be polarized either transverse
magnetic (TM) or transverse electric (TE) relative to the z' axis and is
invariant with respect to z'.

We seek to determine the total fields everywhere in space in the
presence of the medium discontinuity and the diffracting PEC half-plane.
The more practical result developed, however, is the field at great
distances from the edge of the half-plane, that is, that which results
from applying asymptotic evaluation techniques to the inverse Fourier
transform integrals of the Wiener-Hopf solutions obtained.

This problem may be formulated in terms of an unknown quantity which
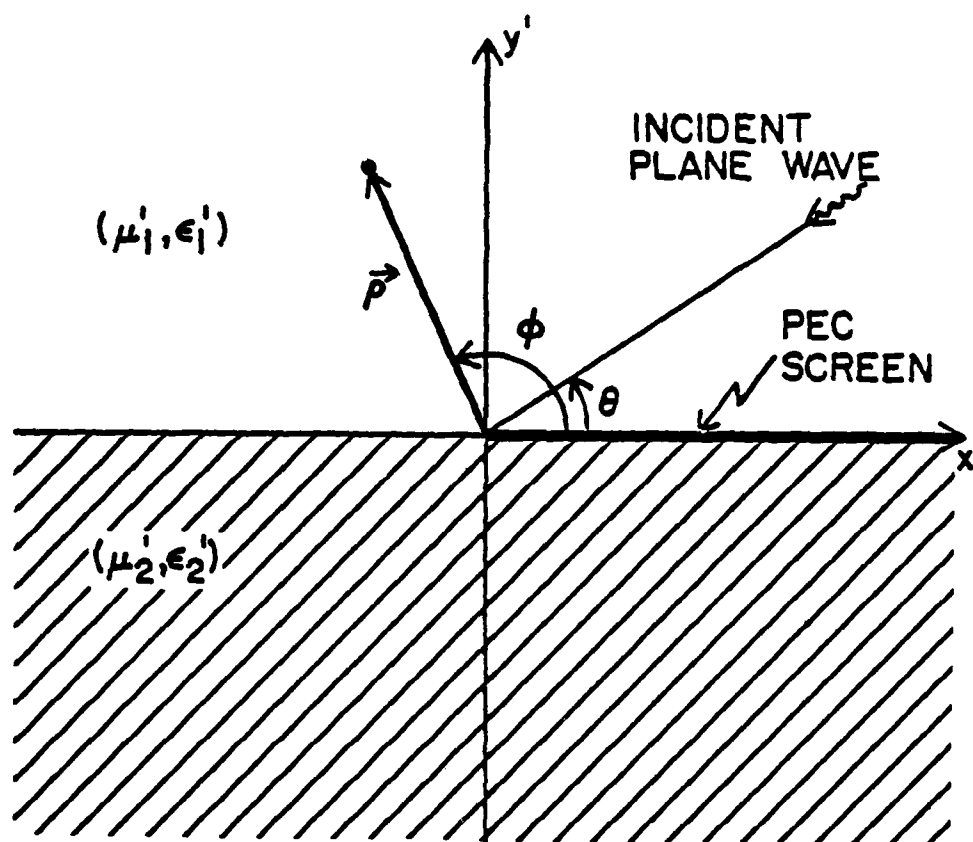
Figure 3.1. Geometry of the interface problem.

resides on the interface and which is non-zero only over half of the domain, that is, for x' in $(-\infty, \infty)$. Either the component of the total electric field tangential to the interface plane is considered unknown for x' in $(-\infty, 0)$ or the surface current density on the PEC half-plane for x' in $(0, \infty)$ is considered as unknown. In either case the quantity in question vanishes on the complementary semi-infinite domain by the physics of the problem.

We proceed in this chapter to state four integral equations resulting from the two incident field polarizations viewed both from the aperture and the PEC half-plane formulations. The particular case of TM incidence formulated over the aperture is treated in detail. The other three integral equations admit to similar treatment. We conclude the chapter by relating them to the TM aperture formulation.

3.2 Integral Equation Formulations

We begin by considering the formulation of the TM scattering problem as an integral equation with the tangential electric field over the aperture plane $(x' < 0)$ as the unknown. The problem configuration is shown in Figure 3.1. The analysis follows the procedure described by Butler and Umashankar (1976). The problem is viewed as the composition of two subsidiary problems, one equivalent problem for the half space above the interface plane $(y' > 0)$ and another below the interface $(y' < 0)$. In each equivalent problem the PEC half-plane is extended to cover the entire interface plane and an unknown surface magnetic current is intro-

duced to provide the correct continuity across the shorted aperture of the tangential components of the fields. The resulting integro-differential equation is given below:

$$h_x^{inc}(x') = -j\omega\epsilon_1' \left[1 + \frac{1}{(k_1')^2} \frac{\partial^2}{\partial x'^2}\right]_{x_0=-\infty} \int^0 e_z(x_0) \cdot g_1(x',x_0)dx_0$$

$$+ j\omega\epsilon_2' \left[1 + \frac{1}{(k_2')^2} \frac{\partial^2}{\partial x'^2}\right]_{x_0=-\infty} \int^0 e_z(x_0) \cdot g_2(x',x_0)dx_0 \quad (3.2.1)$$

for $x' \in (-\infty, 0)$,

where $k_x^{inc} = \dfrac{-E_0 e^{jk_1'x'\cos\theta}}{\eta_1'}\sin\theta$ is the component of the incident

magnetic field which is tangential to the interface plane (E_0 is the magnitude of the electric field of the incident plane wave at the edge of the PEC screen and $\eta_1' = \sqrt{\mu_1'/\epsilon_1'}$),

e_z is the total electric field over the aperture,

$(\epsilon_1', k_1'), (\epsilon_2', k_2')$ are the permittivity and wavenumber for the medium in the upper/lower half-spaces respectively,

and g_1, g_2 are the Green's functions appropriate to the respective problems:

$$g_{\binom{1}{2}}(x',x_0) = -\frac{1}{4} H_0^{(2)}(k_{\binom{1}{2}}'|x' - x_0|) \quad .$$

The TM problem can also be formulated in terms of the z'-directed current induced on the PEC half-plane as an electric field integral equation. The resulting integral equation is

$$e_z^{NP} = -\int_{x_0=0}^{\infty} j_z(x_0) \cdot a(x',x_0) dx_0 \quad (3.2.2)$$

for $x' \in (0,\infty)$,

where e_z^{NP} is the total electric field present with the PEC half-plane removed, that is, the total scattered field in the presence of only the discontinuity of the media,

j_z is the unknown induced electric current on the PEC half-plane,

a is the Green's function which serves as the kernel.

The kernel is usually expressed in the spectral domain as it involves a Sommerfeld integral. For this problem the Fourier transform of the kernel $a(x')$ is

$$A(k_x') = \frac{\omega}{\sqrt{2\pi}\left(\dfrac{\beta_1'}{\mu_1'} + \dfrac{\beta_2'}{\mu_2'}\right)} \quad . \tag{3.2.3}$$

Similar procedures can be formulated for the TE case. The problem can be formulated as an integro-differential equation either over the aperture or over the PEC half-plane. The resulting equations are shown below:

Aperture Formulation

$$h_z^{inc}(x') = \frac{\omega}{4} \int_{x_0 = -\infty}^{0} e_x(x_0) \times \tag{3.2.4}$$

$$[\epsilon_1' \cdot H_0^{(2)}(k_1'|x'-x_0|) + \epsilon_2' \cdot H_0^{(2)}(k_2'|x'-x_0|)]dx_0$$

for $x' \in (-\infty, 0)$

PEC Formulation

$$e_x^{NP}(x') = j\omega\mu_1' \left[1 + \frac{1}{(k_1')^2} \frac{\partial^2}{\partial x'^2}\right]_{x_0=0} \int^\infty j_x(x_0) \cdot a(x',x_0)dx_0 \quad (3.2.5)$$

for $x' \in (0,\infty)$, where $a(x',x_0)$ is the kernel of the integral equation in the TM case. The Fourier transform of this kernel is

$$A(k_x') = \frac{-j\ \epsilon_1'}{\sqrt{2\pi}\ (\beta_1')^2 \left[\frac{\epsilon_1'}{\beta_1'} + \frac{\epsilon_2'}{\beta_2'}\right]} \quad . \quad (3.2.6)$$

It is noted that equations (3.2.1) and (3.2.5) are integro-differential equations. As a result, the subsequent Fourier transformation of them requires integration by parts which results in the formation of a term commonly referred to as the bilinear concomitant. A detailed examination of the conditions for the vanishing of this term results in a boundary condition on the applicability of the Wiener-Hopf equation in the transform domain. The remaining two integral equations are seen to involve Sommerfeld integrals as part of the Green's function in the kernel. On examining the regions of validity for the Fourier transform of the integral equations resulting from the two formulations in a particular polarization, it is found that the regions are complementary in the spectral domain; that is, the union of the domains for the two formulations is always a strip in the transform domain which is bounded by the branch points for that wavenumber in the problem which is closest to the real axis. As a result if the strip of analyticity vanishes in one formulation due to the angle of the incident plane wave, it is found that

the other formulation will have a non-vanishing Wiener-Hopf strip.

3.3 Wiener-Hopf Formulation for TM Incidence: Aperture Formulation

The integral equation (3.2.1) may be formally extended to apply on an infinite domain as in (2.4.4) in order to allow it to be Fourier transformed into the form of (2.4.5) with the result

$$a(x') + b(x') = -j\omega\varepsilon_1' \left[1 + \left(\frac{1}{k_1'}\right)^2 \frac{\partial^2}{\partial x'^2}\right] \int_{-\infty}^{\infty} \phi(x_0) \cdot g_1(x',x_0)dx_0$$

$$\tag{3.3.1}$$

$$-j\omega\varepsilon_2' \left[1 + \left(\frac{1}{k_2'}\right)^2 \frac{\partial^2}{\partial x'^2}\right] \int_{-\infty}^{\infty} \phi(x_0) \cdot g_2(x',x_0)dx_0$$

where

$$a(x') = \begin{cases} 0 & , \quad 0 < x' < \infty \\ \\ h_x^{inc}(x') & , \quad -\infty < x' < 0 \end{cases} \quad , \tag{3.3.2}$$

$$b(x') = \begin{cases} \text{unknown function} & , \quad 0 < x' < \infty \\ \\ 0 & , \quad -\infty < x' < 0 \end{cases} \quad , \tag{3.3.3}$$

$$\phi(x') = \begin{cases} 0 & , \quad 0 < x' < \infty \\ \\ e_z(x') , \text{ the desired,} & -\infty < x' < 0 \\ \quad \text{unknown function} \end{cases} \quad . \tag{3.3.4}$$

The unknown function $b(x')$ is, of course, not required by the original integral equation. It is an artifice in the Wiener-Hopf procedure and is ultimately eliminated.

The extended domain integral equation (3.3.1) can be Fourier transformed according to (2.1.2) to obtain

$$A'(k_x') + B'(k_x') = -j\omega\epsilon_1' \sqrt{2\pi} \left[1 - \left(\frac{k_x'}{k_1'}\right)^2\right]\left[\Phi'(k_x') \cdot G_1(k_x')\right]$$

$$-j\omega\epsilon_2' \sqrt{2\pi} \left[1 - \left(\frac{k_x'}{k_2'}\right)^2\right]\left[\Phi'(k_x') \cdot G_2(k_x')\right] \quad , \tag{3.3.5}$$

where we have used the convolution theorem of Fourier transforms. The transformed kernels $G_{1,2}$ contain the Fourier transforms of Hankel functions and are given in (2.1.3) with $y = 0$.

At this point we introduce the following substitutions and normalizations:

$$\frac{A_-(k_x)}{\eta_0 k_0} = A'(k_0 k_x) = \frac{1}{\eta_0 k_0} \frac{j E_0 \sin\theta}{\sqrt{2\pi} \eta_1(k_1\cos\theta + k_x)} , \tag{3.3.6}$$

$$\frac{B_+(k_x)}{\eta_0 k_0} = B'(k_0 k_x) = \text{unknown function} , \tag{3.3.7}$$

$$\Phi_-(k_x) = \frac{-k_0 \Phi'(k_0 k_x)}{2} = \frac{-k_0 E_z'(k_0 k_x)}{2} , \tag{3.3.8}$$

$$\frac{\beta_1}{\eta_0\mu_1} = \frac{1}{\omega}\frac{\beta_1'}{\mu_1'} \quad . \tag{3.3.9}$$

With these normalizations, the result is that for [1]

$$(-\min(k_{1i}, k_{2i}) = \tau_-) < \tau < (\tau_+ = \min(k_{2i}, k_{1i} \cos\theta)) \qquad (3.3.10)$$

where $k_x = \sigma + j\tau$ and $k = k_r - jk_i$,

the following equation holds in the Fourier transform domain:

$$A_-(k_y) + B_+(k_x) = \left[\frac{\beta_1}{\mu_1} + \frac{\beta_2}{\mu_2}\right] \Phi_-(k_x) \ . \qquad (3.3.11)$$

This is the Wiener-Hopf equation which we must solve for Φ_-, the Fourier transform of the electric field in the aperture on the interface between the two media.

Requisite to the Wiener-Hopf procedure is the determination of the common strip of analyticity in the k_x plane for the quantities appearing in (3.3.11). One must consider the region of existence of the transform domain functions appearing in this equation in the light of the Wiener-Hopf factorization defined in (2.4.8).[2]

Figure 3.2 depicts the complex k_x plane and the boundaries delimiting the half planes of analyticity for the functions involved and the directions from each boundary in which the regular regions extend. (The

---

[1]This restriction on the region of validity of the Wiener-Hopf equation arises from the analyticity and existence of the various constituent transforms and is discussed subsequently.

[2]We consistently use the (+) subscript to denote a function which is regular and non-zero in the upper half plane and (−) to denote similar behavior in the lower half plane.
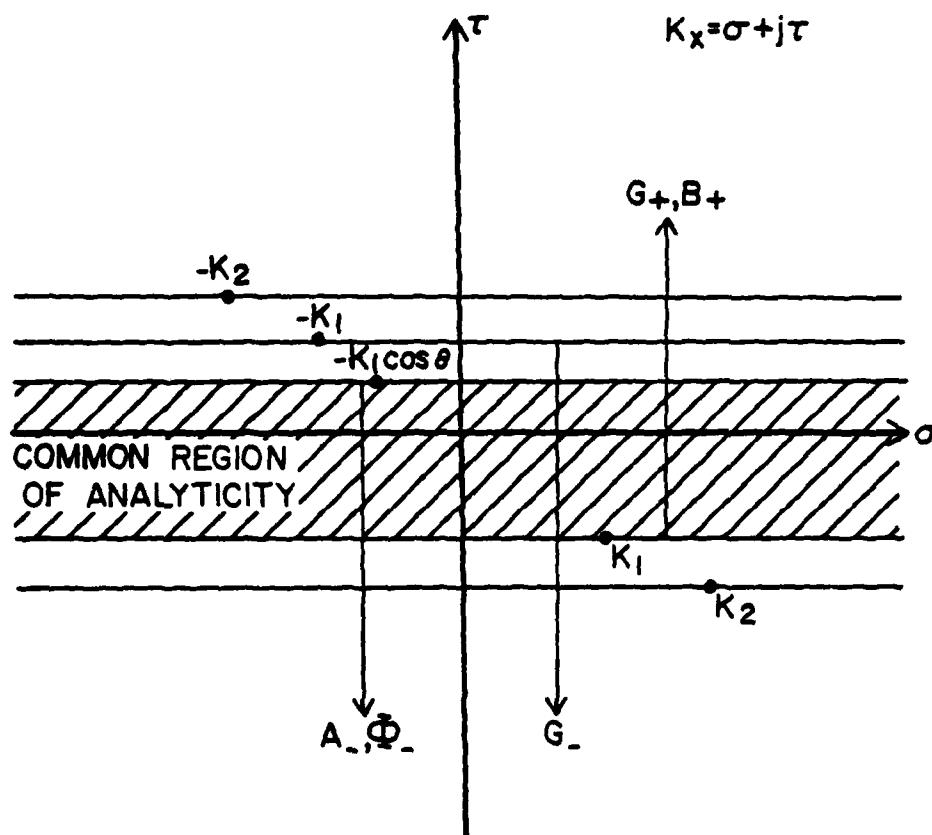
Figure 3.2.   Regions of analyticity of functions
in (3.3.11).

subscript notation introduced in equations (3.3.6) through (3.3.9) refers to the regions of regularity for the functions defined there in anticipation of the Wiener-Hopf analysis which follows.) The common region of analyticity for all the components is observed to be bounded by (3.3.10). We also note that the Wiener-Hopf equation, when formulated over the aperture, does not apply when $\tau_+ < \tau_-$ which occurs if $k_{1i}\cos\theta < -k_{2i}$. Observe that this can only occur for $\theta > \pi/2$ when $k_{1i} > k_{2i}$.

Our Wiener-Hopf system is (3.3.11) and applies in the domain defined by (3.3.10). To use the Wiener-Hopf procedure, it is necessary to form the factors G_+ and G_- defined in (2.4.8).

3.4 Factorization of $G(k_x)$

We consider in this section the factorization of the kernel in the Wiener-Hopf equation (3.3.11)

$$G(k_x) = \frac{\beta_1}{\mu_1} + \frac{\beta_2}{\mu_2} \qquad . \qquad (3.4.1)$$

Before proceeding to formulate a formal factorization integral for $G(k_x)$ some observations about the function are in order. $G(k_x)$ is analytic except on the branch cuts of $\beta_1 = \sqrt{k_1^2 - k_x^2}$ and $\beta_2 = \sqrt{k_2^2 - k_x^2}$, and is bounded in any finite region of the complex k_x plane. It is a multiple-sheeted function with four Riemann sheets. It is also an even function. There is a total of four zeros on all sheets and they occur in pairs on a sheet. Hence two sheets will have no zeros and two will have two zeros each.

It is useful to partially factorize $G(k_x)$ by identifying explicit factors which are regular over the requisite half planes

$$G(k_x) = G_1(k_x) \cdot G_2(k_x) = \left[\frac{\mu_1 + \mu_2}{\mu_1\mu_2} \beta_1\right]\left[\frac{\mu_2}{\mu_1 + \mu_2} + \frac{\mu_1}{\mu_1 + \mu_2}\frac{\beta_2}{\beta_1}\right] \quad (3.4.2)$$

The first factor $G_1(k_x)$ is factorized by inspection:

$$G_1(k_x) = \left[\frac{\mu_1 + \mu_2}{\mu_1\mu_2}\right]^{\frac{1}{2}}\sqrt{k_1 + k_x} \cdot \left[\frac{\mu_1 + \mu_2}{\mu_1\mu_2}\right]^{\frac{1}{2}}\sqrt{k_1 - k_x} \quad . \quad (3.4.3)$$

The G_2 factor is now the function which remains to be factorized. We note that it is bounded except at $k_x = \pm k_1$. In particular $G_2(k_x) \rightarrow 1$ as $|k_x| \rightarrow \infty$. It is a two sheeted function since the branch points are introduced only in the ratio of (β_2/β_1). This is apparent if one considers the value of the function on a closed path which encircles two of the four branch points. It is an even function (as is $G(k_x)$) and is bounded everywhere except at $k_x = \pm k_x$. Since there are two branches of $G_2(k_x)$, there will only be two roots which will occur and they will be located at the following positions:

$$k_x = \pm\sqrt{\frac{k_2^2\mu_1^2 - k_1^2\mu_2^2}{\mu_1^2 - \mu_2^2}} \; , \; \mu_1 \neq \mu_2 \quad (3.4.4)$$

If $\mu_1 = \mu_2$, there are no roots of $G_2(k_x)$ unless $\epsilon_1 = \epsilon_2$, i.e. unless the media are identical signifying the degeneration of the two media problem to the classical half-plane problem. It is readily determined on which sheet of $G_2(k_x)$ the roots occur by substituting the roots of (3.4.4) into

equation (3.4.2) for $G_2(k_x)$. They can only occur on one sheet.

The two different choices of branch cuts shown in Figure 3.3 prove useful in defining G_2 in subsequent developments. The cuts shown in Figure 3.3a are sectors of hyperbolas which are asymptotic to the coordinate axes and pass through the branch points. A pair of these cuts is associated with the respective branch points at $+ k_1$ and $+ k_2$ and their choice ensures that

$$\text{Im } \beta_1 \leq 0 \ , \ \text{Im } \beta_2 \leq 0 \qquad (3.4.5)$$

for all points in the k_x plane as discussed in section 2.2. With β_1 and β_2 defined by the hyperbolic branch cuts, it is difficult to discuss the occurrence of the roots on the top sheet of $G_2(k_x)$. It is desirable to consider an analytic continuation of the definition of the top sheet of $G_2(k_x)$ which manifests the fourth quadrant branch cut as a curved line connecting the branch points k_1 with k_2 (and, similarly, another line connecting $-k_1$ with $-k_2$). The branch cuts for this analytic continuation of $G_2(k_x)$ are shown in Figure 3.3b and account for the two-sheeted nature of G_2. That this branch cut deformation is permissible is a result of the radicals in G_2 appearing as a quotient only. The precise definition of this branch cut and the properties of the new top sheet of $G_2(k_x)$ are discussed below.

In order to examine the functional behavior of $G_2(k_x)$ with the new branch cut configuration, the functional mappings implied by $G_2(k_x)$ can be viewed as a series of conformal mappings. For simplicity, only values
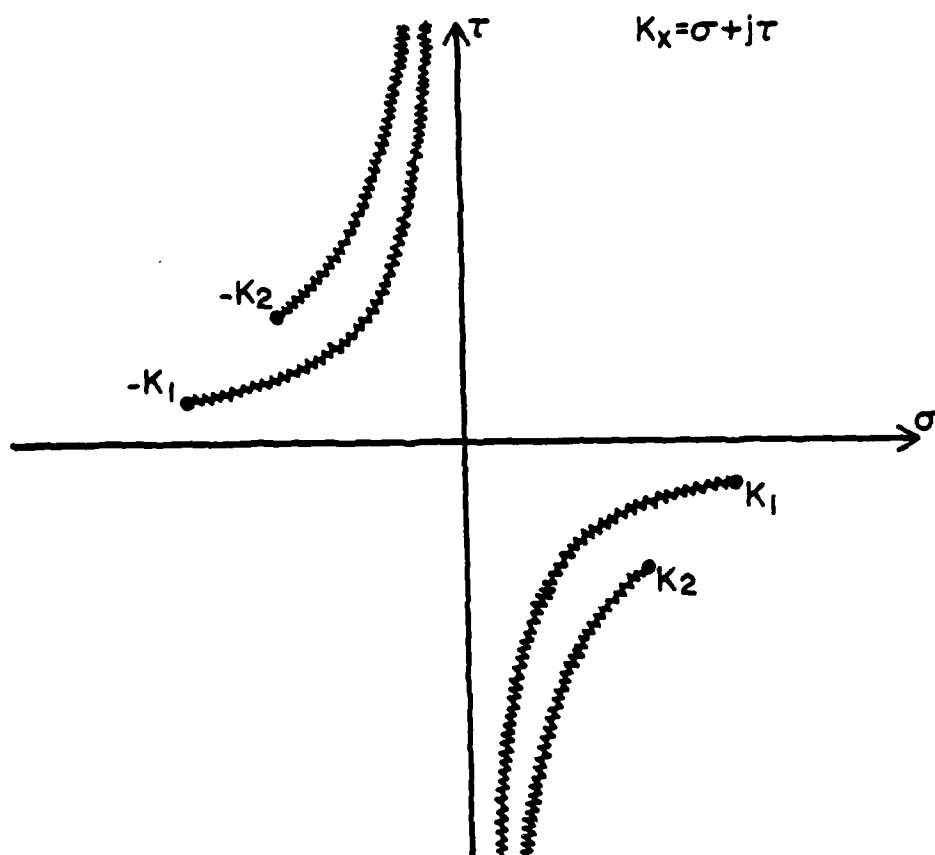
Figure 3.3.a.   Definition of $G_2(k_x)$ with hyperbolic
branch cuts.
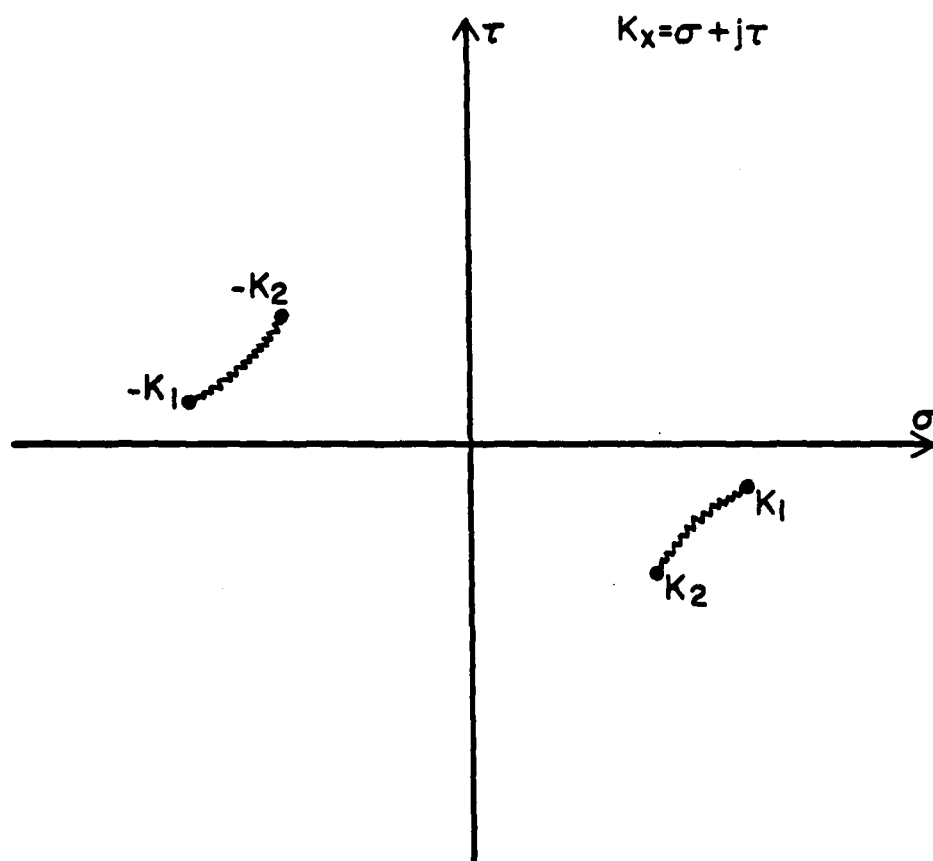
Figure 3.3.b. Definition of $G_2(k_x)$ with finite-length hyperbolic branch cuts.

of k_x with $Im(k_x) < 0$ will be considered. (Similar arguments apply for $Im(k_x) > 0$ also.) The mappings are depicted in Figure 3.4 along with the critical points $k_x = k_1$, k_2, ∞.

The definition of the new branch cut of $G_2(k_x)$ is shown in the γ plane of Figure 3.4. The branch cut connecting k_1^2 and k_2^2 is a straight line which, of course, goes through $k_x = \infty$. The transform shown as $B(k_x)$ is a Mobius mapping and hence circle-preserving. However $B(\infty) = 1$ and $B(k_2) = 0$ which causes the branch cut to map into the negative real axis in the B plane. In order to define $D = \sqrt{B}$, it is necessary to specify both the branch cut and a point on the top sheet of D. For this reason the point $D(\infty) = 1$ is used. This causes $G_2(k_x) \to 1$ as $|k_x| \to \infty$ and pre- serves the asymptotic behavior of $G_2(k_x)$ required by the integral factor- ization theorem which we apply later. Since $B(\infty) = D(\infty) = 1$ and $D = \sqrt{B}$, it is clear that the specified branch cut maps into the imaginary axis in the D plane. Observe that the root of $G_2(k_x)$ occurs at $D = -(\mu_2/\mu_1)$. Since both μ_1 and μ_2 are, in general, complex numbers in the fourth quadrant, their ratio is a complex number restricted to the first or fourth quadrants. Therefore, $(-\mu_2/\mu_1)$ must lie in the left half of com- plex D plane; that is, the root of D must lie on the lower sheet of D. This proves that the branch definition of G_2 which is specified by the straight cut between k_1 and k_2 (and hence $-k_1$ and $-k_2$) in the $\gamma = k_x^2$ plane and the asymptotic value of $\lim G_2(k_x) = 1$ as $|k_x| \to \infty$ has no roots on the top sheet. This cut in the γ plane may be mapped back into the k_x plane, of course. However it proves less complicated and no more

Mapping Function	Critical Points	Mapping

1. $\gamma = \alpha^2$

$\gamma(K_1) = K_1^2$

$\gamma(K_2) = K_2^2$

$\gamma(\infty) = \infty$

2. $B = \dfrac{K_2^2 - \gamma}{K_1^2 - \gamma}$

$B(K_1) = \infty$

$B(K_2) = 0$

$B(\infty) = 1$

3. $D = \sqrt{B}$

$D(K_1) = \infty$

$D(K_2) = 0$

$D(\infty) = 1$
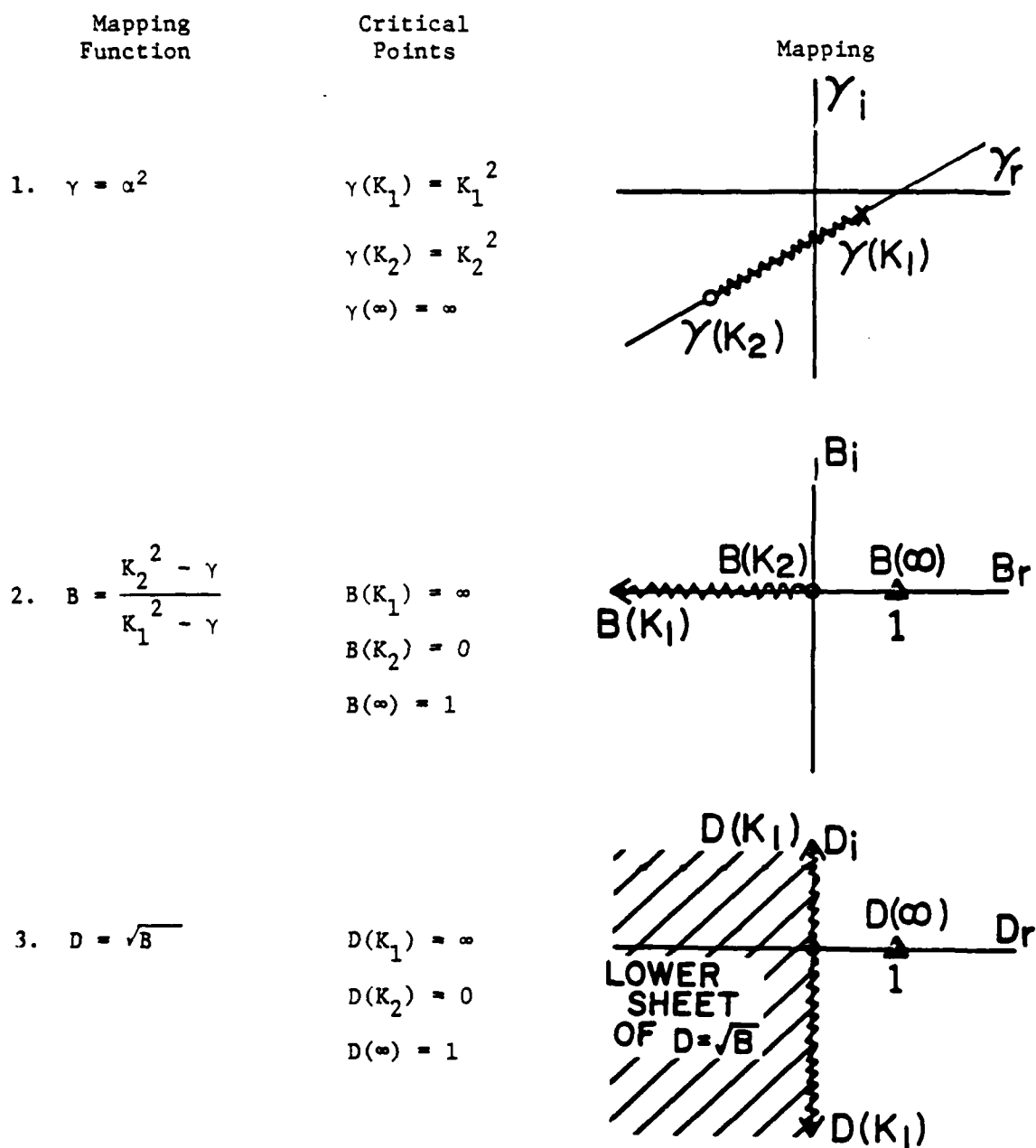
Figure 3.4. Conformal mappings implied by $G_2(k_x)$.

costly to transform the integral in k_x to an integral in γ and thereby obviate the need to explicitly define the cut in the k_x plane.

We proceed to perform a formal integral factorization of $G_2(k_x)$ defined in (3.4.2). The following factorization theorem (Mittra and Lee (1971a), Noble (1958)) is applicable to G_2 as we have constructed it:

Let $G_2(k_x)$ be regular and nonzero in the strip $\tau_- < \tau < \tau_+$. Within this strip, $G_2(k_x) \to 1$ uniformly as $|\sigma| \to \infty$. Then $G_2(k_x)$ can be factorized such that

$$G_2(k_x) = G_2^+(k_x) \cdot G_2^-(k_x) \ ,$$

where

$$G_2^+(k_x) = \exp\left\{ \frac{1}{2\pi j} \int_{-\infty+jc}^{\infty+jc} \frac{\ln[G_2(\delta)]}{\delta - k_x} \, d\delta \right\}, \quad \tau_- < c < \tau < \tau_+ \quad (3.4.6)$$

is regular and nonzero in the upper half k_x-plane defined by $\tau > \tau_-$; and

$$G_2^-(k_x) = \exp\left\{ \frac{-1}{2\pi j} \int_{-\infty+jd}^{\infty+jd} \frac{\ln[G_2(\delta)]}{\delta - k_x} \, d\delta \right\} , \quad \tau_- < \tau < d < \tau_+ \quad (3.4.7)$$

is regular and nonzero in the lower half k_x-plane defined by $\tau < \tau_+$.

Let us consider the integral in (3.4.6). Figure 3.5 shows the inte-
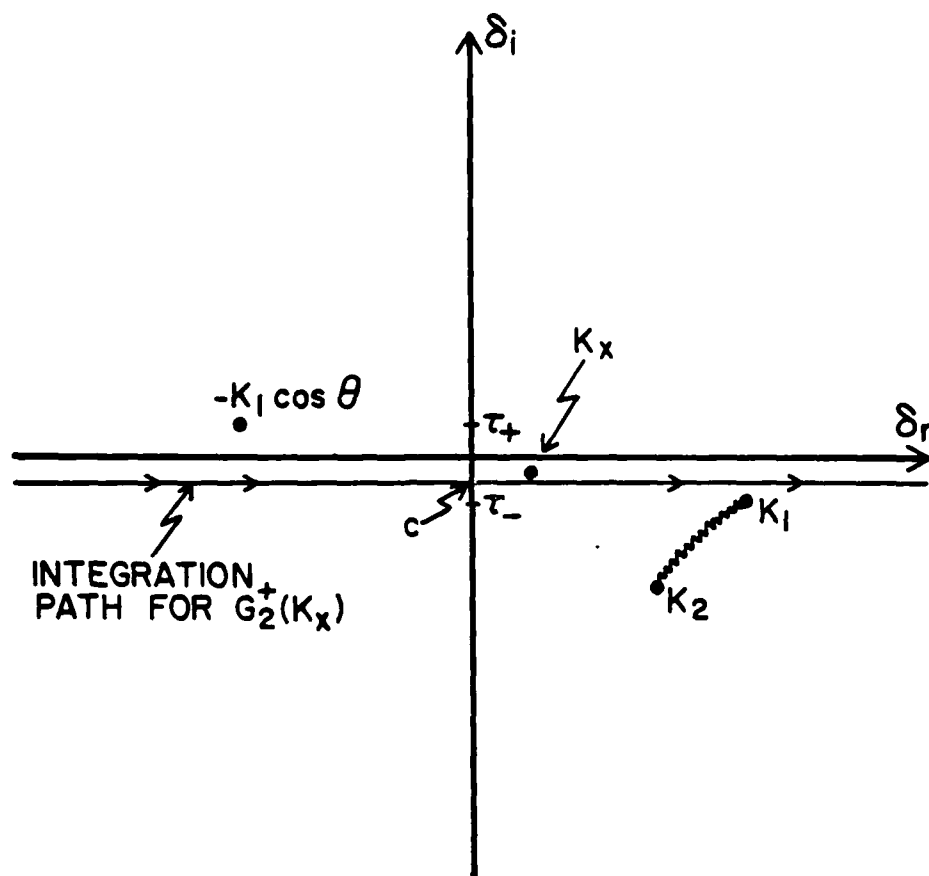
Figure 3.5. Integration path for the integral factorization $G_2^+(k_x)$.

gration path in the δ plane. Since we are considering a case which has no roots of G_2 on the top sheet, no additional cuts are required for the logarithm. This analytic continuation of G_2 has precisely the same values in the complex δ plane as the original definition of the top sheet of G_2 at all points except those in the region bounded by the hyperbolic cuts and the new branch cut connecting k_1 and k_2 (and the symmetric image of this region in the second quadrant). Since no roots occur in this definition of the top sheet of G_2 and the function is bounded at all points in the δ plane except $\delta = \pm k_1$, it is clear that no branch cut of the logarithm specified in equation (3.4.6) need appear on the top sheet of the integrand shown in Figure 3.5.

We observe that the principal value of the logarithm is an acceptable definition for the integrand in (3.4.6). Such a definition can be seen to have the logarithmic branch cut on the lower sheet of the integrand. Considering the plot of the D plane in Figure 3.4, the logarithmic cut will run from the root of G_2 along a line connecting $D(\infty) = 1$ and the root. It will run to $D(k_1) = \infty$ in the direction opposite to $D(\infty) = 1$.

We may close the integration contour at infinity either up or down with no change in the value of the integral since the integrand is uniformly asymptotic to zero along any arc at infinity. Closure down is shown in Figure 3.6 where we show the integration path taken in the negative direction (for convenience later). The region enclosed by the contour is analytic and therefore the contour integral equals zero. Also the contributions from C_1 and C_2 cancel while all contributions
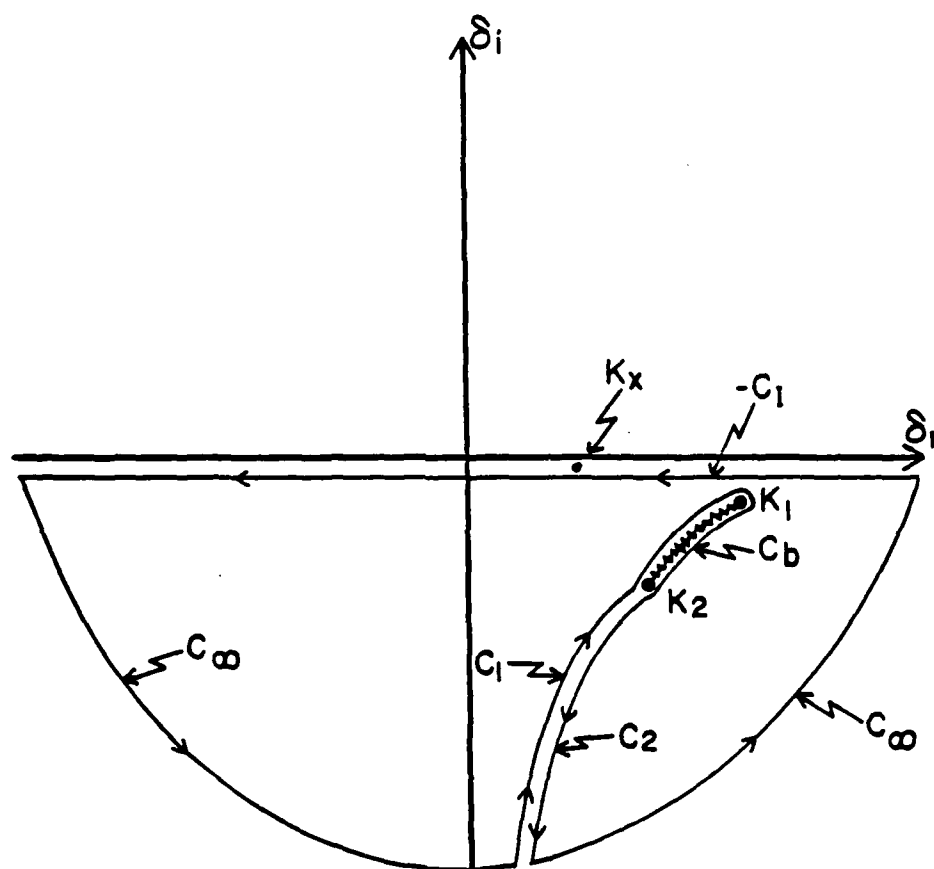
Figure 3.6.   Closure of the integration contour.

from C_∞ are zero. Therefore we have

$$\int_{(C_I)} = -\int_{(-C_I)} = \int_{C_b} \tag{3.4.8}$$

We have converted the original infinite line integral into a finite loop integral encircling the branch cut from $\delta = k_1$ to $\delta = k_2$.

We now consider the loop integral around the branch cut. The loop integral may be considered as four separate integrals as shown in Figure 3.7. We have taken the branch cut as the line connecting k_1 and k_2 specified implicitly by the straight cut in the $\gamma = k_x^2$ plane. Therefore we have the following:

$$\int_{-\infty+jc}^{\infty+jc} \frac{\ln G_2(\delta)}{\delta - k_x} d\delta = \int_{C_b} = \int_{C_1} + \int_{C_2} + \int_{C_3} + \int_{C_4} . \tag{3.4.9}$$

Using standard analysis one can show that the contour contributions vanish on the two semi-circular arcs C_2 and C_4. Thus the original integral reduces to

$$\int_{-\infty+jc}^{\infty+jc} \frac{\ln G_2(\delta)}{\delta - k_x} d\delta = \int_{C_1 + C_3} \frac{\ln G_2(\delta)}{\delta - k_x} d\delta . \tag{3.4.10}$$

For purpose of computation it is necessary to establish the value of G_2 for points on the integration path C_1. This is straightforward since the path specified by C_1 does not cross the original hyperbolic cuts in Figure 3.7 and the original hyperbolic branch values of the square roots may be used along C_1. This can be shown by observing that the hyperbolas
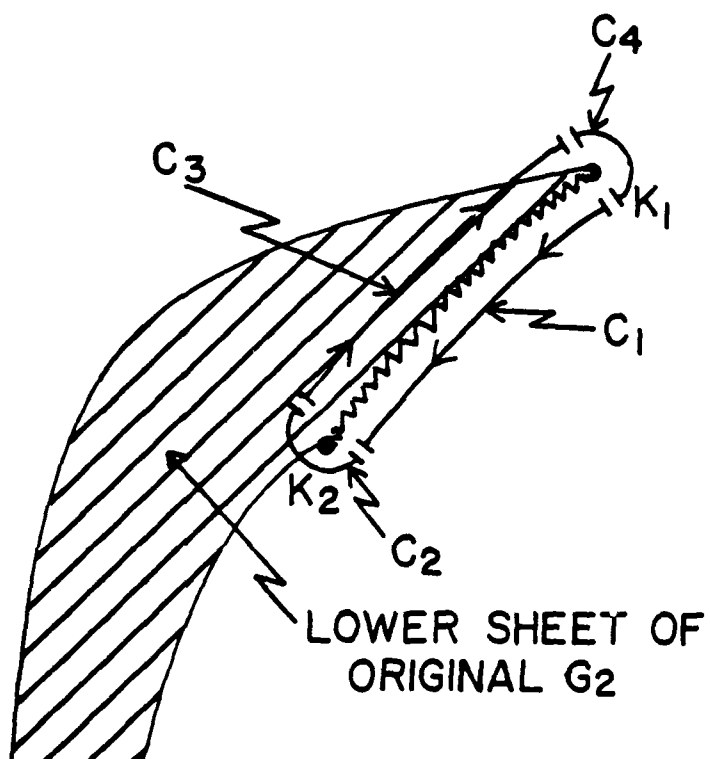
Figure 3.7. Detail of the integration contour in the vicinity of the branch cut.

correspond to straight lines in the $\gamma = k_x^2$ plane which are parallel to the real axis and pass through the branch points. Hence the hyperbolic lines through k_1 and k_2 in the k_x plane of a problem will map into straight parallel lines in the γ plane while path C_1 maps into a straight line which connects the branch points. So the value of G_2 on a path C_1 will always be that associated with the hyperbolic branch cut definition.

As depicted in Figure 3.7, the integral along C_1 (path from k_1 to k_2) is on the original top sheet of the hyperbolic definition of G_2 and the integral along C_3 is on the original lower sheet of G_2 (in the limit as C_3 approaches the branch cut). This is due to the fact that in the problem shown in Figure 3.7, the point $\delta = k_1$ lies on the original hyperbolic branch cut which was nearer the coordinate axes in the δ plane. Had k_2 lain on the inside hyperbola, we would have found that the path from k_1 to k_2 would have been C_3 rather than C_1. This suggests an algorithm for establishing values of $\ln(G_2)$ on the line integral.

The path C_1, as defined, is always on the original top sheet of G_2 so that β_1 and β_2 are clearly and simply defined on C_1 (with the hyperbolic branch cuts). Also we observed that C_3 lies just across the square root branch cut from C_1 which simply means a change of sign for (β_2/β_1). Therefore we have

$$\int_{-\infty+jc}^{\infty+jc} \frac{\ln G_2(\delta)}{\delta - k_x} d\delta = \int_{C_1} \frac{\ln[a + b \, \beta_2/\beta_1]}{\delta - k_x} d\delta - \int_{C_2} \frac{\ln[a - b \, \beta_2/\beta_1]}{\delta - k_x} d\delta$$

$$\tag{3.4.11}$$

$$= \int_{C_1} \frac{1}{\delta - k_x} [\ln(a+b \, \beta_2/\beta_1) - \ln(a-b \, \beta_2/\beta_1)] d\delta \quad ,$$

where $a = \mu_2/(\mu_1+\mu_2)$ and $b = \mu_1/(\mu_1+\mu_2)$.

We have reduced the original infinite line integral to a finite line integral. Since the ratio of the logarithm arguments in (3.4.11) is less than π, it is permissible to express the integral as

$$\int_{-\infty+jc}^{\infty+jc} \frac{\ln G_2(\delta)}{\delta - k_x} d\delta = \int_{C_1} \frac{\ln\left[\dfrac{a + b\,\beta_2/\beta_1}{a - b\,\beta_2/\beta_1}\right]}{\delta - k_x} d\delta = \int_{C_1} \frac{\ln\left[\dfrac{a\beta_1 + b\beta_2}{a\beta_1 - b\beta_2}\right]}{\delta - k_x} d\delta,$$

$$(3.4.12)$$

For k_1 on the inner hyperbola (branch cut nearest the real and imaginary δ axes):

$$\int_{-\infty+jc}^{\infty+jc} = \int_{C_1} \frac{\ln\left[\dfrac{\mu_2\beta_1 + \mu_1\beta_2}{\mu_2\beta_1 - \mu_1\beta_2}\right]}{\delta - k_x} d\delta \quad , \qquad (3.4.13)$$

β_1 and β_2 maintain the hyperbolic definition and ln is the principal value. For k_2 on the inner hyperbola:

$$\int_{-\infty+jc}^{\infty+jc} = - \int_{C_1} \frac{\ln\left[\dfrac{\mu_2\beta_1 + \mu_1\beta_2}{\mu_2\beta_1 - \mu_1\beta_2}\right]}{\delta - k_x} d\delta \qquad . \qquad (3.4.14)$$

To consolidate these expressions we define a function $DIR(k_1)$:

$$DIR(k_1) \equiv \begin{cases} +1, \text{ when } k_i \text{ is on the inner hyperbola} \\[20pt] -1, \text{ when } k_1 \text{ is on the outer hyperbola} \end{cases} \qquad (3.4.15)$$

This leaves us with the final result

$$\int_{-\infty+jc}^{\infty+jc} \frac{\ln G_2(\delta)}{\delta-k_x}\, d\delta = [DIR] \cdot \int_{C_1} \frac{\ln\left[\dfrac{\mu_2\beta_1 + \mu_1\beta_2}{\mu_2\beta_1 - \mu_1\beta_2}\right]}{\delta-k_x}\, d\delta \quad . \quad (3.4.16)$$

Note that $\ln((\mu_2\beta_1+\mu_1\beta_2)/(\mu_2\beta_1-\mu_1\beta_2))$ is a well-behaved function for δ on a line between k_1 and k_2. As $\delta \to k_1$, $\ln \to \pm j\pi$ and as $\delta \to k_2$, $\ln \to 0$.

The function (3.4.16) is analytic in the region around the integration path except at k_1 and k_2. In fact, the integral is a Cauchy type integral since the logarithm is analytic along the integration path except at k_1 and k_2 (see Markushevich (1977), Gakhov (1966)). That is, the logarithm function is continuous on the integration path. The value of the integral is an analytic function of k_x for all points off of the integration path and tends uniformly to zero for $|k_x| \to \infty$. We can characterize the jump in the value of the integral as k_x traverses the path of integration using the Plemelj formulas. The important point is that the integral constructed has well-behaved properties in the variable k_x. At this point we observe that the expression for G_2^+, given by the formal factorization formula, was asserted to hold just for k_x such that $\tau_- < \tau < \tau_+$. We now have a well-behaved form which is the analytic continuation of G_2^+ onto the entire k_x plane. Therefore we have the factorization of the original function $G(k_x)$, (3.4.1), given as follows:

$$G_+(k_x) = \sqrt{\frac{\mu_1 + \mu_2}{\mu_1\mu_2}} \cdot \sqrt{k_1-k_x} \cdot \exp\left\{\frac{DIR}{2\pi j} \int_{C_1} \frac{\ln\left[\frac{\mu_2\beta_1(\delta) + \mu_1\beta_2(\delta)}{\mu_2\beta_1(\delta) - \mu_1\beta_2(\delta)}\right]}{\delta - k_x} d\delta\right\}$$

(3.4.17)

where β_1, β_2 and $\sqrt{k_1-k_x}$ are the original values defined in Chapter 2, ln is the principal value of the logarithm and C_1 is the path from k_1 to k_2 specified by $\delta^2 = (k_2^2-k_1^2)t+k_1^2$ where t is a real parameter and t is contained in $[0,1]$.

It is a straightforward exercise to formulate the integral in terms of the real parameter t, which is used to characterize δ on C_1. Direct substitution results in the following:

$$G_+(k_x) = \sqrt{\frac{\mu_1 + \mu_2}{\mu_1\mu_2}} \cdot \sqrt{k_1-k_x} \cdot \exp\left\{\frac{(k_2^2 - k_1^2) \cdot DIR}{4\pi j} \times \int_{t=0}^{1} \left[\frac{\ln\left[\frac{\mu_2\beta_1(\delta) + \mu_1\beta_2(\delta)}{\mu_2\beta_1(\delta) - \mu_1\beta_2(\delta)}\right]}{(\delta - k_x)\delta}\right]_{\delta(t)} dt\right\}$$

(3.4.18)

where $\delta(t) = \sqrt{(k_2^2-k_1^2)t+k_1^2}$, using the principal value of the square root.

We now establish a useful relation between $G_+(k_x)$ and $G_-(k_x)$. It is clear that $G(k_x)=G_+(k_x)\cdot G_-(k_x)$ is an even function of k_x. Therefore,

$$\frac{G_+(k_x)}{G_-(k_x)} = \frac{G_+(-k_x)}{G_-(-k_x)} \quad for \quad G_-(-k_x), G_-(k_x) \neq 0 .$$

(3.4.19)

Each side of the above equation is an entire function since $G_+(k_x)/G_-(-k_x)$

is analytic for $\tau > \tau_-$ and $G_+(-k_x)/G_-(k_x)$ is analytic for $\tau < \tau_+$. By the concept of analytic continuation we assert that the two sides are equal for all k_x on the top sheet and are entire functions. As $|k_x| \to \infty$, we have by construction that $G_+(-k_x) \to \sqrt{k_x}$, since the exponential goes to 1 and, similarly, $G_-(k_x) \to \sqrt{k_x}$. Therefore, $G_+(-k_x)/G_-(k_x) \to 1$ as $|k_x| \to \infty$. Hence $G_+(-k_x)/G_-(k_x)$ is an entire function, bounded at infinity. By Liouville's theorem from complex analysis, we have that $G_+(-k_x)/G_-(k_x)$ is a constant for all k_x and hence is equal to unity. So we have that $G_+(-k_x) = G_-(k_x)$ and we see that this symmetry will be true of the factorization of any even function $G(k_x)$ which can be used in a Wiener-Hopf analysis.

We note that $G_-(k_x)$ is analytic in the lower half of the k_x plane. Since $G_+(k_x) = G(k_x)/G_-(k_x) = G(k_x)/G_+(-k_x)$, the integral for $G_+(-k_x)$ in this expression will converge more quickly for k_x near the integration path from k_1 to k_2 than will the original expression for $G_+(k_x)$. The judicious use of these two representations for $G_+(k_x)$ ensures convergence of the integral which is to be evaluated numerically.

In a similar manner to the analysis leading to (3.4.18), we can derive the integral representation for $G_-(k_x)$ from (3.4.7). It can also be shown using these two expressions for $G_+(k_x)$ and $G_-(k_x)$ that, in fact, $G_+(k_x) \cdot G_-(k_x) = G(k_x)$. It is also clear from their form that the functions are analytic in the upper and lower portions of the complex k_x plane as required. The symmetry of the two functions $(G_+(k_x) = G_-(-k_x))$ is also apparent from the factorization integrals.

Before leaving the subject of the factorization of G, it is

appropriate to examine the location of the roots of $G_+(k_x)$ and $G_-(k_x)$.
We observed that the integrals in the exponentials are analytic functions
except on the integration paths (k_1, k_2) and $(-k_1, -k_2)$. They are bounded
except possibly in the vicinity of those lines. Therefore G_+ and G_-
must be bounded except possibly in the immediate vicinity of those lines
(which are actually branch cuts of G_+ and G_-). Now we know that $G(k_x)$
has four roots which occur in symmetric pairs on two of its four sheets.
If two of these roots occur on the top sheet of G then they also exist
for $(G_+ \cdot G_-)$. However the arguments of the exponential factors
which appear in the expressions for the functions G_+ and G_- (using the al-
tered branch cut definitions) must be bounded and hence G_+ and G_- cannot
be zero (except possibly at the branch points $k_x = \pm k_1$). This is a de-
monstration that G_+ and G_- have no roots on the top sheet except possibly
at the branch points themselves if G has no roots on the top sheet with
the deformed branch cuts. Therefore the roots of G, G_+ and G_- lie on
the sheets adjacent to the top sheet. As noted above G_+ and G_- are
related functions and therefore will each contain one root on the
improper sheet.

In closing this section on the factorization of G, we reiterate that
a knowledge of the position of the roots of G and construction of a cut
which placed them off of the top sheet is crucial to the formation of
the simplified integral expression (3.4.17) and is subsequently seen to
be important in forming an efficiently computable solution to a Wiener-
Hopf problem.

3.5 Decomposition

In the analysis below we carry only the formal functional expressions $G_+(k_x)$ and $G_-(k_x)$ to represent the functions derived in the preceeding section. As pointed out there, the analytical behavior of the factorized functions is simply inferred from their form, and they are straightforward to evaluate numerically. Therefore, having performed the factorization, we may now proceed with the decomposition operation specified in Section 2.4 (equation (2.4.9)). The function to be decomposed is

$$S(k_x) = A_-/G_+ = \frac{\Omega}{(k_1 \cos\theta + k_x) \cdot G_+(k_x)} = S_+(k_x) + S_-(k_x) \quad (3.5.1)$$

where

$$\Omega = \left(\frac{j E_0 \sin\theta}{\sqrt{2\pi} \; \eta_1} \right) \quad .$$

The decomposition is seen directly. $G_+(k_x)$ with its branch cuts must be part of $S_+(k_x)$ while the other singularity due to the root of $(k_x + k_1 \cos\theta)$ will clearly lie in S_-, so that

$$S_-(k_x) = \left[\frac{\Omega}{G_+(-k_1 \cos\theta)} \right] \frac{1}{(k_x + k_1 \cos\theta)} \quad (3.5.2)$$

and

$$S_+(k_x) = \Omega \left[\frac{1}{G_+(k_x)} - \frac{1}{G_+(-k_1 \cos\theta)} \right] \frac{1}{(k_x + k_1 \cos\theta)} \quad , \quad (3.5.3)$$

Note that the pole of S_+ due to the zero of the denominator of the second factor is cancelled by a zero in the first factor. An application

tion of L'Hospital's rule shows that the function S_+ is bounded at this point. Having performed the decomposition, we proceed with the Wiener-Hopf analysis as follows:

$$\Phi_- \cdot G_- - S_- = \frac{B_+}{G_+} + S_+ \quad . \qquad (3.5.4)$$

We observe that the left side of the equation is an analytic function in the upper k_x half plane ($\tau > \tau_-$) and that the right side is an analytic function in the lower k_x half plane. The equality stated in (3.5.4) holds in the domain ($\tau_- < \tau < \tau_+$). Therefore by analytic continuation we can assert that the two functions are analytic continuations for the upper and lower half plane of an entire function $P(k_x)$.

Consider the asymptotic behavior of $G_+(k_x)$ and $G_-(k_x)$ as $|k_x| \to \infty$. Clearly the integrals in the exponents vanish since k_x appears only in the denominator of the finite integral. Hence $G_+ \sim G_- \sim |k_x|^{\frac{1}{2}}$, and from the expressions for the decomposition functions, we see that the asymptotic behavior is as follows:

$$S_+(k_x) \text{ and } S_-(k_x) \sim |k_x|^{-1} \text{ as } |k_x| \to \infty. \qquad (3.5.5)$$

If we examine $\Phi(x) = e_z(x)$, we have from the edge condition that $\phi(x) \sim x^{\frac{1}{2}}$. It can be shown (Mittra and Lee(1971a)) that this implies $\Phi(k_x) \sim k_x^{-3/2}$. Therefore we have

$$P(k_x) = \Phi_- \cdot G_- - S_- \sim [(k_x^{-3/2})(k_x^{-1/2}) - k_x^{-1}] \to 0 \quad . \qquad (3.5.6)$$

We now have need of the asymptotic behavior of $B_+(k_x)$ which is essentially the Fourier transform of the difference current on the conducting

half-plane due to the edge. It can be shown that $B_+(k_x) \sim k_x^{\frac{1}{2}}$. Therefore we see that $P(k_x) \sim k_x^{-1}$ for $|k_x| \to \infty$ and hence $P(k_x) = 0$ for $|k_x| = \infty$.

We have shown that upon completion of the decomposition step we can create a bounded entire function $P(k_x)$. By Liouville's theorem we know that $P(k_x)$ is equal to a constant. However we know that $P(k_x) = 0$, hence within the strip of analyticity of the Wiener-Hopf problem we arrive at (2.4.6).

Therefore we obtain the following result for the transform of the total electric field over the aperture of the interface problem:

$$E_z(k_x) = -\frac{2}{k_0} \left[\frac{S_-(k_x)}{G_-(k_x)} \right] = \frac{\sqrt{2\pi}}{k_0} \ \xi \left[\frac{1}{(k_x + k_1 \cos\theta) \ G_-(k_x)} \right], \quad (3.5.7)$$

where
$$\xi = \left[\frac{-jE_0 \sin\theta}{\pi \ \eta_1 \ G_+(-k_1 \cos\theta)} \right].$$

CHAPTER IV

ASYMPTOTIC ANALYSIS OF THE INTERFACE PROBLEM

4.1 Fields in the Transmission Region (y < 0)

4.1.1 General Formulation

As a result of solving the Wiener-Hopf problem for the interface
geometry in Chapter III, we have determined the Fourier transform of the
total tangential electric field over the plane y = 0. From aperture the-
ory we know that this can be directly related to e_z anywhere in the tran-
smitted region (see Collin and Zucker (1969)). The electric field has
only the z component since the excitation is transverse magnetic to the
z direction.

Because the transform variable, k_x, is normalized to the free space
wavenumber $k_0 = \omega\sqrt{\mu_0 \cdot \varepsilon_0}$, it is necessary to normalize distance to free
space: $x = k_0 \cdot x' = (2\pi \cdot (\text{distance in wavelengths}))$ where x' is the unnor-
malized distance. This ensures that $k \cdot x = k' \cdot x'$, where the unprimed
quantities are normalized and the primed ones are not.

The total electric field e_z in the transmitted region may be con-
structed to be

$$e_z(x',y') = \frac{1}{\sqrt{2\pi}} \int_{k_x' = -\infty + jc'}^{\infty + jc'} E_z(k_x') \, e^{-j(\vec{k}' \cdot \vec{\rho}')} \, dk_x' \quad \text{for } y' < 0. \qquad (4.1.1)$$

55

where $k' = (k_x')\hat{x}-(k_y')\hat{y}$, $k_y' = \beta_2' = \sqrt{k_2'^2-k_x'^2}$, $\vec{\rho}' = (x')\hat{x}+(y')\hat{y}$.

Reverting to normalized parameters and substituting in $E_z(k_x)$ from (3.5.7), we have

$$e_z(x,y) = \xi \int_{k_x=-\infty+jc}^{\infty+jc} \frac{e^{-j(\beta_2 y+k_x x)}}{(k_x+k_1\cos\theta)G_-(k_x)} dk_x \quad \text{for } y < 0 , \quad (4.1.2)$$

where c places the inversion path in the strip of analyticity fixed in the Wiener-Hopf procedure, i.e. that of (3.3.10) with ξ given in (3.5.7).

Equation (4.1.2) is an exact field representation of the solution to the interface problem in the transmitted region. It is largely a formal result, however, since it manifests the computational formidability typical of inversions of continuous spectra. For diffraction computation, the asymptotic evaluation of (4.1.2) for large ρ is quite useful, however, and we turn our attention to this task.

The choice of the branch cut due to β_1 in $E_z(k_x)$ will not affect the convergence of the inversion integral (since β_1 does not occur in the exponential). The factor G_- contains cuts due to β_1 and β_2. Moving the semi-infinite cut for β_1 does not affect the convergence of the Fourier inversion integral since G_- does not have an exponential behavior. It is useful later to exercise this freedom in the asymptotic evaluation of (4.1.2). We can analytically continue $G_-(k_x)$ into the extended form with the semi-infinite hyperbolic branch cuts from $-k_1$ and $-k_2$ without affecting the integral or the convergence behavior at $|k_x| \to \infty$. In so doing we may expose a root of G_- which resides on the exposed portion of the lower sheet. Also the method for evaluating $G_-(k_x)$ in this region of

the k_x plane is to use $G_- = G/G_+$ where we use the original definition of $G(k_x)$. This continuation of G causes the integrand to have the hyperbolic branch cuts extending from $-k_1$ and $-k_2$ to ∞ in the second quadrant.

4.1.2 Angular Spectral Mapping

We now make use of the trigonometric substitution $k_x = k_2 \sin\alpha$, where α is a complex variable, to map the integral onto the α domain. Such a mapping is conventionally referred to as determining the angular spectral domain, α. The cuts become the lines in Figure 4.1 which are asymptotically vertical and pass through $\alpha = + \pi/2$ and $-\pi/2$. The lower sheet of the original plane is mapped into the regions indicated with crosshatching in Figure 4.1. The former two-sheeted plane of $\beta_2(k_x)$ thus becomes the periodic plane shown in Figure 4.1 with the role of the branch cuts replaced by lines which are their images . The effect of this mapping is to open up the function $\beta_2 = \sqrt{k_2^2 - k_x^2}$, and fix a saddle point in the integral which may be used in a steepest descent analysis. Substituting $k_x = k_2 \sin\alpha$, $x = \rho \cos\phi$, $y = \rho \sin\phi$ for $-\pi < \phi < 0$ into (4.1.2), we obtain

$$e_z(\rho,\phi) = \xi \int_\Gamma \frac{k_2 \cos\alpha}{G_-(k_2\sin\alpha) \cdot (k_2\sin\alpha + k_1\cos\theta)} e^{-j(k_2\rho) \cdot \sin(\alpha-\phi)} \, d\alpha,$$

$$(4.1.3)$$

where Γ is the mapping of the integration path with k_x on $(-\infty+jc, +\infty+jc)$.

In Figure 4.1 is shown the portion of the complex α plane which is
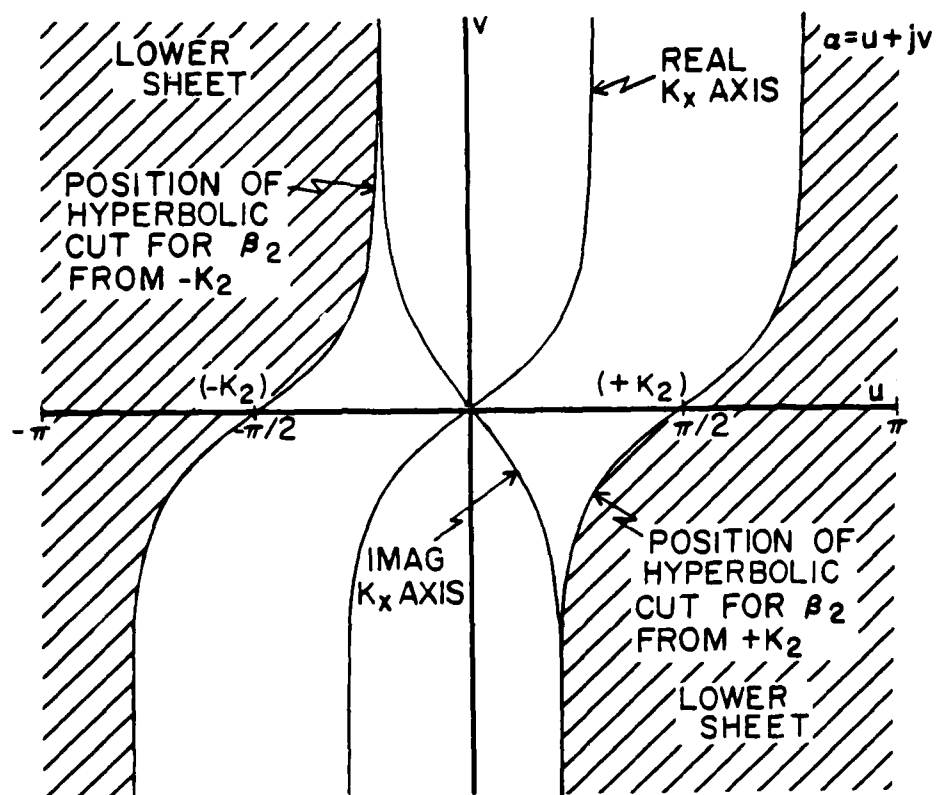
Figure 4.1. The angular spectral plane, $k_x = k_2 \sin \alpha$.

of interest and the position of several key features of the k_x plane.
For simplicity and definiteness we take the inversion path to be the real
k_x axis (this is correct for $0 < \theta < \pi/2$). A discussion of the equations
for various α plane contours of interest is given in Appendix A. As not-
ed above, the boundary of the top sheet in the k_x plane, which is defined
by the branch cuts of β_2, corresponds in the α plane to the curve repre-
senting the image of the real k_x axis moved to intersect the real α axis
at $\alpha = \pm \pi/2$ (see Figure 4.1).

The next stage in the asymptotic analysis of e_z is to deform the
integration path to the steepest descent path (SDP) through the saddle
point. In the process of deforming to the SDP, singularities of the
integrand may be crossed and must be considered separately. The saddle
point is characterized as a point in the α plane at which the derivative
ot the exponent vanishes.

$$\frac{d}{d\alpha_s} [-j\ k_2\ \rho \sin(\alpha_s-\phi)] = -j\ k_2 \rho \cos(\alpha_s-\phi) = 0 \qquad (4.1.4)$$

$$\alpha_s = \phi + \frac{n\pi}{2}, n \text{ is an integer (only } n = 1 \text{ is of interest).}$$

Note that as the angle of observation moves from $\phi = 0$ (on the lower edge
of the PEC half-plane) to $\phi = -\pi$ (on the lower edge of the interface aper-
ture), the saddle point moves from $\alpha = \pi/2$ to $\alpha = -\pi/2$. The shape of SDP
is a function of $(\alpha-\phi)$ and hence of $(\alpha-\alpha_s)$, therefore it is unaffected
as the observation angle changes. That is, the SDP's shape is fixed for
a specific problem but its position moves so that it crosses the real α

axis at α_s. Therefore, once the curve of the SDP is found, only the region of the α plane between the integration path and the SDP need be examined for singularities of the integrand. Hence a graphical procedure can be used to locate the dominant contributors to the far field.

The total field is represented, after deformation of Γ to the SDP, as the sum of an integral along the SDP and the singularity contributions swept during the deformation. For $|k_2\rho| \rightarrow \infty$, the SDP contribution is asymptotic to a term containing the value of the integrand of (4.1.3) at the saddle point. The contributors to the far field are the following:

1. <u>SDP integral contribution</u> — Present in all cases and is equivalent to the diffracted ray for the half-plane in a homogeneous region,

2. <u>Pole due to the root of $(k_2\sin\alpha+k_1\cos\theta)$</u> — Contributes when swept and is the counterpart to the geometrical optics field in the homogeneous half-plane problem,

3. <u>Pole due to the root of G_-</u> — Contributes if crossed in the deformation to the SDP,

4. <u>Branch point of G_- at $k_x=-k_1$</u> — Contributes when swept and denotes a term arising from the presence of the semi-infinite opposing half space which is filled with a contrasting medium.

All the singularity contributions are functionally characterized by the integrand evaluated at the singularity position in the α plane :

$$e_z = (e_z)_{\substack{\text{saddle} \\ \text{point}}} + (e_z)_{\substack{\text{g.o.} \\ \text{pole}}} + (e_z)_{\substack{\beta_1 \\ \text{branch} \\ \text{cut}}} + (e_z)_{\substack{\text{root} \\ \text{of } G_-}} \quad (4.1.5)$$

When the terms of (4.1.5) are evaluated asymptotically, they exhibit an exponential behavior which is determined by the position of each contributor in the α plane. It is useful to determine what region of the α plane will correspond to outwardly decaying waves (and therefore, physical ones). Clearly these waves have the real part of the exponent less than zero,

$$\text{Re}[-j \, k_2 \, \sin(\alpha-\phi)] = -k_{2i}\sin(u-\phi)\cosh v + k_{2r}\cos(u-\phi)\sinh v \quad (4.1.6)$$

where $\alpha = u+jv$ and $k_2 = k_{2r} - jk_{2i}$. Therefore the boundary of the α plane corresponding to physical waves has

$$k_{2i} \, \tan(u - \phi) = k_{2r} \, \tanh(v). \quad (4.1.7)$$

We observe that the mapping of the real k_x axis into the α plane is given by: $k_{2i} \, \tan(u) = k_{2r} \, \tanh(v)$. Hence the boundaries of physical waves are given by the real k_x axis mapping shifted to the position $u = \phi$ and $u = \phi + \pi$ (the region from $\pi/2$ to the left of the saddle point over to $\pi/2$ to the right of the saddle point).

If the inversion path Γ is the mapping of the real k_x axis (which is permissible if $0 < \theta < \pi/2$), then we are guaranteed that only

singularities for decaying waves can be crossed for all observation angles $-\pi < \phi < 0$. See Figure 4.2 for the case $\phi = -\pi$ (maximum negative position of the saddle point). On the other hand, if $\pi/2 < \theta < \pi$, then the integration path in the k_x plane must be below the real axis and map into a curve to the right of the mapping of the real axis. Because the path lies to the right of the mapped real axis, as $\phi \to -\pi$ it is possible to sweep a region between the real axis mapping and the path of integration which causes non-decaying components. However we observe that there are no zeros of $G(\alpha)$ in this region of the α plane. Hence the only possible singularity is the pole at $(k_2 \sin\alpha + k_1 \cos\theta) = 0$. Though it appears to be anomalous that a field contributor can become unbounded as one moves to an infinite distance from the diffracting edge of the half-plane, this can occur and is interpreted as follows. For $\pi/2 < \theta$, the incident field along the interface becomes unbounded as $x \to -\infty$. For $\phi < \phi_0$ (which is the angle that the refracted wavefront makes with the half-plane), the observation direction cuts across planes of growing amplitude as $\rho \to \infty$. Therefore this nonphysical behavior of the pole is due to the fact that a plane wave in a lossy medium does, in fact, correspond to a wave which decays as it propagates in from $\rho = \infty$. We note that the pole arising from the root of $(k_2 \sin\alpha + k_1 \cos\theta = 0)$ corresponds to the geometrical optics pole in the half-plane diffraction problem in homogeneous space and gives rise to the simple transmitted field for the unobscured portion of the half space below the interface. It is therefore clear that, with the exception of the geometrical optics field, this problem can only give rise to decaying, outgoing fields in the transmitted region.
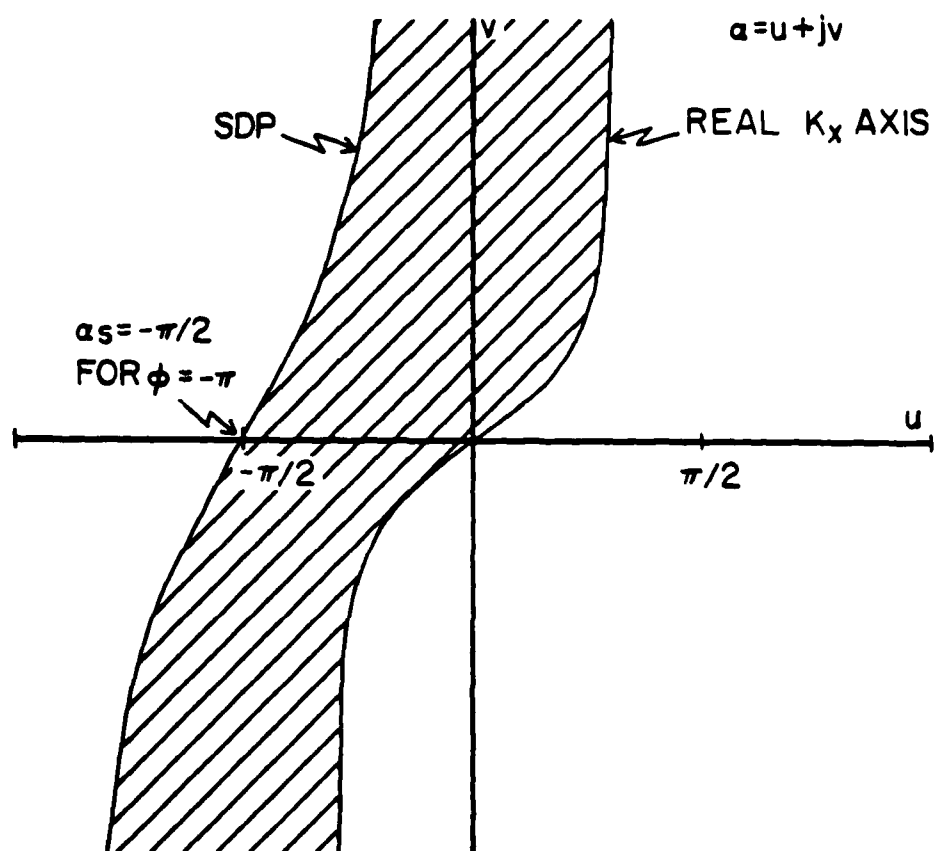
Figure 4.2. Region swept in the deformation to the steepest descent path through $\alpha_s = -\pi/2$.

4.1.3 Identification of Asymptotically Dominant Singularities

In diffraction problems where the media are lossless, the exponential behavior of dominant field contributors is that of a propagating wave and the asymptotically dominant field terms are identified based on the exponential decay of the non-propagating factor. The presence of material loss introduces a new complexity in that all of the singularities are complex-valued and exponential decay occurs concomitantly with propagation. We therefore must identify relative rates of this exponential decay for the various contributors and identify the dominant terms.

Since all observation angles contain the diffracted field due to the steepest descent integral, it is useful in the spirit of the above analysis to compare the exponential decay of swept singularity waves to that of the SDP diffraction wave as one moves radially away from the edge of the PEC screen. Saddle point analysis allows an asymptotic approximation of the SDP integral to be made for $\rho \rightarrow \infty$ (see Appendix B) yielding

$$[e_z]_{\substack{\text{saddle} \\ \text{point}}} \quad \frac{-j\sqrt{\frac{2}{\pi}}\, E_0 k_{ob} \sin\theta \sin|\phi| \sqrt{\dfrac{-1}{j(k_{ob}\rho)}}^{PV}}{\eta_1 G_+(-k_1\cos\theta) G_+(-k_{ob}\cos\phi)(k_{ob}\cos\phi + k_1\cos\theta)}\, e^{-jk_{ob}\rho} ,$$

(4.1.8)

where $\sqrt{}^{PV}$ is the principal value, and $k_{ob} = k_2$. Note that this is the leading term in the asymptotic expansion of the saddlepoint integral and represents the contribution to the radiation field (varies as $\rho^{-1/2}$) of that integral. For observation angles in the vicinity of the

interface, the dominant contribution is a lateral wave type field (varies as $\rho^{-3/2}$) and the relative significance of these two fields is discussed in Appendix B.

The dominant far field contributor (or contributors) is determined by identifying regions in the α plane which have greater or lesser exponential decay than Re $(-jk_2\rho)$. For $\phi = 0$, this region is bounded by a contour defined by

$$\text{Re}[-jk_2\sin(\alpha-\phi)] = -k_{2i}$$

$$- k_{2i}\sin u \cdot \cosh v + k_{2r}\cos u \cdot \sinh v = -k_{2i} \tag{4.1.9}$$

where $\alpha = u+j\,v$. After algebraic manipulations we have

$$\sinh v = \left[\frac{1 \pm \cos|u'| \cdot \sqrt{1 + \left(\dfrac{k_{2i}}{k_{2r}}\right)^2}}{\left(\dfrac{k_{2r}}{k_{2i}}\sin^2 u' - \dfrac{k_{2i}}{k_{2r}}\cos^2 u'\right)} \right] \sin u' \,, \tag{4.1.10}$$

where $u' = (u-u_s)$, u_s is the position of the saddle point. Note the following properties:

   Use (+) for the $(v > 0)$ leg (bounded by $- (\pi-u_{res}) \le u' \le (\pi-u_{res})$)

   Use (-) for the $(v < 0)$ leg (bounded by $-u_{res} \le u' \le u_{res}$ where

        $u_{res} = \tan^{-1}(k_{2i}/k_{2r})$, principal value).

The double sign on the square root reflects the fact that there are two curves in the α plane on which the exponential decay is the same as that of the saddle point contribution.

A typical plot of the equal decay contours derived above is shown in Figure 4.3. It is seen that these contours divide the α plane into four regions in which the exponential decay is either greater than that at the saddle point or less than it. Clearly the SDP will lie in the two regions of greater decay and therefore identify them. Several observations are appropriate. While the expression for the equal decay curves was derived for $\phi = 0$, it applies for any ϕ with u replaced by $(u - \phi)$ in (4.1.9). These curves cross the real α axis at the saddle point just as the SDP does and therefore the entire set of curves (SDP, equal decay contours) can be considered a template which slides across the α plane as ϕ moves from 0 to $-\pi$. We refer to this collection of curves as the dominance template.

The foregoing analysis allows the determination of the most significant contributors in a particular problem for any specific angle of observation. Most of the α plane lies in the region of greater decay than the saddle point value and hence any singularities occurring there can be ignored since the greater exponential decay implies asymptotic insignificance as $\rho \to \infty$. On the other hand, if a singularity lies in the region of lesser decay, then the saddle point value can be ignored. Only the dominant contribution needs to be considered asymptotically in the far field, therefore this analysis of the significance of the various contributors is fundamental to the problem for observation points which are far removed from the edge of the PEC half-plane. Note that the equal decay contours are functions only of k_2 and do not involve k_1.
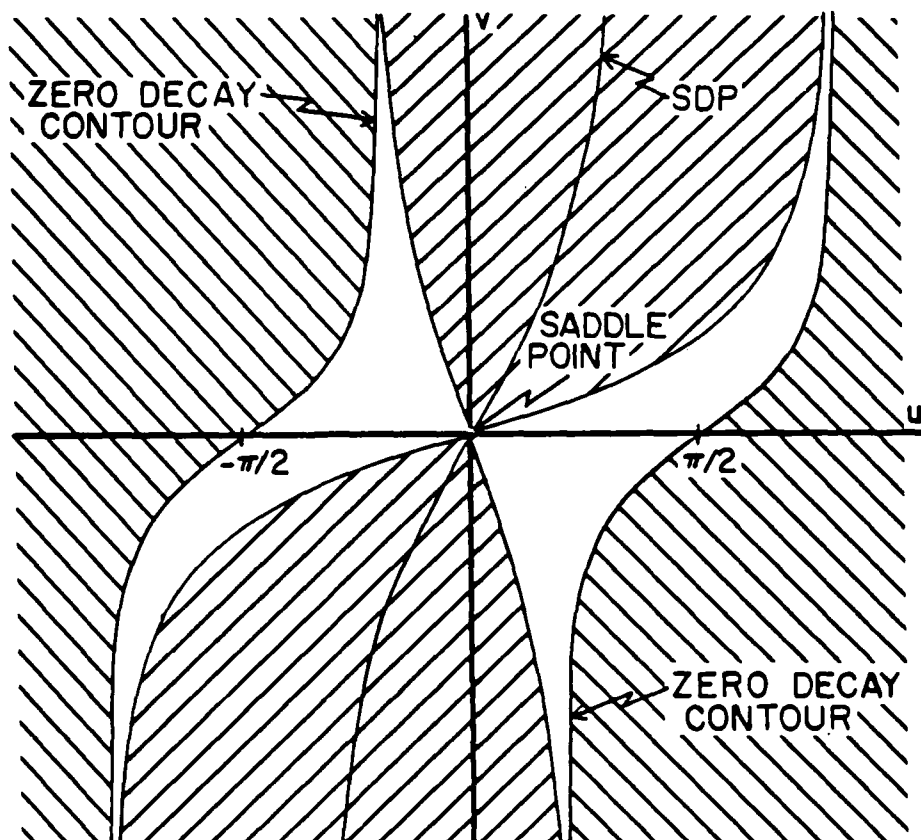
Region containing singularities which represent waves with exponential growth, non-physical

Region containing singularities which represent waves with greater exponential decay than the saddle point

Region containing singularities which represent waves with less exponential decay than the saddle point

Figure 4.3. Demarcation of regions in the α plane about the saddle point characterizing the exponential decay rate of waves associated with singularity locations. (Dominance contours).

As $k_{2i} \to 0$ (medium 2 becomes lossless), one equal decay contour coincides with the real α axis in the vicinity of the saddle point. Thus, in the lossless case, the geometrical optics pole and the diffracted (saddle point) contribution manifest the same exponential decay rates, i.e. no decay. For lossy media the two contributions will not be of the same asymptotic order since the exponential decay rates will be different. For $k_{2i} \ll k_{2r}$ the region of exponential dominance over the saddle point contribution collapses to a narrowly defined region. Then it is approximately true that any singularity off the real α axis can be ignored. However as k_{2i} increases, this is not valid and the significance of the various regions of the α plane must be considered.

Another interesting question is to determine what portion of the plane gives rise to outgoing waves and what portion gives rise to incoming waves. These regions are separated by lines of zero phase given by

$$\text{Im}[-jk_2\sin(\alpha-\phi)] = -k_{2r}\sin(u-\phi)\cosh v - k_{2i}\cos(u-\phi)\sinh v = 0 \quad (4.1.11)$$

or for $\phi = 0$

$$\tanh v = -\frac{k_{2r}}{k_{2i}} \tan u \quad . \quad\quad (4.1.12)$$

This is the equation for the mapping of the imaginary k_x axis onto the α plane and, in particular, it describes two loci shifted so that they intersect the real α axis at $u = u_s \pm \pi/2$ where u_s is the saddle point location. The region between these two lines has a negative phase change as ρ increases (outgoing wave) while the region outside of these lines

has a positive phase change (incoming wave). This wave interpretation can be incorporated into the dominance template discussed above as shown in Figure 4.4.

Diffracted waves must manifest the phase progression of outgoing waves only. Incoming waves are excluded in the solution process due to the fact that the swept region characterized by incoming waves cannot contain singularities. For example, Figure 4.5 shows the largest region swept between the real axis and the SDP for $\phi = 0$ that violate outgoing wave behavior. A similar plot can be made for $\phi = -\pi$ with the saddle point at $\alpha_s = -\pi/2$. It is clear that the swept regions of outgoing waves in these extreme cases lie in the mappings of the first and third quadrants of the original k_x plane. There are no singularities of the interface problem occurring in those quadrants.

Summarizing these results, we see that given a specific complex medium, k_2, one can construct a dominance template which centers on the saddle point and divides the α plane into quadrants of exponential growth or decay relative to the diffraction term of the saddle point contribution. The dominant contribution can be determined graphically (or by simple algorithms on the computer). Since the only possible scattered waves are decaying, outgoing waves, one can infer that no singularities arise in regions of the α plane which would violate this property.

The contribution of the geometrical optics pole which arises from the factor $(k_2\sin\alpha + k_1\cos\theta)$ in the denominator of the inversion integral is given as follows (see Appendix B):

Region containing singularities which represent outwardly
propagating waves

Region containing singularities which represent inwardly
propagating waves
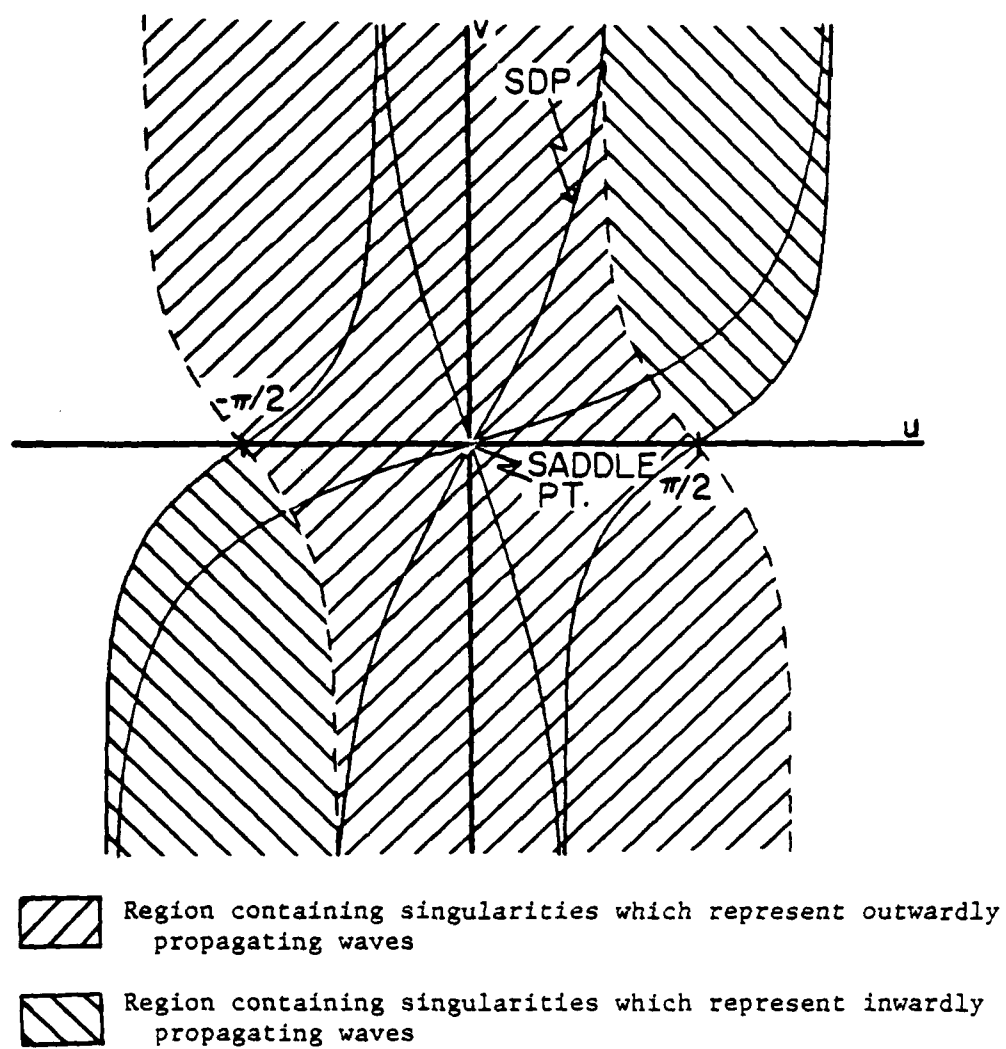
Figure 4.4.   Dominance contours supplemented with phase behavior.
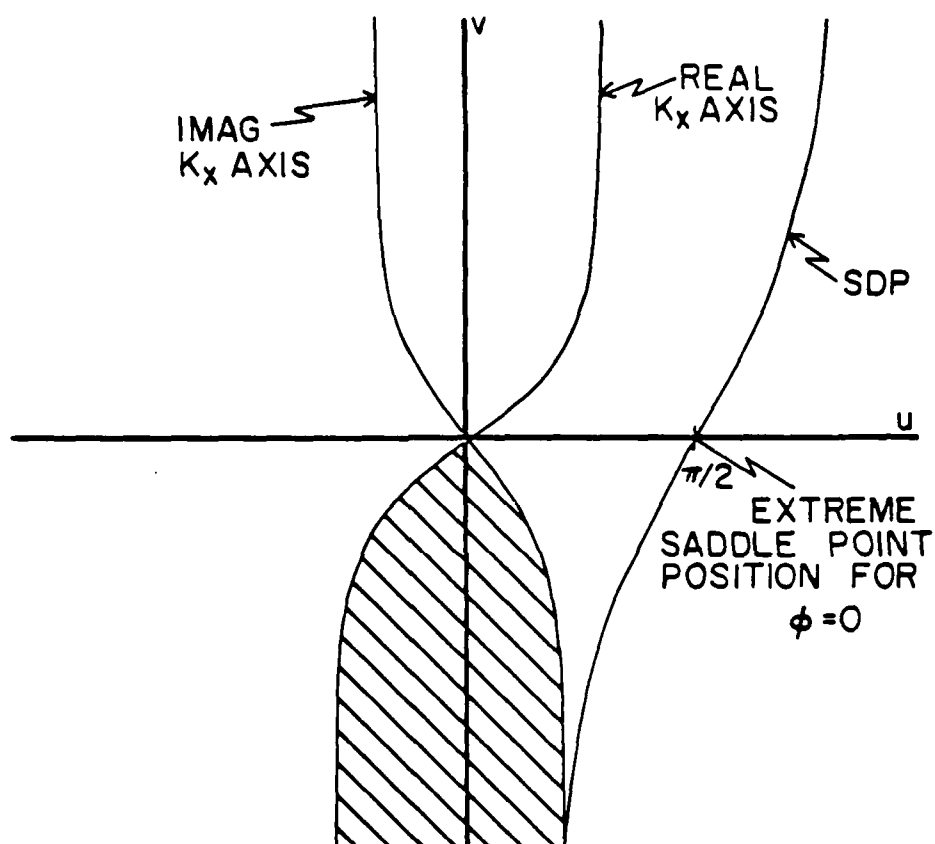
Region containing singularities which represent inwardly
propagating waves

Figure 4.5. Example of the integration path deformation to the
steepest descent path through $u = \tau/2$.

$$[e_z]_{\substack{\text{geom.} \\ \text{optics} \\ \text{pole}}} = \frac{2E_0\sin\theta}{\eta_1 G(-k_1\cos\theta)} e^{-j(k_{ob}\rho)} \sin(\alpha_r + |\phi|) , \qquad (4.1.13)$$

where α_r is the pole location and $k_{ob} = k_2$, $G(\alpha) = (3.4.1)$.

Also the contribution at the root of $G_-(\alpha)$ is given as follows (see Appendix B):

$$[e_z]_{\substack{\text{root} \\ \text{of } G_-}} = \left[\frac{2E_0\sin\theta}{\eta_1 G_+(-k_1\cos\theta)}\right]\left[\frac{G_+(k_{ob}\sin\alpha_r)}{(k_{ob}\sin\alpha_r + k_1\cos\theta)G'(k_{ob}\sin\alpha_r)}\right]$$

$$\times e^{-j(k_{ob}\rho)} \sin(\alpha_r + |\phi|) , \qquad (4.1.14)$$

where α_r is the root location, $k_{ob} = k_2$, $\mu_{ob} = \mu_2$, $\mu_{opp} = \mu_1$,

and

$$G'(\alpha_r) = \left[\frac{\mu_{ob}^2 - \mu_{opp}^2}{\mu_{ob}\mu_{opp}^2}\right]\tan\alpha_r .$$

Note that when $\mu_1 = \mu_2$ no root of G_- occurs (see (3.4.4)).

4.1.4 Branch Cut Contribution

In order to consider the evaluation of the branch cut contribution, it is necessary to review (4.1.8,13,14) and consider how the function $G_+(\alpha)$ is to be evaluated. From (3.4.17), we observe that the factor $\sqrt{k_1 - k_x}$ exhibits a simple square root branch cut running from $k_x = k_1$, while the exponential factor has a branch cut running from k_1 to k_2. As noted in section 3.4, the factor $G_2(k_x)$ (which factorizes positively into

the exponential in (3.4.17)) is a two-sheeted function; and if the β_1 and β_2 cuts are chosen to coincide, they can be viewed as annihilating each another, resulting in a finite branch cut. If the β_1 and β_2 branch cuts of $G_2^+(k_x)$ are allowed to separate, we can view the process as evolving as shown in Figure 4.6. If the result shown in Figure 4.6c is combined with $G_1^+(k_x)$, the derived value of $G_+(k_x)$ uses the simple hyperbolic values for β_1 and β_2. However it is difficult to see how to perform this continuation in light of the integral factorization available in (3.4.17). The simplest procedure is to view $G_+(k_x)$ as follows:

$$G_+(k_x) = \begin{cases} (3.4.18); \text{for } Im(k_x)>0 \text{ or if } Im(k_x)=0, \text{ then } Re(k_x)\leq 0 \\ \\ G(k_x)/G_-(k_x) = G(k_x)/G_+(-k_x); \text{otherwise} \end{cases} \qquad (4.1.15)$$

$$\text{where } G(k_x)=(3.4.1) \text{ and } G_+(-k_x)=(3.4.18)$$

Here we are assuming that the branch cuts for β_1 and β_2 do not cross the real k_x axis. Observe that $G_+(-k_x)$ is unambiguously given by the integral factorization formula for k_x in the lower half of the complex k_x plane. The branch cut behavior is contained in the factor $G(k_x)$ and can be dealt with conveniently in this form since the effect of shifting the branch cuts is manifest directly in $G(k_x)$ as the functions β_1 and β_2 .

It is useful to recognize this method of evaluating $G_+(k_x)$ since in the process of evaluating the branch cut contribution to the radiation integral (4.1.3), it is necessary to deform the β_1 branch cut and the various singularity contributors can be swept by the branch cut. When a contributor is swept, the evaluation procedure given in (4.1.15)
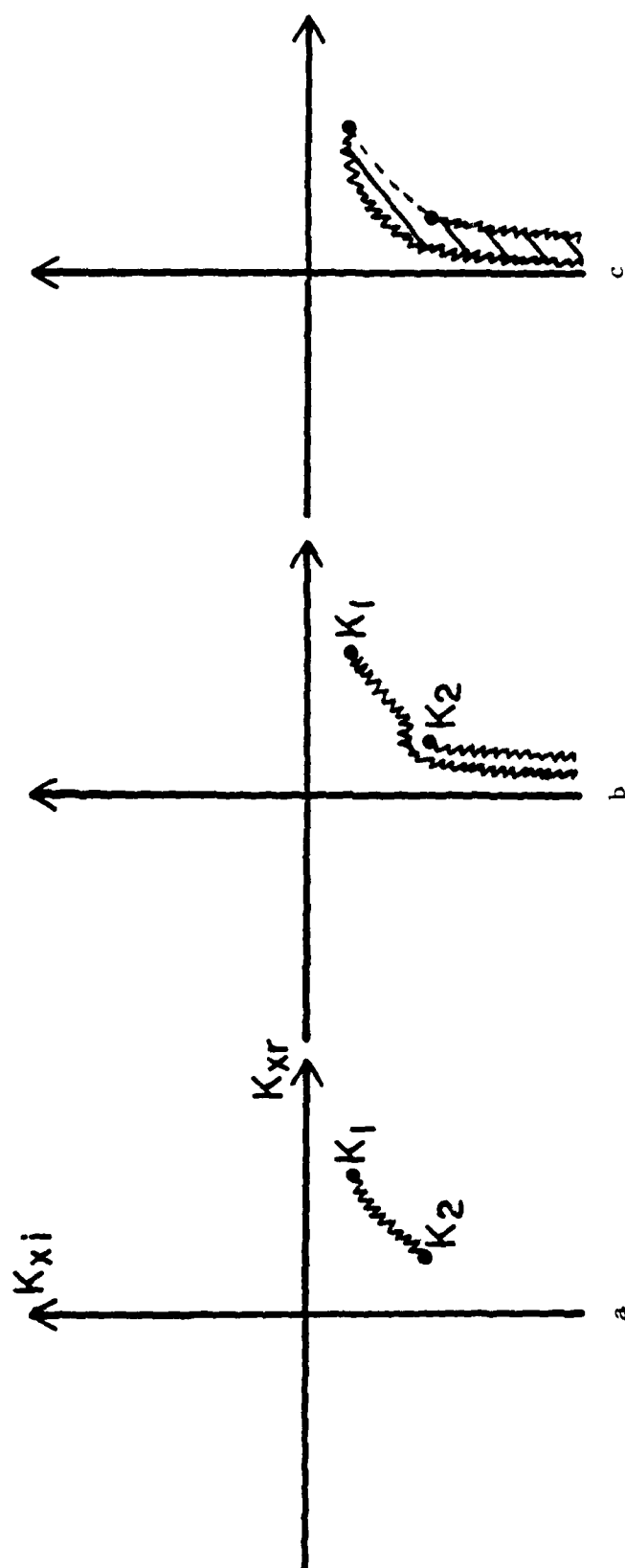
Figure 4.6. Deformation of the branch cuts of G_2^+.

allows the factor β_1 given in $G(k_x)$ to be easily determined.

The development of the asymptotic formula for the branch cut contribution for $k_x = -k_1$ follows the analysis of Felsen and Marcuvitz (1973a). It requires that the branch cut from $k_x = -k_1$ be deformed in the α plane so that it lies along the steepest descent path (SDP_b) from the branch point. It must be emphasized that the SDP_b changes as the saddle point moves. The locus along which the SDP_b lies is a line of constant phase of the exponential and points on this line have the greatest possible change in the magnitude of the exponential factor. Hence these lines are contours in the α plane where (4.1.11) equals a constant $\gamma \leq 0$. Figure 4.7 shows such a set of phase contours in the α plane. Clearly these phase contours move with the saddle point (since $\gamma = -k_{2r}$ corresponds to the SDP). Hence the SDP_b, which must lie on the phase contour running through the branch point corresponding to $k_x = -k_1$ and be asymptotic to the SDP through the saddle point, changes continuously as the saddle point moves with varying observation angles. A detailed discussion of the formulas describing these SDP_b contours and the effect on the other asymptotic contributors is given in Appendix C. We summarize below the conclusions given there.

In deforming the branch cut in the α plane for the branch point corresponding to $(-k_1)$ to a line along the SDP_b, we may be forced to cross a singularity contributor, α_x. The result is that the value of $\beta_1(\alpha_x)$ which we must use in the asymptotic formulas is given by

$$(\beta_1(\alpha_x))_{swept} = -(\beta_1(\alpha_x))_{original\ hyperbolic\ definition}.$$
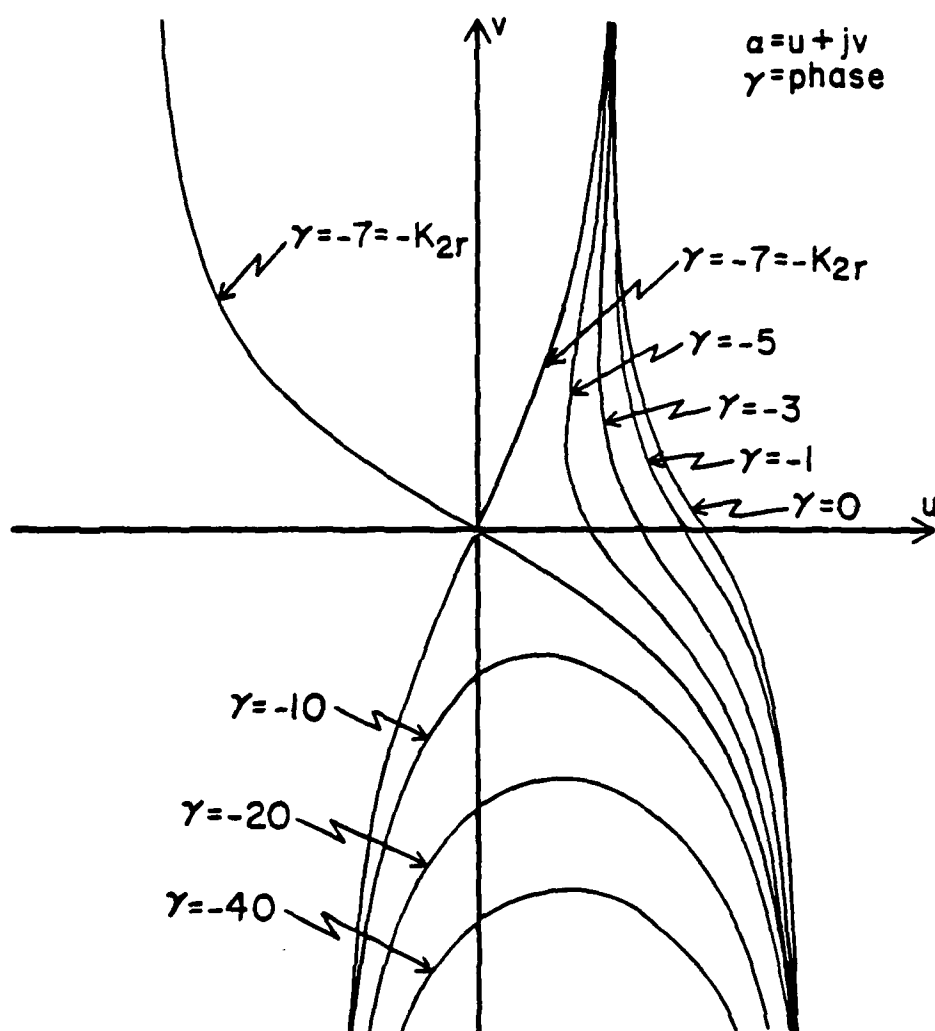
Figure 4.7. Contours of constant phase in the α plane about the saddle point location.

Looking at the asymptotic formulas (4.1.8,14) we see that $G_+(-k_1\cos\theta)$ must be evaluated. One of the results of Appendix C is that the geometrical optics pole for an observation point in the transmission region ($y < 0$) is never swept by the β_1 branch cut. Hence $G_+(-k_1\cos\theta)$ may be evaluated in all cases using the original definition of β_1 (Section 2.2). Also, in the process of deforming the branch cut for β_1 to the SDP_b configuration, a portion of the lower sheet of $G_-(\alpha)$ is brought onto the top sheet. This may result in the root of $G_-(\alpha)$ being brought onto the top sheet, a detail which is dealt with in Appendix C.

Having performed this deformation we observe that when the branch point is crossed, the entire cut is crossed. The branch cut contribution is now amenable to an asymptotic analysis somewhat similar to the usual steepest descent analysis about the saddle point. The rather complicated result is stated below:

$$
[e_z]_{\substack{\text{branch} \\ \text{cut,} \\ -k_{opp}}} \sim \frac{\xi\,\mu_{ob}^2\,G_+(-k_{opp})\sqrt{2\pi k_{opp}}^{PV}\,\exp\left[j\,\dfrac{3\theta_+}{2}\right]}{\mu_{opp}(k_{opp}-k_1\cos\theta)\sqrt{k_{ob}\cos\alpha_b}^{PV}\,|k_{ob}\rho\cos(\alpha_b+|\phi|)|^{3/2}}
$$

$$
\times\,e^{-j(k_{ob}\rho)\,\sin(\alpha_b+|\phi|)}\,,
\tag{4.1.16}
$$

where $(k_{ob}, \mu_{ob}) = (k_2, \mu_2)$; $(k_{opp}, \mu_{opp}) = (k_1, \mu_1)$; $\sqrt{}^{PV}$ is the principal value; θ_+ is the angle of the SDP_b from α_b (corresponds to $k_x = -k_{opp}$) in the α plane relative to a ray from α_b in the positive real direction, where $\theta_+ > [\mathrm{Arg}(k_{opp})-\mathrm{Arg}(k_{ob}\cos(\alpha_b))]$, modulo 2π (that is, if

$[\text{Arg}(k_{opp}) - \text{Arg}(k_{ob} \cdot \cos(\alpha_b))] = \theta_g$, then $\theta_g < \theta_+ < \theta_g + 2\pi$).

4.1.5 Uniform Asymptotic Expansion

In general the wavenumbers for the two media involved in the inter-face problem have *different loss tangents* and as a result will not lie on a common line in the k_x plane running through the origin. One expects that the geometrical optics pole will lie on a curve in the α plane which only intersects the saddle point locus at the origin. As a result the asymptotic expansion of the radiation integral given in (4.1.8) is an adequate representation for observation point sufficiently removed from the edge of the PEC half-plane.

In practice one would like to have an asymptotic form which is applicable at smaller radii. This necessitates utilizing a uniform asymptotic expansion of the steepest descent integral. The resulting expression is given as follows:

$$[e_z]_{\substack{\text{saddle} \\ \text{point,} \\ \text{g.o. pole}}} = \left[-j\sqrt{\frac{2}{\pi\rho}} \, \frac{E_0 \sin\theta}{\eta_1} e^{-jk_{ob}z} \right] \times$$

$$\left\{ -\frac{1}{\sqrt{-jk_{ob}}}^{PV} \frac{k_{ob} \cdot \sin|\phi|}{G_+(-k_{ob}\cos\theta) \cdot G_+(-k_1\cos\theta) \cdot (k_{ob}\cos\theta + k_1\cos\theta)} \right.$$

$$(4.1.17)$$

$$+ \left[\frac{1}{\sqrt{-jk_{ob}}}^{PV} \frac{1}{2 \cdot G(k_1\cos\theta) \cdot \sin\left(\frac{\alpha_p - \alpha_s}{2}\right)} \right.$$

$$\left. \pm j \, \frac{\sqrt{2\rho} \; e^{j2k_{ob}\rho\sin^2\left(\frac{\alpha_p - \alpha_s}{2}\right)}}{G(k_1\cos\theta)} \times \right.$$

$$\left. \left. Q\left[\mp j\sqrt{-j2k_{ob}\rho}^{\,PV}\sin\left(\frac{\alpha_p - \alpha_s}{2}\right) \right] \right] \right\}$$

for $\text{Im}\left[\sqrt{-j2k_{ob}}^{PV} \cdot \sin((\alpha_p - \alpha_s)/2) \right] \lessgtr 0$, where $k_{ob} = k_2$, α_s is the saddle point location in the α plane and α_p is the geometrical optics pole location, $Q(y)$ is the complementary error function defined by

$$Q(y) = \int\limits_y^\infty e^{-x^2} dx \qquad (4.1.17.a)$$

The first term in the braces in (4.1.17) is the original non-uniform expanson contribution (4.1.8).

4.1.6 Remarks Concerning the Asymptotic Analysis

It is clear from the form of these asymptotic constituents to the far field that their exponential factors depend on the location of the singularities causing them as stated earlier regarding the dominance analysis of the various contributors. Extreme care must be exercised in this analysis to determine whether or not the root of $G_{-}(\alpha)$ occurs on the top sheet of the integrand used for the asymptotic analysis. The expression for the saddle point contribution given in (4.1.8) is the non-uniform asymptotic version where no singularities are assumed to lie in the vicinity of the saddle point. For the transmitted region (as long as k_2/k_1 is not purely real) this is the case. In the homogeneous half-plane problem, the geometrical optics pole (a function of θ, the angle of incidence) lies on the real α axis between $(-\pi/2, \pi/2)$. Therefore as the observation angle ϕ approaches the shadow boundary (which is in the transmission region), the saddle point expansion becomes unbounded due to the breakdown of the asymptotic analysis. To avoid this singular behavior, several uniform asymptotic expansions are available for a pole in the vicinity of the saddle point. However, in the interface problem when k_2/k_1 , the contrast ratio of the media, has a significant imaginary part relative to the real part, then the geometrical optics pole follows a locus as a function of θ(the angle of incidence) which is off the real α axis and crosses it at $\alpha = 0$. Nonetheless, a uniform asymptotic expansion is given in (4.1.17) to allow a more accurate evaluation of the saddle point contribution for small observation radius.

An interesting physical interpretation can be given to the smooth behavior of the steepest descent integral when the observation angle brings the saddle point near the geometrical optics pole (Felsen(1982)). In the well-understood problem of diffraction by a half-plane residing in a homogeneous medium, the singular behavior of the saddle point contribution (diffracted wave) in the vicinity of the boundary between the region lit by the incident wave and that shadowed by the half-plane (hence, the shadow boundary) clearly indicates the physical importance of the shadow boundary. Therefore, the fact that the contribution of the diffracted term is well-behaved for distant observation points near the position of the shadow boundary in the interface problem means that the complex contrast ratio causes a "smearing" of the shadow boundary into a smooth transition from the lit space to the shadowed space. This is true except for the case of normal incidence when the geometrical optics pole is located at $\alpha = 0$. Therefore the complexity of uniform asymptotic analysis is not warranted in the transmission region for distant points of observation. Equations describing the locus of the geometrical optics pole are given in Appendix A.

It is important to realize that in some problems where the medium of the transmitted region is significantly lossy, it is quite possible for the diffraction term arising from the saddle point to be dominated by one of the terms arising from the singularities mentioned for some observation angles. It is not possible to discard these field constituents until the problem is specified and the positions of the singularities

is determined. The saddle point contribution is a homogeneous cylindrical wave which appears to emanate from the edge of the PEC half-plane. The other waves are, in fact, inhomogeneous plane waves which exist in a region bounded by a ray (extending from the edge of the PEC at a critical angle) and the interface plane and do not appear to come from the edge. This can be seen by considering the exponential

$$e^{-j(k_2\rho)\sin(\alpha-\phi)}$$

where ρ is the normalized distance from the edge, ϕ is the observation angle ($-\pi < \phi < 0$) and α is the position of the mode singularity. Considering the constant phase planes, we have the following:

$$\text{Im}[-j(k_2\rho)\,\sin(\alpha-\phi)] = \text{Im}[\,jk_y y - jk_x x] = [k_{yr}y - \sigma x] = 0 \qquad (4.1.18)$$

where $k_x = k_2\sin\alpha = \sigma+j\tau$ and $k_2 = k_{2r}-jk_{2i}; k_{2r},k_{2i}\geq 0$. Recognizing that the direction which is normal to a constant phase plane (given by θ_p) is characterized by $\tan\theta_p = 1/(-dy/dx) = -k_{yr}/\sigma$, we have

$$\tan\theta_p = \frac{k_{2i}\tan u \cdot \tanh v - k_{2r}}{k_{2i}\tanh v + k_{2r}\tan u} \qquad , \qquad (4.1.19)$$

where $\alpha = u+jv$, θ_p is the apparent angle of phase progression relative to the interface ($\theta_p = 0$ is the positive x direction) and does not refer to the edge of the half-plane.

A similar derivation for the constant amplitude planes, ignoring algebraic decay, leads to an angle θ_a of apparent maximum decay:

$$\tan \theta_a = \frac{k_{2r}\tan u \cdot \tanh v + k_{2i}}{k_{2r}\tanh v + k_{2i}\tan u} \quad . \tag{4.1.20}$$

It is clear from these expressions that, in general $\theta_a \neq \theta_p$. If k_2 is taken as lossless ($k_{2i} = 0$), it is apparent that the two directions are normal to each other, the usual property of inhomogeneous plane waves in a lossless medium.

4.2 Solution in the Reflection Region (y > 0)

From the solution of the Wiener-Hopf equation we have the Fourier transform for the total electric field along the interface. An expedient way of constructing the solution in the upper half space is to consider the total field as composed of three terms: the incident field, the short circuit reflected field, and the field due to the scattering from the interface structures. The sum of the incident field and the short circuit reflected field has a null at the interface by definition. If we now include that field which gives the correct tangential electric field on the interface, then the solution is complete. The field which we must construct below is the field due to e_z on the interface. This is simply the field in the aperture radiating into the upper region. Therefore the inversion integral is closely related to that for the transmission region,

$$e_z(x,y) = \xi \int_{k_x=-\infty+jc}^{\infty+jc} \frac{1}{(k_x+k_1\cos\theta) \cdot G_-(k_x)} e^{-j(\beta_1 y + k_x x)} dk_x \tag{4.2.1}$$

for $y > 0$ where c is in the strip of analyticity of the Wiener-Hopf formulation and where

$$\xi = \frac{-jE_0\sin\theta}{\pi \eta_1 G_+(-k_1\cos\theta)}$$

and

$$\beta_1 = \sqrt{k_1^2 - k_x^2}$$

At this point the mapping $k_x = k_1\sin\alpha$ is used and the resulting equation is found to be

$$e_z(\rho,\phi) = \xi\int_\Gamma \frac{k_1\cos\alpha}{G_-(k_1\sin\alpha) \cdot (k_1\sin\alpha + k_1\cos\theta)} e^{-j(k_1\rho)\sin(\alpha+\phi)} d\alpha \quad , \quad (4.2.2)$$

where $0 < \phi < \pi$.

The analysis follows in the same way as in the transmitted case. The asymptotic forms there are valid here also if (k_{ob}, μ_{ob}) are taken as (k_1, μ_1) and (k_{opp}, μ_{opp}) are taken as (k_2, μ_2). We observe that the saddle point is now given by $\alpha_s = \pi/2 - \phi$, so that we may take $\alpha_s = \pi/2 - |\phi|$ as characterizing the saddle point in both half space inversion integrals. One significant difference between the two solutions is that the geometrical optics pole now moves along the real α axis between $(-\pi/2, \pi/2)$ regardless of the medium parameters. Hence the reflection boundary will be a distinct physical feature of the problem as in homogeneous problem. The problem of a uniform asymptotic expansion for the saddle point integral in the vicinity of the geometrical optics pole is an issue here. There-

fore the uniform asymptotic expansion given in (4.1.17) with $k_{ob} = k_1$ must be used when the saddle point is in the vicinity of the geometrical optics pole to avoid the singularity resulting from the non-uniform expasion given in (4.1.8).

4.3 Validation and Sample Data

It is clear that the solution of the interface problem should reduce to the diffraction from a half-plane in a homogeneous space as the media parameters limit to each other. It is also clear that the numerical evaluation of the factorization integral in (3.4.18) will become unstable as the two media limit to the homogeneous case since the integration path vanishes while the integrand becomes unbounded. As a test of the algorithm, the case shown below was evaluated on a computer:

$$\mu_1 = 1.-j.001, \; \varepsilon_1 = 1. \text{ resulting in } k_1 = 1.-j.000500 \qquad (4.3.1)$$

$$\mu_2 = 1.-j.0003, \; \varepsilon_2 = 1.-j.001 \text{ resulting in } k_2 = 1.-j.000650$$

Incidence angle, $\theta = 45^{\circ}$ and observation radius, $\varrho = 5$ ‹

in free space.

The resulting evaluation of (4.1.8) for the cylindrical wave of the diffracted field was compared with the Keller diffraction coefficient. Plots of the two diffracted field computations were found to overlay one another except in the vicinity of the observation angle, $\phi = 180^{\circ}$. The modulus of the diffracted field for the parameters given above is plotted in Figure 4.8 as a function of the observation angle, ϕ, taken with respect to the illuminated side of the PEC half-plane where $0^{\circ} < \phi < 360^{\circ}$.

The anomaly in the vicinity of $\phi = 180^{\circ}$ arises from the vanishing
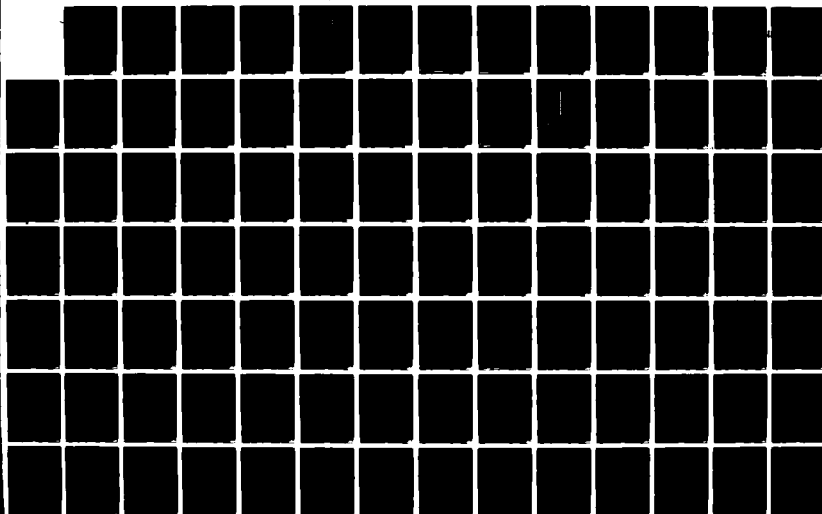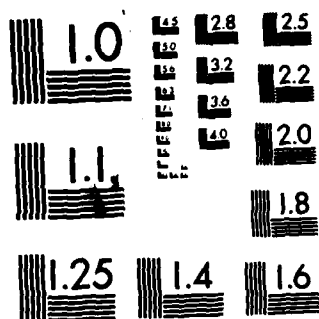
MICROCOPY RESOLUTION TEST CHART

NATIONAL BUREAU OF STANDARDS-1963-A
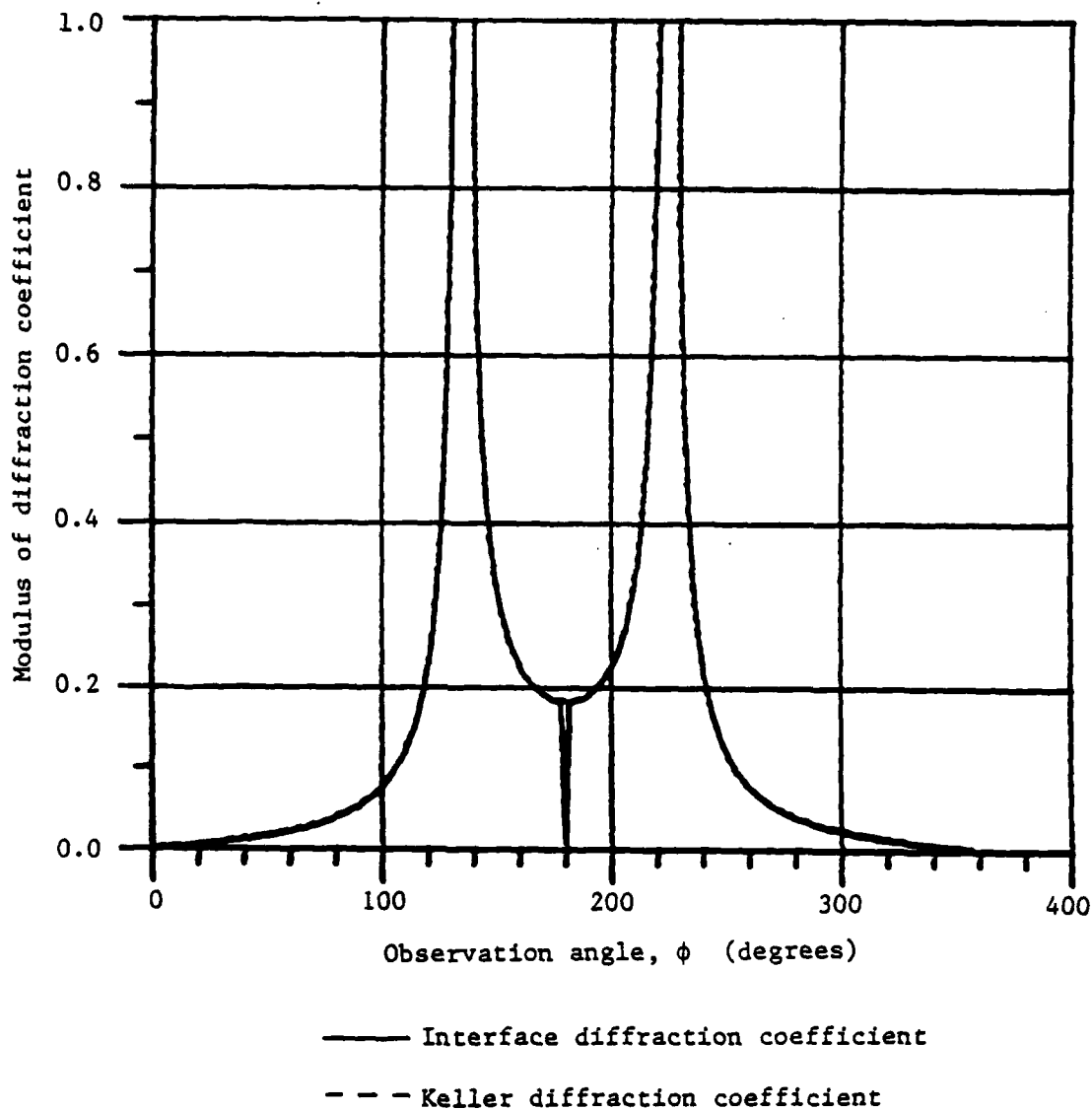
Figure 4.8. Comparison of diffraction coefficients from the interface problem with the Keller values. The two agree closely except in the vicinity of $\phi = 180^\circ$.

of the leading term in the asymptotic expansion of the steepest descent
integral about the saddle point as discussed in Appendix B. As indicated
there, this failure of the leading term to suffice in the asymptotic exp-
ansion is localized to roughly a $\pm 2°$ sector about the interface in the
present example. As the contrast between the media is increased, the de-
parture from the Keller diffraction coefficient around $\phi = 180°$ is en-
hanced. This behavior is seen in Figure 4.9.

In Figure 4.9 another feature of the diffracted field is apparent,
namely, the spur occuring at $\phi = 156°$. For this configuration the angle
of total internal reflection is $\phi = 24°$. The spur occurs at this criti-
cal angle and always lies in the more dense medium (i.e., that medium
having the larger magnitude of the real part of the complex wave
number). Figure 4.10 is the same configuration as in Figure 4.9 but view-
ed at an observation radius of $\rho = 50 \lambda$ from the edge of the PEC half-
plane. It is evident that the spur is diminished as the observation ra-
dius increases.

The spur arises when the two media have almost the same loss tangent.
In that case the branch point for the less dense medium ($-k_2$ for the ex-
ample shown in Figure 4.10) approaches the line in the k_x plane which con-
nects the branch point of the denser medium ($-k_1$) to the origin. This
line segment maps into the line segment between $\alpha = -\pi/2$ and $\alpha = 0$ which
is the locus of the saddle point. In essence, the spur represents the ef-
fect of the branch point due to ($-k_2$) on the saddle point integral as the
saddle point passes near the branch point.
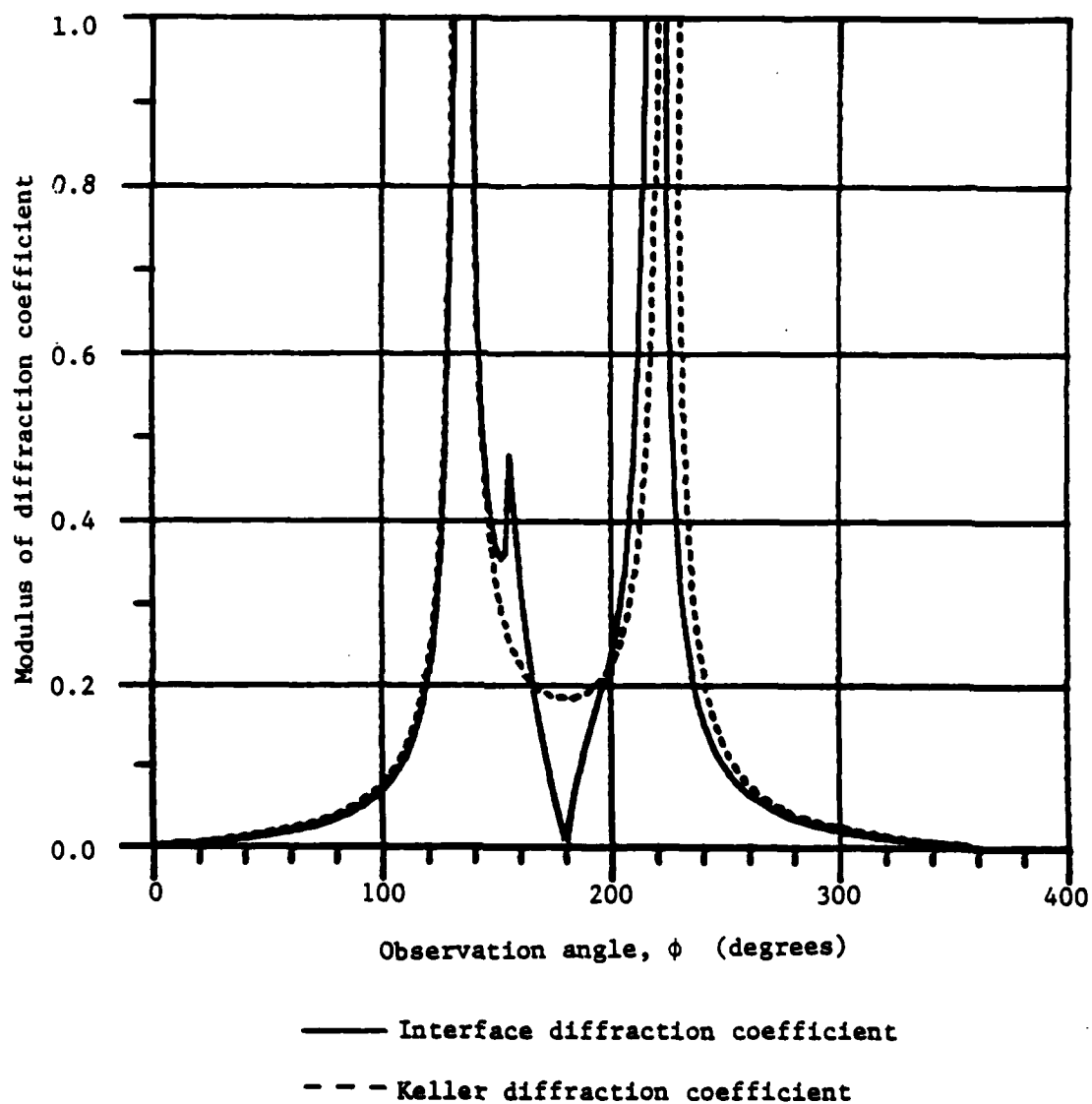
Figure 4.9. Comparison of the interface and Keller diffraction coefficients for dissimilar media. Observation radius, $\rho = 5 \lambda$ in free space; incidence angle, $\theta = 45°$.
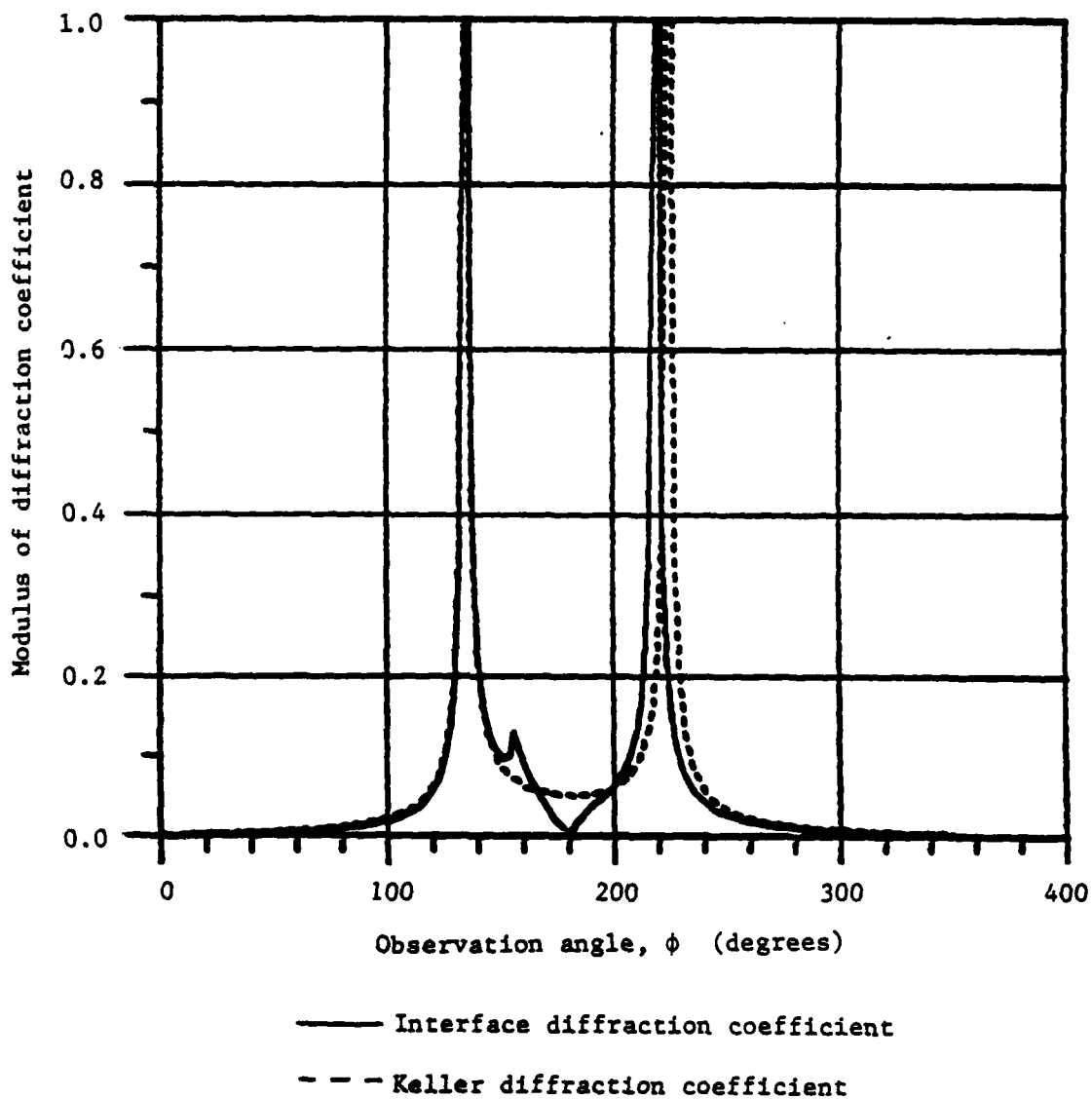
Figure 4.10. Data for Figure 4.9 at an observation radius of $\rho = 50\lambda$, free space.

The validity of the asymptotic expansion is questionable for observation angles near the spur unless ρ is large. In order to determine under what conditions the asymptotic saddle point expansion is valid, it is necessary to establish a minimum limit for the observation radius, ρ. This can be done by considering the value of the exponential envelope of the integrand in the saddle point integral. We may consider a circular region in the α plane which is centered on the saddle point and has the branch point on its boundary (the region of validity for the Taylor's series expansion of the integrand). If we require the magnitude of the exponent in the integrand to drop to one tenth of its value at the saddle point then it can be shown that the smallest observation radius for which the simple asymptotic value of the saddle point integral is valid is given by

$$\rho \approx .73/r^2 , \qquad\qquad (4.3.2)$$

where ρ is the observation radius in wavelengths in the medium containing the observation point, r is the separation of the branch point and the saddle point in the α plane.

It must be said, however, that the spur is a valid phenomenon in the far field of the diffraction pattern and represents an interaction between the radiation portion of the saddle point contribution and the branch point of the opposing medium. If the loss tangents of the two media are fixed and the contrast is decreased, the spur is seen to move toward $\phi = 180°$.

A typical situation is shown in Figure 4.11, where all the terms con-
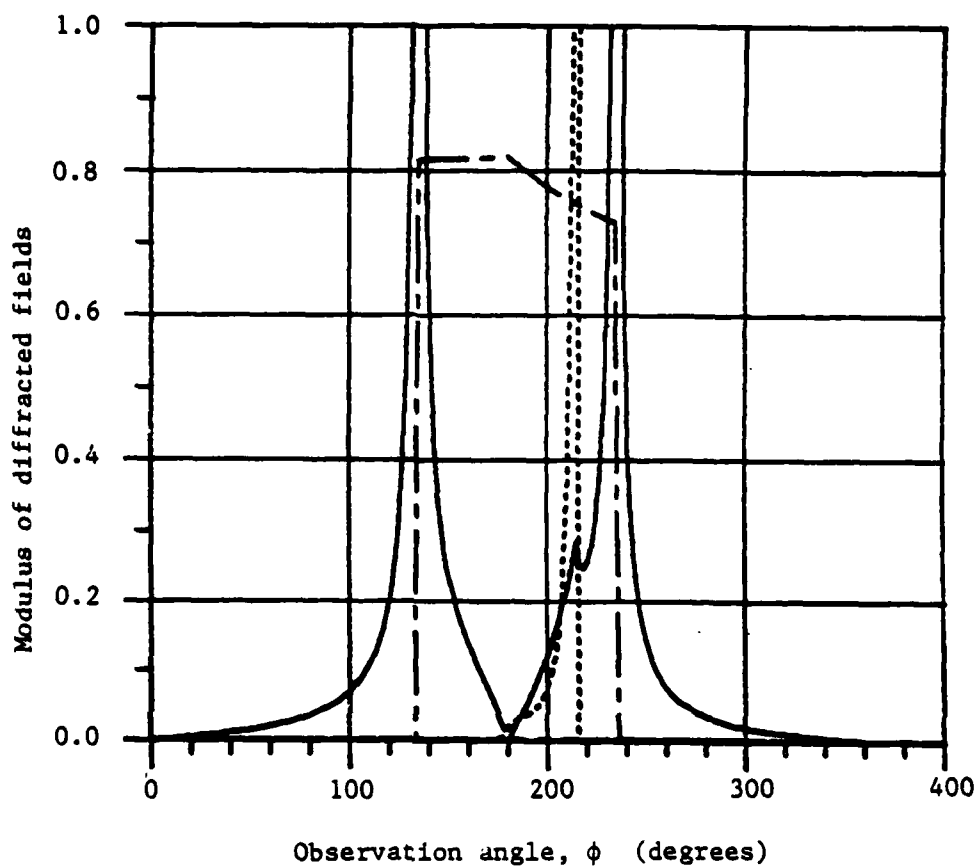
Figure 4.11. Typical result of scattering from a PEC half-plane on an interface between dissimilar media. (Parameters — $\mu_1 = \mu_2 = 1$, $k_1 = 1.-j.0005$, $k_2 = 1.2248-j.0041$, $\rho = 5\lambda$ (free space), $\theta = 45°$)

tributing to the scattered field are shown. The geometrical optics field contributes in the region bounded by the reflection and shadow boundaries of geometrical optics. In the reflection region ($y > 0$) the total geometrical optics field is composed of the sum of the short circuit field (that due to the incident plane wave reflecting off of the interface plane where the PEC half-plane has been extended to cover the aperture) and the scattered field of the geometrical optics pole. In the portion of the reflection region which lies beyond the reflection boundary ($\pi-\theta < \phi < \theta$) these two constituents must sum to equal the field that would exist with no half-plane present. As a result the field of the geometrical optics pole can have a magnitude greater than one in a lossless configuration due to phasing between the short circuit and geometrical optics pole fields.

In the transmitted region ($y < 0$) the geometrical optics pole is the total geometrical optics field. Since we require the total tangential fields to be continuous across the interface and the short circuit field vanishes at the interface, it is seen that constituents of different radial behavior must be continuous across the interface.

The decrease in the geometrical optics field as ϕ moves away from the interface is a manifestation of the greater loss in medium 2 since the ray must attenuate more quickly as the ray path in medium 2 increases. If medium 1 is much more lossy than medium 2, it is possible that the geometrical optics pole field will actually increase in magnitude with increasing ϕ from the interface. It is noted that when medium 1 is more dense than medium 2 and the angle of incidence exceeds the critical

angle of total internal reflection, a cutoff effect of the diffracted field structure is seen in medium 2.

The lateral wave field arises from the branch cut integral and is seen to lie in the more dense medium with its peak magnitude occurring near the critical angle for internal reflection. As is seen in Figure 4.11, it seems probable that the mechanism which creates the spur on the saddle point diffraction field represents some interaction with the lateral wave as both occur at approximately the same observation angle.

In Figure 4.12 the configuration of Figure 4.8 is shown versus increasing radius. It is clear that the lateral wave suffers a larger algebraic and exponential attenuation than the other contributors and therefore decays more quickly with distance.

An interpretation of the phenomena may be offered to suggest the physical mechanism which gives rise to them. The lateral wave has been described in numerous places (Felsen and Marcuvitz (1973b,c), Felsen (1967)) as the result of a ray which propagates along the media interface in the less dense medium and leaks energy into the more dense medium at the critical angle due to refraction of the ray. In these interface problems one may visualize the initial scattering from the PEC half-plane as launching a homogeneous cylindrical wave as in the diffraction from a PEC half-plane in a homogeneous medium. However the ray bundle which propagates along the interface experiences precisely the same environment as a lateral wave source ray. The differing phase velocity of the two media refracts energy into the more dense medium as the source

Observation angle, ϕ (degrees)
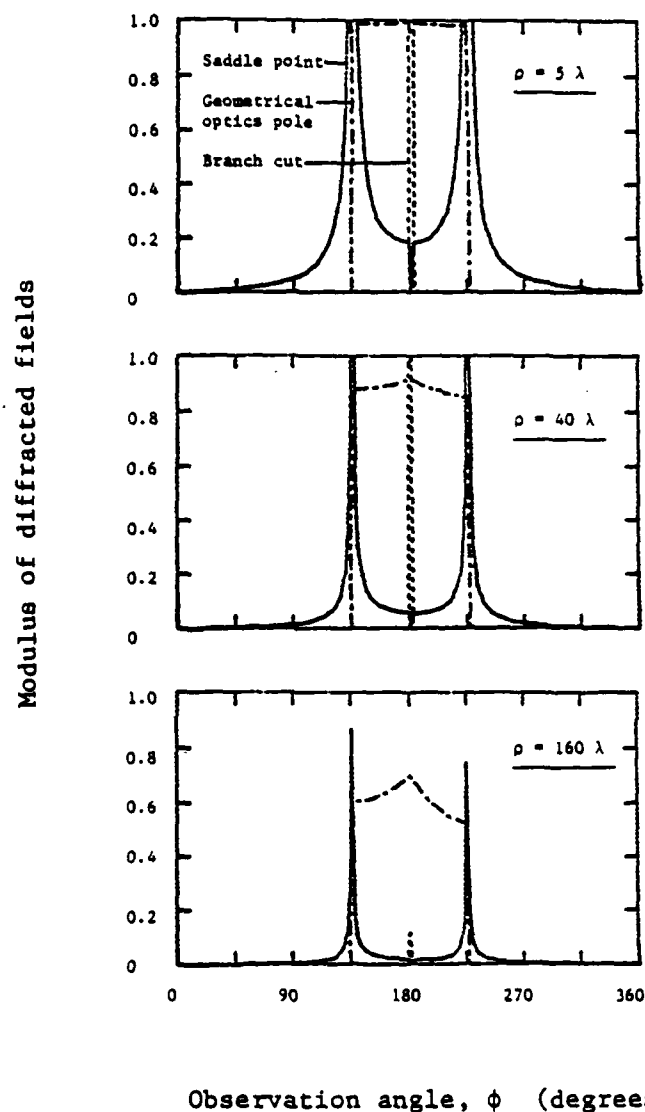
Figure 4.12. Scattering for the case described by (4.3.1) with increasing observation radius. Incidence angle, $\theta = 45^\circ$.

ray propagates and depletes the energy of the cylindrical diffraction wave in the vicinity of the interface. The greater the contrast, the greater the energy loss of the diffraction field, thereby minimizing the scattered energy in the direction of the interface.

This viewpoint also explains the mechanism by which the lateral wave is launched. One asks the following question: how can the diffracted field propagate with $e^{-jk_1\rho}$ in the upper region and $e^{-jk_2\rho}$ in the lower region along the interface and represent a valid solution to the boundary value problem? Surely even an approximate solution will manifest continuity of the tangential electric field across the interface. The solution to this paradox lies in the realization that the radiation field (which varies as $\rho^{-\frac{1}{2}}$) arising from the asymptotic evaluation of the steepest descent integral at the saddle point vanishes along the interface and the second term in the expansion is the leading term. Recognizing that both the saddle point and branch cut contributions vary as $\rho^{-3/2}$ but with a propagation behavior of $e^{-jk_1\rho}$ and $e^{-jk_2\rho}$ respectively, one suspects that the saddle point contribution for region 1 will equal the branch cut contribution for region 2. This can be shown to be the case. Therefore we see that the lateral wave contribution is essential along the interface to match the saddle point contribution for the other medium and to provide continuity of the total diffracted field across the interface. This viewpoint would seem to explain the mathematical necessity of the existence of the lateral ray to provide continuity of phase and attenuation across the interface when combined with the saddle point contribu-

tion. It also provides a useful device for estimating the magnitude of the second term in the asymptotic expansion for the saddle point integral. That is, the second term will equal the lateral wave term. Clearly for $\rho = 5 \lambda$ this contribution is small as seen in the data presented below.

In Figures 4.13-4.18 sample data is presented for a number of possible media combinations. All media parameters are normalized to free space. In all cases $\mu_1 = \mu_2 = 1$, the permeability of free space. Plots to the left are associated with higher loss in medium 2, while those further down are associated with increasing contrast (that is, the modulus of $\varepsilon_2/\varepsilon_1$) between the two media . The data in Figure 4.13 serve as a reference case where the angle of incidence is $\theta = 45°$, the radius of observation is $\rho = 5 \lambda$ in free space. The contrast ratio increases by a factor of three as one moves down and the ratio is one on the top row. It is clear that increasing contrast causes the angle of refraction of the geometrical optics ray to increase and causes the lateral wave peak to shift away from the interface. Also a general flattening of the diffraction contribution from the saddle point (particularly about the interface) is seen with increasing contrast . Increasing the loss of medium 2 is seen primarily to attenuate the fields in the transmitted region.

Figure 4.14 is identical to Figure 4.13 but with the radius of observation increased to $\rho = 20$ wavelengths in free space. The magnitude of the lateral wave in the case of no contrast (top row) is explained by noting that the middle picture depicts a case of almost equal loss tangent in the two media. Clearly the branch point which gives rise
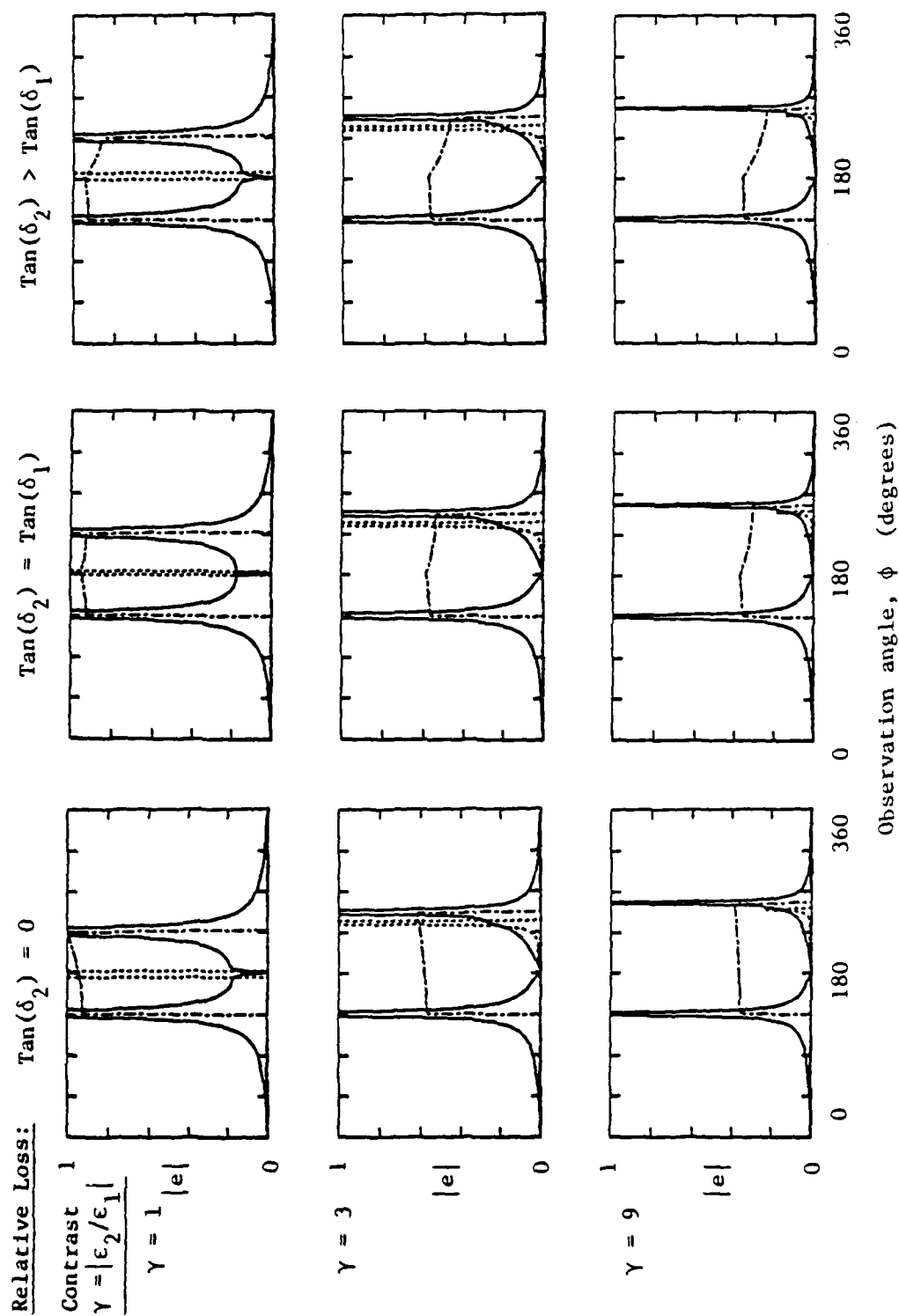
Figure 4.13. Comparison of data when contrast (ϵ_2/ϵ_1) and loss tangent $(\tan \delta_2)$ of medium 2 are varied. Medium 1 is fixed $(k_1 = 1. - j.0025)$. $\theta = 45°$; $\rho = 5\lambda$, free space.
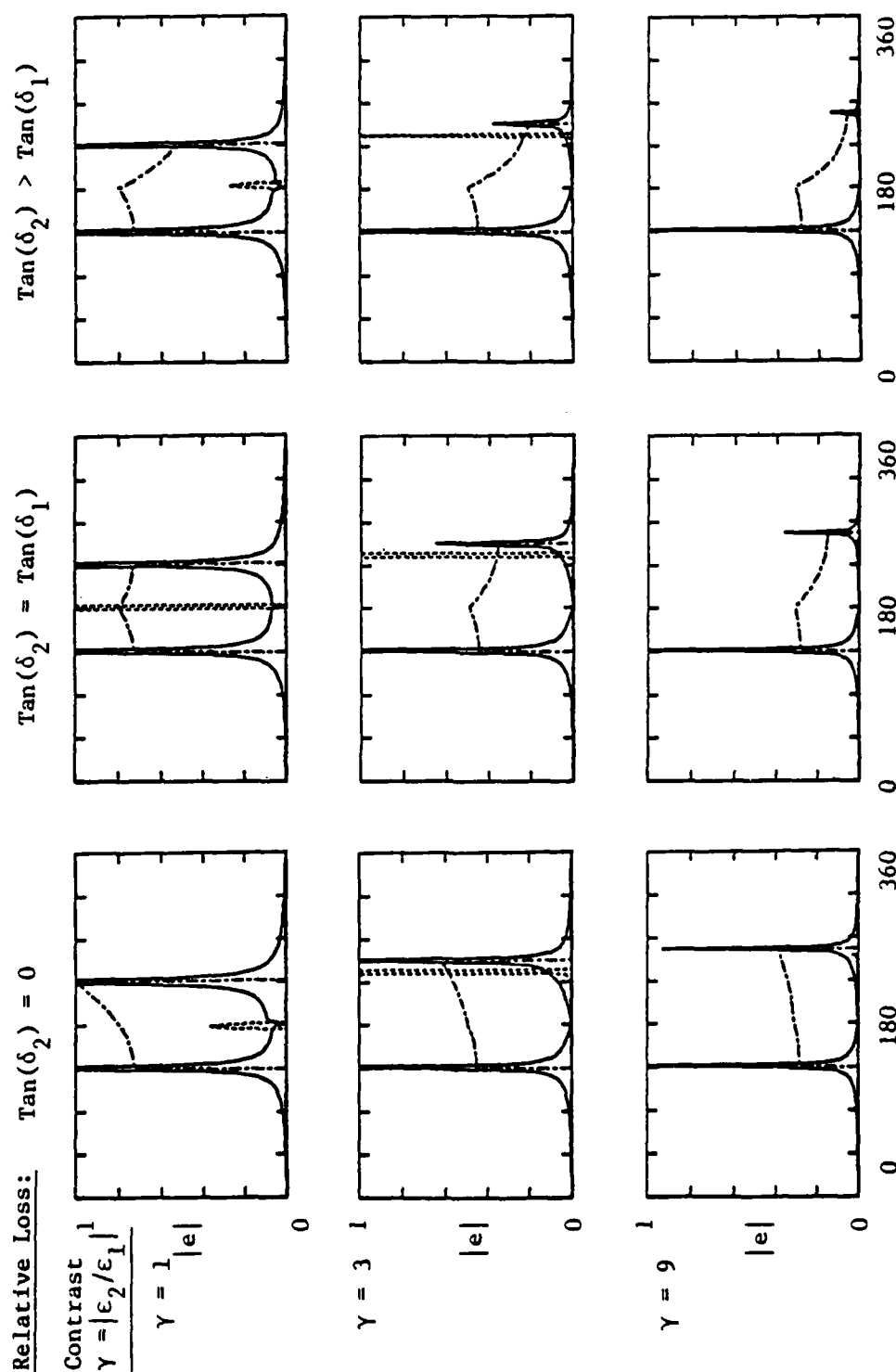
Figure 4.14. Same case as Figure 4.13 with $\rho = 20\lambda$, free space.
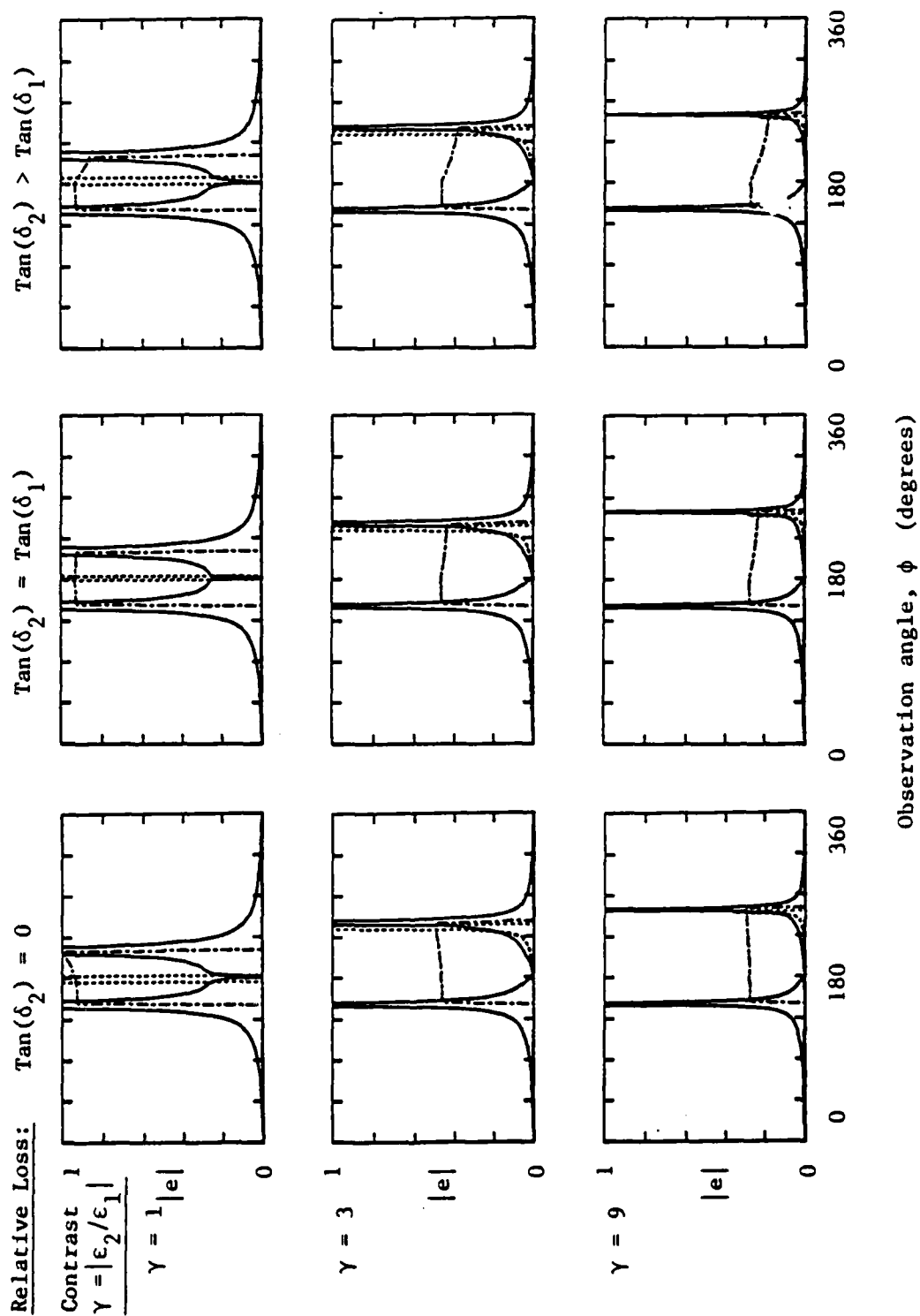
Figure 4.15. Same case as Figure 4.13 with angle of incidence, θ = 30°.

Observation angle, φ (degrees)

Relative Loss: Tan(δ₂) = 0   Tan(δ₂) = Tan(δ₁)   Tan(δ₂) > Tan(δ₁)
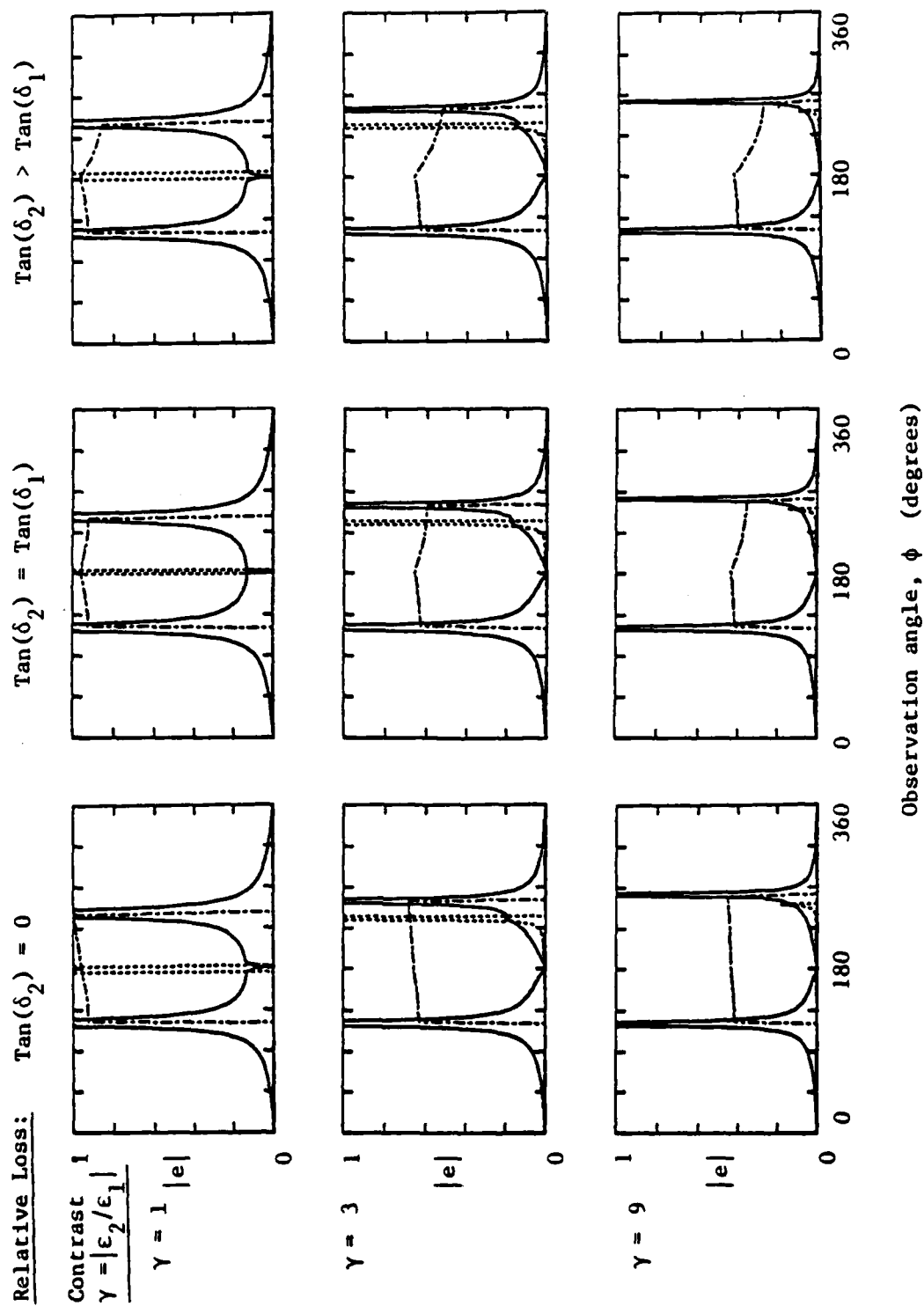
Figure 4.16. Same case as Figure 4.13 with angle of incidence, θ = 60°.
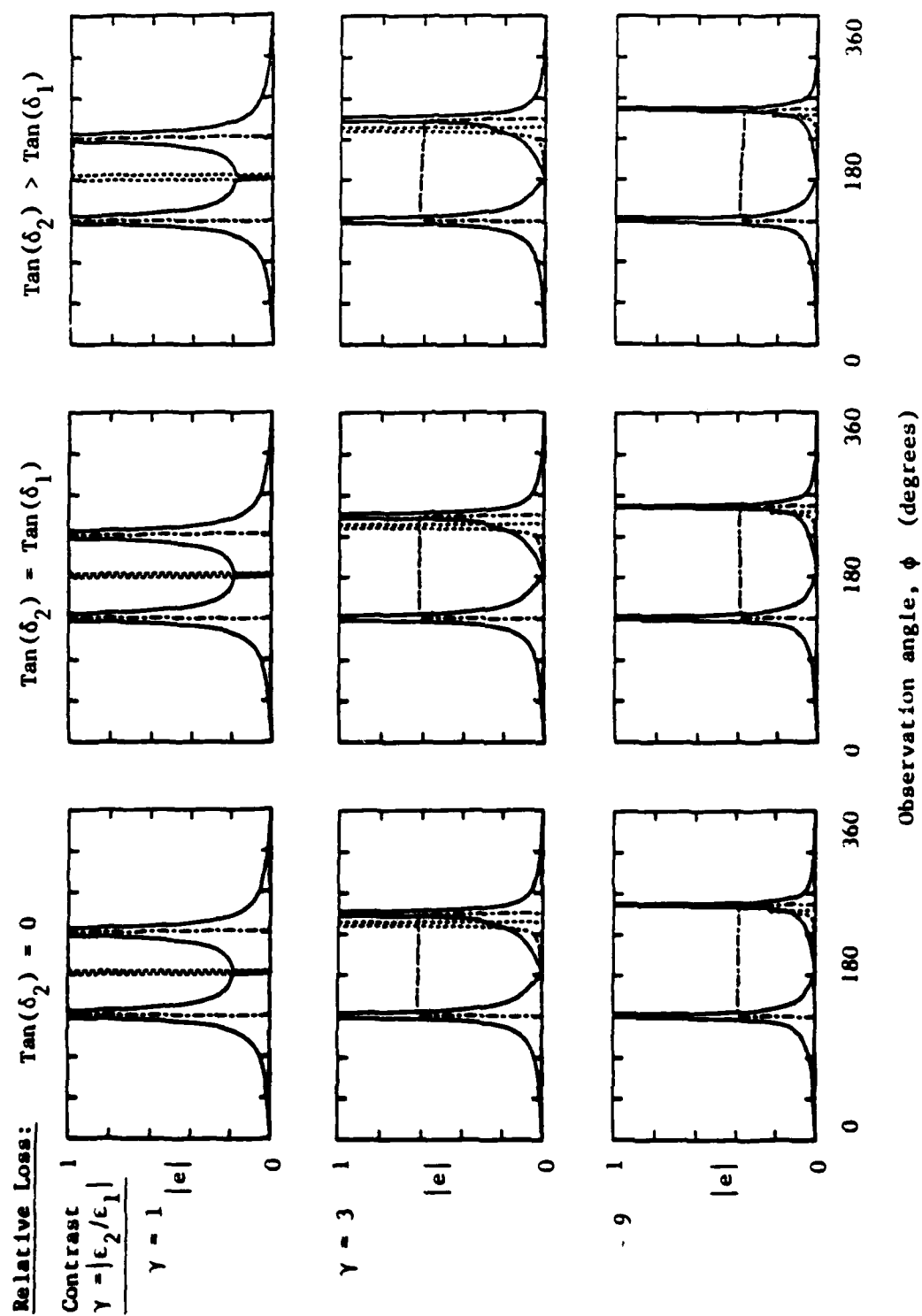
Figure 4.17. Comparative data for medium 1 almost lossless ($k_1 = 1. - j.00005$).
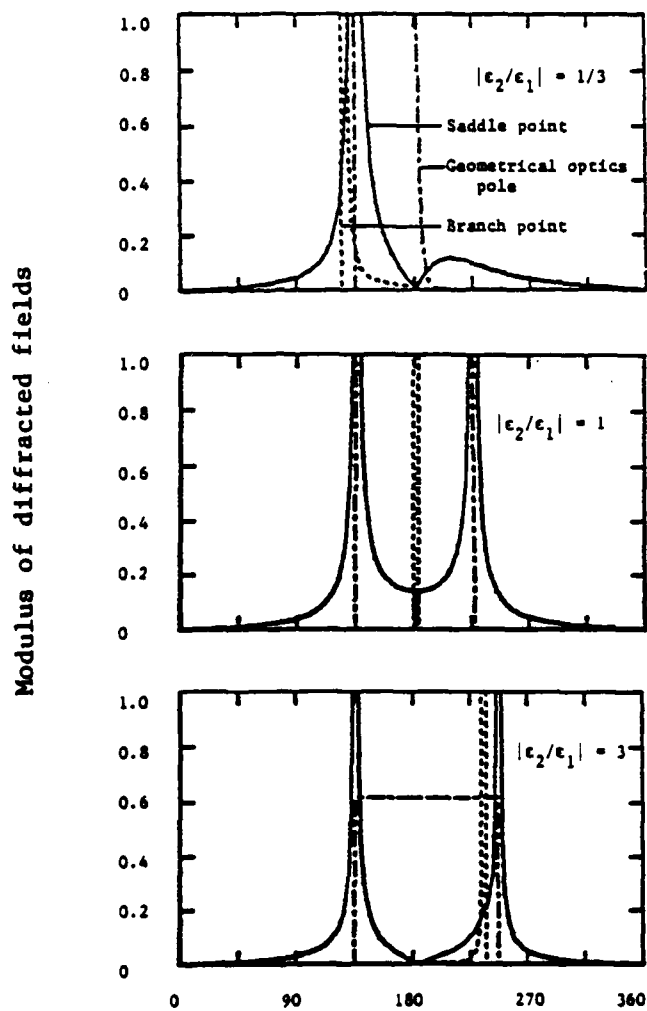
Figure 4.18. Comparative data with increasing contrast (ϵ_2/ϵ_1) and medium 1 fixed $(k_1 = 1.732 - j.000029)$.

to the lateral wave is nearer the real axis of the α plane than in the two surrounding pictures on the top row of Figure 4.13. Therefore the lateral wave contribution should be greater at a given observation radius. Also noticeable is the fact that the peak of the saddle point term is greater on the reflection boundary than on the shadow boundary. In fact, the peak on the reflection boundary is truly a singularity (of the non-uniform asymptotic expansion) since the geometrical optics pole resides on the real α axis for observation points in the incident medium. The peak on the shadow boundary is not truly singular since the geometrical optics pole will lie on the α axis only at $\alpha = 0$ ($\phi = 90°$) for problems involving media with unequal loss tangents.

Figures 4.15 and 4.16 are given for comparison with Figure 4.13 and depict the same case but with the incidence angle shifted to $\theta = 30°$ and $60°$ respectively. As anticipated the shift in the reflection and shadow boundaries is apparent. Figure 4.17 is included as an example where medium 1 is essentially lossless ($k_1 = 1.-j.00005$). The second row in this figure corresponds to a value of ϵ_2 such that $Re(\epsilon_2) = 3$ which is typical of many plastic dielectric materials. The third row characterizes medium 2 with $Re(\epsilon_2) = 9$ which is near the value for ceramic dielectrics. In contrast to the earlier cases, Figure 4.18 depicts a case where medium 1 is relatively dense ($k_1 = 1.732-j.000029$). The top row of this figure represents a contrast ratio which is less than 1 ($|\epsilon_2/\epsilon_1| = 1/3$) as opposed to equality as in all of the earlier figures. This implies a critical angle of total internal reflection of about 55° and therefore the

plot of this figure exhibits the phenomenon of total reflection.

Figure 4.19 depicts the case given by

$$\mu_1 = \mu_2 = 1$$

$$\epsilon_1 = 1.-j.00001, \quad k_1 = 1.-j.000005$$

$$\epsilon_2 = 3.-j.00001, \quad k_2 = 1.732-j.000003 \qquad (4.3.3)$$

$$\rho = 5\lambda \text{ in freespace}$$

Unlike the earlier figures, this one shows the diffraction as the angle of incidence increases from 15° to the maximum incidence angle for the validity of the Wiener-Hopf analysis ($-Im(k_1 \cos\theta_{max}) = Im(k_2)$) which for this case is $\theta_{max} = 137^O$.

It must be pointed out that in none of the data computed has the pole due to the root of G_- significantly contributed to the field structure in a problem. This pole is associated with the root of (3.4.1) and seems to correspond to the Zenneck pole contributed since they both are roots of the same equation. This pole contribution arises only when the branch cut in the α plane exposes the pole. No clear determination has been possible to extablish the actual existence of the contribution of this term to the far field structure in a problem.

4.4.   Interpretation of Results

The intent of the analysis in the study of the interface problem is to provide a means for readily computing the various ray optic contributors which arise and thus a means to apply the GTD to configurations that contain features for which the interface problem is
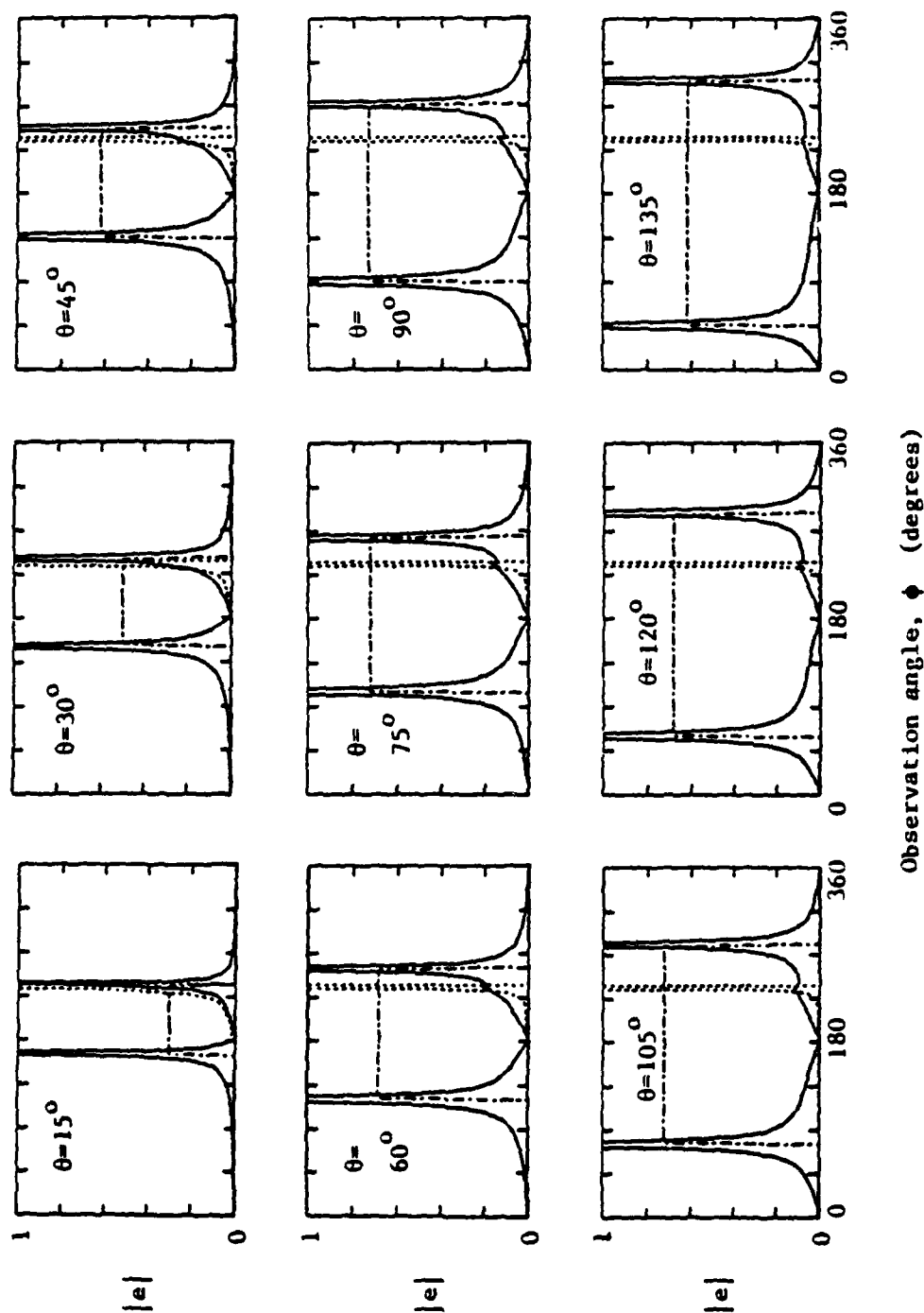
Figure 4.19. Scattered fields for the case described by (4.3.3) with increasing angle of incidence, θ. ρ = 5λ, free space.

a suitable canonical geometry. It is desirable, therefore, to discuss the scattered fields in physical configuration space (that is, the spatial domain) and describe the relative magnitudes of the ray contributors.

A ray representation of the contributing fields given by (4.1.8), (4.1.13) and (4.1.16) is shown in Figure 4.20 where both media are assumed to be lossless, and the lower medium is assumed to be the more dense. That the Zenneck pole contribution (4.1.14) arises is a possibility, too. As discussed above, however, no cases have been found where it does arise, and no further address is made to it here.

As shown in Figure 4.20 the geometrical optics field in the upper half space is given by the simple reflection off the PEC half-plane in the region lying between the half-plane (at $\phi = 0$) and the reflection boundary (at $\phi = \phi_{refl}$). For the remaining portion of the upper half space the geometrical optics field is simply the reflection of the incident wave off the media interface. In the lower medium the transmitted wave is seen to bend to an angle ϕ_{refr} and represents the refraction of the incident wave at the media interface.

The presence of the edge of the half-plane launches two different waves: an edge-diffracted wave and a lateral wave. The diffracted wave, which appears as a cylindrical wave propagating away from the edge of the PEC, is seen in all observation directions. When the media parameters are equal, this wave is described by the Keller diffraction coefficients (see Figure 4.8). However, as the contrast is increased, the diffracted wave is quite different from the "Keller" wave (for
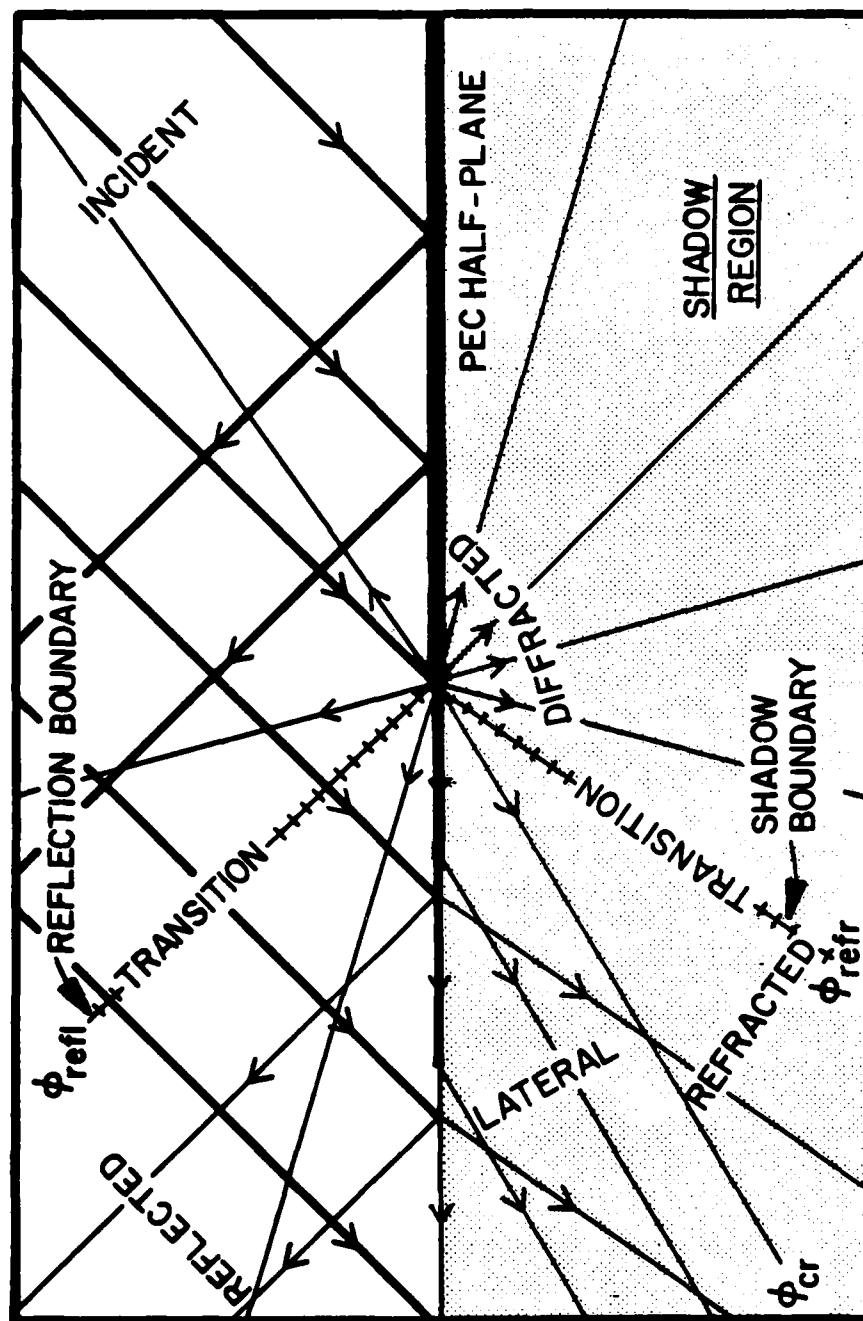
Figure 4.20. Ray paths along which energy is conveyed in the interface problem. It is assumed that the lower medium is the more dense for the case shown.

example, the diffracted wave decreases to near zero as the observation angle approaches the interface while the "Keller" wave does not, see Figure 4.9).

The lateral wave is launched by the PEC half-plane. This wave is an inhomogeneous plane wave which may be represented by a ray bundle emanating from the edge and propagating along the interface in the less dense medium, shedding energy into the more dense medium through refraction. This energy thus propagates away from the interface at the critical angle of total internal reflection, ϕ_{cr}. This field is present in the region of space between the boundary ray emanating from the edge of the PEC half-plane at an angle of ϕ_{cr} and the interface. The lateral wave is a plane wave which propagates in the direction ϕ_{cr} and is most intense along the boundary ray at ϕ_{cr}. At a fixed radius the magnitude of the lateral wave decays rapidly as the angle of observation rotates from ϕ_{cr} toward the interface. This lateral wave is a unique manifestation in problems involving an interface between media and does not occur unless dissimilar media are present in a scattering configuration. Note that in Figure 4.20 the lateral wave is shown propagating into the lower medium. This is due to the assumption that the lower medium is more dense than the upper medium. Had the reverse been assumed then the lateral wave would propagate into the upper medium.

Figure 4.20 shows all the possible ray contributors at an observation point. It is clear that when the upper medium is less dense, any observation point in that medium will receive scattered

radiation from the geometrical optics field and the cylindrical edge-diffracted field. The geometrical optics field will dominate in the upper half space when lossless media are involved except for observation points near the reflection boundary ϕ_{refl} where the geometrical optics field and the edge-diffracted field will be of the same magnitude. It is noted that since the lower medium is assumed more dense, the lateral wave contribution in the upper medium is quite small and evanescent in nature, decaying away from the interface.

In the lower medium, it is seen that observation points in the shadow region will only be illuminated by the edge-diffracted field. For observation angles between the interface and the shadow boundary, ϕ_{refr}, the geometrical optics field contributes as does the edge-diffracted field and the lateral wave contributes in the sector between the interface and the ray at ϕ_{cr}, the critical angle of total internal reflection. Throughout most of the "lit" region of the lower medium the dominant contributor is the geometrical optics field and the least important contributor is the lateral wave field. However, the lateral wave dominates the others in a small angular sector bounded by the ray at ϕ_{cr}. In essence a pencil beam of lateral rays appears to be emanating from the edge roughly in the direction ϕ_{cr} and is the dominant field contributor there. The hierarchy of contributions to the total field is summarized in the table in Figure 4.21.

It is emphasized here that when the two media are different, the edge-diffracted field is substantially different from that in the homogeneous problem. The lateral wave also is a manifestation of the

Region	Hierarchy of Contributors	
1	i.	Geometrical optics field
	ii.	Edge-diffracted field
2	i.	Geometrical optics field
	ii.	Edge-diffracted field
3	i.	Geometrical optics field
	ii.	Edge-diffracted field
	iii.	Lateral wave
3a	i.	Lateral wave
	ii.	Geometrical optics field
	iii.	Edge-diffracted field
3b	i.	Geometrical optics field
	ii.	Edge-diffracted field
4	i.	Edge-diffracted field
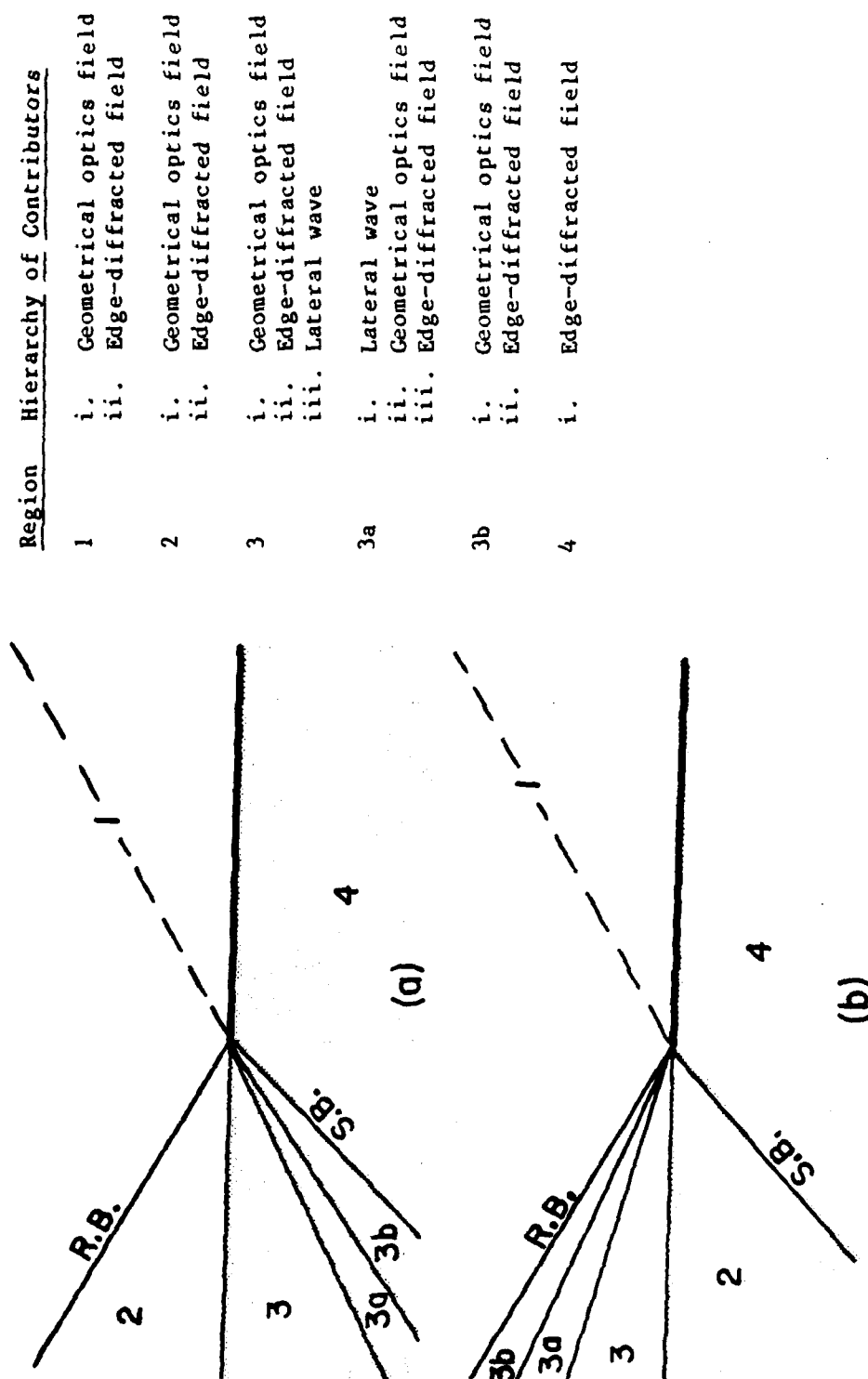
Figure 4.21. Significance of the ray contributors in the scattered field for the interface problem. The lower medium is more dense in (a) and the upper medium is more dense in (b).

presence of the interface. Hence the field structure manifests markedly different features from the classical problem of scattering from a half-plane in a homogeneous medium.

When losses are introduced several interesting changes occur. Most marked is the possibility that the dominance of the geometrical optics field over the edge-diffracted field in the lower medium can reverse when the constrast ratio of the media wave numbers (k_2/k_1) attains a significant imaginary part. In this circumstance the locus of the geometrical optics pole leaves the real axis in the angular spectral plane and induces the exponential dominance of the edge-diffracted field as discussed in Section 4.1.3. A second manifestation of the presence of media loss is that the shadow boundary is seen to "smear" and lose definition. Further, the significance of the lateral wave contribution is strongly dependent on the contrast ratio (k_2/k_1) between the two media. In some cases the lateral wave will dominate both the geometrical optics wave and the edge-diffracted wave for observation points sufficiently close to the interface.

CHAPTER V

THE SLAB PROBLEM

5.1 Statement of the Problem

The structure considered in this chapter is shown in Figure 5.1. A dielectric slab of thickness t' with constitutive parameters (μ_0', ε_2') is embedded in a surrounding medium with constitutive parameters (μ_0', ε_1') where ε_1' and ε_2' are real and $\varepsilon_2' > \varepsilon_1'$. The upper surface of the slab lies in the plane $y' = 0$. Residing on the slab's upper surface is a PEC screen covering the half-plane $(x' \geq 0)$ with its edge at $x' = 0$. A plane wave is incident from the upper half-space $(y' > 0)$ and propagates toward the slab at an angle θ with respect to the PEC half-plane. The incident wave is assumed to be polarized transverse magnetic (TM) to the z' axis. As in the interface problem, we assume no variation in the z' direction and so this is a strictly two-dimensional problem. It is noted that only loss-less media are admitted. This stands in contrast to the general media considered in the slab problem.

5.2 Wiener-Hopf Formulation over the PEC Half-Plane

For this problem we structure the integral equation over the PEC half-plane rather than over the aperture (as in the interface problem) to demonstrate the features of this formulation and how they contrast to

113
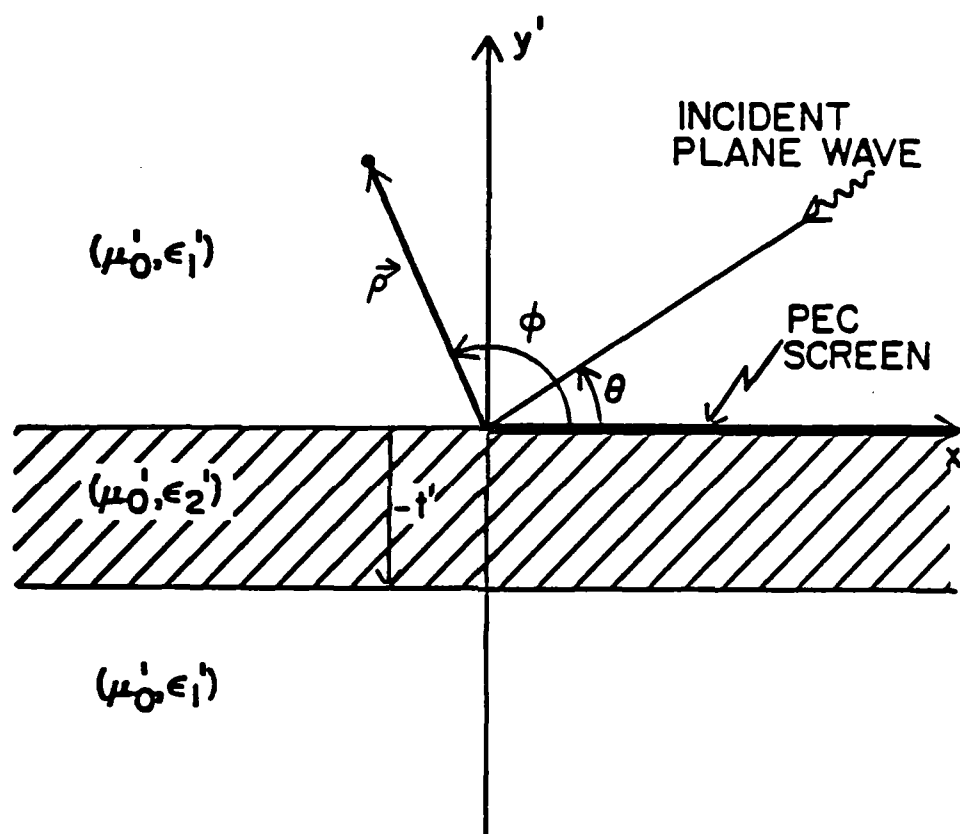
Figure 5.1.   Geometry of the slab problem.

the features of the aperture field formulation used to solve the interface problem. The resulting integral equation is an electric field integral equation (EFIE) which enforces that the total tangential electric field over the PEC screen be zero and has the electric current on the screen as the unknown function. Since we are considering the TM case we see that the surface current on the plane is purely z' directed and therefore induces only the z' component of the magnetic vector potential, A_z. To formulate the integral equation, we must solve two associated problems. First, the problem of a z' directed filamentary source of z' directed electric current located on the upper surface of the slab (at $x' = 0$) is used to establish the Green's function for the integral equation. Second, the problem of the plane wave incident on the slab with the PEC screen removed is used to establish the source field for the integral equation. Having established these two functions, we form the EFIE,

$$e_z^{NP}(x') = -e_z^{Rad}(x') = -\frac{1}{\sqrt{2\pi}} \int_{x'=0}^{\infty} j(x_0')k(x',x_0')dx_0' \qquad (5.2.1)$$

for $x' \in (0,\infty)$,

where $e_z^{NP}(x')$ is the total field present due to a plane wave impinging on the slab in the absence of the screen and $k(x',x_0')$ is the Green's function relating the z'-directed electric field on the interface electric field on the interface to a z'-directed current filament residing there. It is convenient to consider this equation directly in the Fourier

transform domain, therefore we extend the definition of the functions in the manner described in section 2.4 to arrive at

$$a_+^u(x') + b_-^u(x') = \frac{1}{\sqrt{2\pi}} \int_{-\infty}^{\infty} \phi_+^u(x_0') k(x',x_0') dx_0' \qquad \text{for } x' \epsilon(-\infty,\infty)$$

(5.2.2)

$$= \phi_+^u * k \quad ,$$

where $\phi_+^u(x') = j_z(x')$ and $a_+^u(x') = e_z^{NP}(x')$ for $x' > 0$. Fourier transforming this equation with respect to x', we arrive at

$$A_+^u(k_x') + B_-^u(k_x') = \phi_+^u(k_x') \cdot K(k_x')$$

(5.2.3)

for k_x' within a strip where all the functions are analytic. We now establish the Fourier transform of the known functions, K and A_+^u.

We require the kernel $k(x')$ in (5.2.2), that is, the Green's function relating the e_z field in the $y' = 0$ plane to a z'-directed filament of current in that plane. Actually, since a Wiener-Hopf analysis is subsequently used, we need only the Fourier transform of this kernel. The analysis for the transform is given in Whitmer (1948) and results in

$$a(k_x') = \begin{cases} a_1 & , & y' \geq 0 \\ a_2 & , & -t' \leq y' \leq 0 \\ a_3 & , & y \leq -t' \end{cases}$$

(5.2.4)

where

$$a_1 = \left[e^{-j\beta_2' t'} - \frac{e^{j\beta_2' t'}}{\Gamma} \right] C \, e^{-j\beta_1' y'} \left(\frac{-j}{2\sqrt{2\pi}} \right) \quad , \qquad (5.2.5.a)$$

$$a_2 = \left[e^{-j\beta_2'(y'+t')} - \frac{e^{j\beta_2'(y'+t')}}{\Gamma} \right] C \left(\frac{-j}{2\sqrt{2\pi}} \right) \quad , \qquad (5.2.5.b)$$

$$a_3 = \left[1 - \frac{1}{\Gamma} \right] C \left(\frac{-j}{2\sqrt{2\pi}} \right) e^{j\beta_1'(y'+t')} \quad , \qquad (5.2.5.c)$$

and

$$\Gamma = \frac{\beta_1' - \beta_2'}{\beta_1' + \beta_2'} \quad ,$$

$$C = \frac{2}{(\beta_1' + \beta_2')(\Gamma \, e^{-j\beta_2' t'} - \frac{1}{\Gamma} e^{j\beta_2' t'})}$$

The Green's function which we require for (5.2.3) is given by a above with $y' = 0$. Hence we have

$$K(k_x') = \frac{\omega\mu_0'}{2\beta_1'} F(k_x') \qquad (5.2.6)$$

where

$$F(k_x') = \left\{ 2\beta_1' \left[\frac{(\beta_1' - \beta_2')e^{-j\beta_2't'} - (\beta_1' + \beta_2')e^{j\beta_2't'}}{(\beta_1' - \beta_2')^2 e^{-j\beta_2't'} - (\beta_1' + \beta_2')^2 e^{j\beta_2't'}} \right] \right\} \qquad (5.2.7.a)$$

or equivalently,

$$F(k_x') = \left\{ 2\beta_1't' \left[\frac{j\beta_1't' + \beta_2't'\cot(\beta_2't')}{j[(\beta_1't')^2 + (\beta_2't')^2] + 2(\beta_1't')(\beta_2't')\cot(\beta_2't')} \right] \right\} \qquad (5.2.7.b)$$

An interesting observation can be made at this point regarding (5.2.6). The poles of the Green's function characterize the surface waves for the dielectric slab while the roots characterize the surface waves of the problem of a slab with the upper surface covered by a PEC screen. The problem treated here is a composite of these two problems for the two regions $x' \gtrless 0$. One expects the solution for these two regions to manifest the wave structure appropriate to each region in the vicinity of the slab. As is seen later, one result of the Wiener-Hopf analysis is that both roots and poles of (5.2.6) are singularities of the integrand of the radiation integral and contribute in the two regions $x \gtrless 0$ as expected.

To formulate $A_+^u(k_x')$, which is the Fourier transform of the incident plane wave in the presence of the slab but with the PEC screen removed, we must solve the requisite boundary value problem. The analysis is relatively straightforward and the resulting fields are given below:

$$e_z^{NP} = \begin{cases} E_0\, e^{jk_1'(x'\cos\theta + y'\sin\theta)} + A\, e^{jk_1'(x'\cos\theta - y'\sin\theta)} & , \ y' \geq 0 \\[2em] B\, e^{jk_2'(x'\cos\theta + y'\sin\theta)} + C\, e^{jk_2'(x'\cos\theta - y'\sin\theta)} & , \ -t \leq y' \leq 0 \\[2em] D\, e^{jk_1'(x'\cos\theta + y'\sin\theta)} & , \ y' \leq -t' \end{cases}$$

$$(5.2.8)$$

where $k_1'\cos(\theta) = k_2'\cos(\theta_2)$ and θ, θ_2 are the ray directions for the reflected and transmitted ray respectively from the plane of the slab. The constants in (5.2.8) are

$$A = -E_0 + B + C \qquad\qquad (5.2.9.a)$$

$$B = \left[\frac{\left(\dfrac{\sin\theta}{\eta_1'} + \dfrac{\sin\theta_2}{\eta_2'}\right)}{\Delta}\, e^{jk_2't'\sin\theta_2} \right] \frac{2E_0\sin\theta}{\eta_1'} \qquad (5.2.9.b)$$

$$C = -B\, \frac{\left(\dfrac{\sin\theta}{\eta_1} - \dfrac{\sin\theta_2}{\eta_2'}\right)}{\left(\dfrac{\sin\theta}{\eta_1'} + \dfrac{\sin\theta_2}{\eta_2'}\right)}\, e^{-j2k_2't'\sin\theta_2} \qquad (5.2.9.c)$$

$$D = \frac{2B}{\left(\dfrac{\sin\theta}{\eta_1'} + \dfrac{\sin\theta_2}{\eta_2'}\right)} \ \frac{\sin\theta_2}{\eta_2'} \ e^{j(k_1'\sin\theta + k_2'\sin\theta_2)t'} \tag{5.2.9.d}$$

where

$$\Delta = \left[\left(\frac{\sin\theta}{\eta_1'} + \frac{\sin\theta_2}{\eta_2'}\right)^2 e^{jk_2't'\sin\theta_2} - \left(\frac{\sin\theta}{\eta_1'} - \frac{\sin\theta_2}{\eta_2'}\right) e^{-jk_2't'\sin\theta_2}\right]$$

$$\eta_1' = \sqrt{\mu_0'/\epsilon_1'} \ , \ \eta_2' = \sqrt{\mu_0'/\epsilon_2'}$$

If y' is set to zero in (5.2.8) and the resulting function is then Four-ier transformed (leading to a semi-infinite integral from $x' = 0$ to $x' = \infty$), the resulting transform is

$$A_+^u(k_x') = \frac{j \ F_\theta' \ E_0}{\sqrt{2\pi} \ (k_x' + k_1'\cos\theta)} \tag{5.2.10}$$

where E_0 is the magnitude of the incident plane wave

$$e_z^{inc} = E_0 \ e^{jk_1'(x'\cos\theta + y'\sin\theta)} \qquad \text{and} \ F_\theta' = F(k_x' = k_1'\cos\theta).$$

Applying the normalizations defined in section 2.5, we arrive at the following form for the Wiener-Hopf equation:

$$A_+(k_x) + B_-(k_x) = \Phi_+(k_x) \ G(k_x) \tag{5.2.11}$$

where

$$A_+(k_x) = \frac{j \, F_\theta \, E_0}{(k_x + k_1 \cos\theta)} \; , \; F_\theta = F(k_x = k_1 \cos\theta, t)$$

$$B_-(k_x) = \text{unknown function}$$

$$\Phi_+(k_x) = \omega\mu_0' \sqrt{\frac{\pi}{2}} \, J_z(k_0 \cdot k_x), \; J_z(k_0 \cdot k_x) = F\{j_z(x')\}$$

$$G(k_x) = F(k_x)/\beta_1$$

5.3 Factorization of $G(k_x)$

The next step in the Wiener-Hopf analysis is the factorization of $G(k_x)$ given in (5.2.11). This function is composed of two factors which are considered separately, that is, $1/\beta_1$ and $F(k_x)$. We see that $(1/\beta_1)$ factorizes by inspection as in (3.4.3). Therefore we concentrate on the factorization of F through the formal integral factorization formula given in (3.4.6).

To meet the hypothesis of the integral factorization, we require that $F(k_x) \to 1$ uniformly within the Wiener-Hopf strip of analyticity as $|\sigma| \to \infty$, where $k_x = \sigma + j \tau$. We observe from (5.2.7.a) that as $|k_x| \to \infty$ on the top sheet of F (where β_1 and β_2 assume the original definition of Section 2.2),

$$\text{Re}(-j\beta_2 t) \to -\infty$$

and therefore
$$F \sim 2\beta_1 \left[\frac{0 - (\beta_1 + \beta_2)e^{+j\beta_2 t}}{0 - (\beta_1 + \beta_2)^2 e^{+j\beta_2 t}} \right] = 2\beta_1 \left[\frac{1}{\beta_1 + \beta_2} \right] .$$

However $\beta_1 \sim \beta_2 \sim \sqrt{k_x^2} = \pm k_x$ such that $Im(\beta) < 0$ as $|k_x| \to \infty$. Therefore $F \sim 1$, as $|k_x| \to \infty$. We observe that even if we move to $k_x = \infty$ along the hyperbolic β_2 branch cut (and therefore $Re(-j\beta_2 t) = 0$), again $F \to 1$ as the coefficient $(\beta_1 - \beta_2) \to 0$. It is clear that $F \to 1$ as $|k_x| \to \infty$ anywhere on the top sheet.

We may therefore perform the integral factorization of F and it will apply along the real k_x axis since the Wiener-Hopf strip collapses to the real axis. It is necessary to consider the definition of $\ln(F)$ which appears in the factorization formula (3.4.6). In order to establish an acceptable definition, we must consider in detail the behavior of $F(k_x)$ in the complex k_x plane.

The details of the behavior of F are essentially the same as those for the Green's function of the slab problem and have been considered by several authors (e.g. Whitmer (1948), Barone (1956), Collin (1960)). The important facts concerning F are presented below and in Appendix D.

The points $k_x = \pm k_1$ will be branch points of F due to the function β_1. However, $k_x = \pm k_2$ are not branch points. Observe that F is, in fact, an even function of β_2. If we consider a path encircling k_2 in the k_x plane, we observe that $\beta_2 \to -\beta_2$ but $F \to F$. One can make the observation here that the Fourier transforms of the Green's functions for the slab problem and the interface problem exhibit branch points at the wave numbers for the media which span a half-space but do not exhibit branch points for the media whose extent in the y direction is finite (that is, the slab medium). Therefore the only branch points of F lie at $k_x = \pm k_1$.

In addition to the branch point singularities, F also has poles which occur at the roots of the denominator of F. These roots are considered in Appendix D and they are found to lie on the real k_x axis between k_1 and k_2 (and therefore, by symmetry, between $-k_2$ and $-k_1$). Interspersed alternately between the poles of F are roots of F due to roots of the numerator of F (also constrained to the real k_x axis between $(+k_1, +k_2)$ and $(-k_2, -k_1)$). The number of poles and zeros is a monotonically increasing function of (a $= \sqrt{\epsilon_2 - \epsilon_1}$ t,normalized values). No roots or poles of F exist off of the real axis between $(-k_2, -k_1)$ and between $(+k_1, +k_2)$. If the interval (k_1, k_2) on the positive real k_x axis is considered, the typical distribution of the singularities of ln[F] is shown in Figure 5.2.

Consider F as given in (5.2.7.b). Since k_1 and k_2 lie on the positive real k_x axis with $k_2 > k_1$, we observe that values of k_x in the interval (k_1, k_2) must have $\beta_1 = -j \phi(k_x)$ and $\beta_2 = + \psi(k_x)$ where ϕ, ψ are positive real functions. Substituting for β_1 and β_2 in (5.2.7.b), we see that F is purely real. Therefore if we consider the principal value of the logarithm for ln(F), the branch cuts required will connect respective roots with poles as shown in Figure 5.2 and lie on the real k_x axis. The logarithmic branch cuts are restricted to lie on (k_1, k_2) and similarly on $(-k_2, -k_1)$. We recall that $F \rightarrow 1$ as $|k_x| \rightarrow \infty$, so there are no logarithmic branch cuts running to $k_x = \infty$. It can be shown that a path in the k_x plane which encircles a pole and its adjacent root will not suffer an incrementing of the argument of F as the value of k_x moves around the path. Therefore we have adequately described ln(F) with the branch cuts

$$\text{FOR} \quad a < \pi/2: \quad \underset{K_1}{\text{O}\!\!\sim\!\!\!\times} \qquad\qquad\qquad \underset{K_2}{\square}$$

$$\pi/2 < a < \pi: \quad \square \quad \text{O}\!\!\sim\!\!\!\times \qquad\qquad \square$$

$$\pi < a < 3\pi/2: \quad \text{O}\!\!\sim\!\!\!\times \quad \text{O}\!\!\sim\!\!\!\times \qquad \square$$

$$3\pi/2 < a < 2\pi: \quad \square \quad \text{O}\!\!\sim\!\!\!\times \quad \text{O}\!\!\sim\!\!\!\times \, \square$$
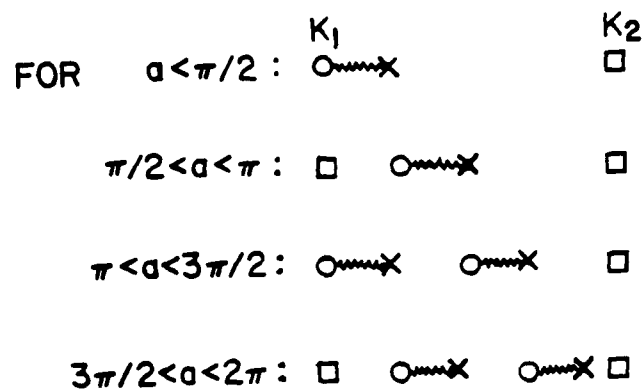
$\sim\!\!\sim\!\!\sim$	Branch cut of the logarithm
O	Root of F (and branch point of ln[F])
X	Pole of F (and branch point of ln[F])

Figure 5.2. Depiction of the branch cuts of ln[F] due to the root and pole progression of the function F in (5.2.7) as the thickness of the slab increases $(a = \sqrt{(\varepsilon_2 - \varepsilon_1)t^2}\,)$

described above using the principal value of the logarithm.

The integral factorization of F is given as

$$F_+(k_x) = \exp\left\{\frac{1}{2\pi j}\int_{\delta=-\infty}^{\infty}\frac{\ln(F)}{\delta-k_x}\,d\delta\right\} \text{ for } \tau = \text{Im}(k_x) = 0 \qquad (5.3.1)$$

where the path of integration is indented below $\delta = k_x$ as shown in Figure 5.3. As noted above $F(k_x) \to 1$ uniformly for $|k_x| \to \infty$, hence we can deform the path of integration of (5.3.1) to that shown in Figure 5.4. It is clear that with this deformed path

$$\int_{-\infty}^{\infty}\frac{\ln(F)}{\delta-k_x}\,d\delta = j2\pi\,\ln[F(k_x)]\cdot u(\sigma) + j2\pi H(k_x) \qquad (5.3.2)$$

$$\text{where } u(\sigma) = \begin{cases} 1 & , \ \sigma > 0 \\ \tfrac{1}{2} & , \ \sigma = 0 \\ 0 & , \ \sigma < 0 \end{cases} \quad \text{with } \sigma = \text{Re}(k_x)$$

and

$$H(k_x) = \frac{1}{2\pi j}\int_{-j\infty}^{j\infty}\frac{\ln[F(\delta)]}{\delta-k_x}\,d\delta \quad ,$$

Therefore,

$$F_+(k_x) = [F(k_x)]^{u(\sigma)} \cdot \exp\{H(k_x)\} \text{ for } \text{Im}(k_x) = 0. \qquad (5.3.3)$$

Let us consider the behavior of (5.3.2) for k_x off of the real axis. Since F is an even function, the integral can be reduced to

$$\int_{-j\infty}^{j\infty}\frac{\ln(F)}{\delta-k_x}\,d\delta = 2k_x\int_{0}^{j\infty}\frac{\ln(F)}{\delta^2-k_x^2}\,d\delta \ . \qquad (5.3.4)$$

Since $\ln(F(\delta)) \to 0$ as $|\delta| \to \infty$ and the integration path is removed from
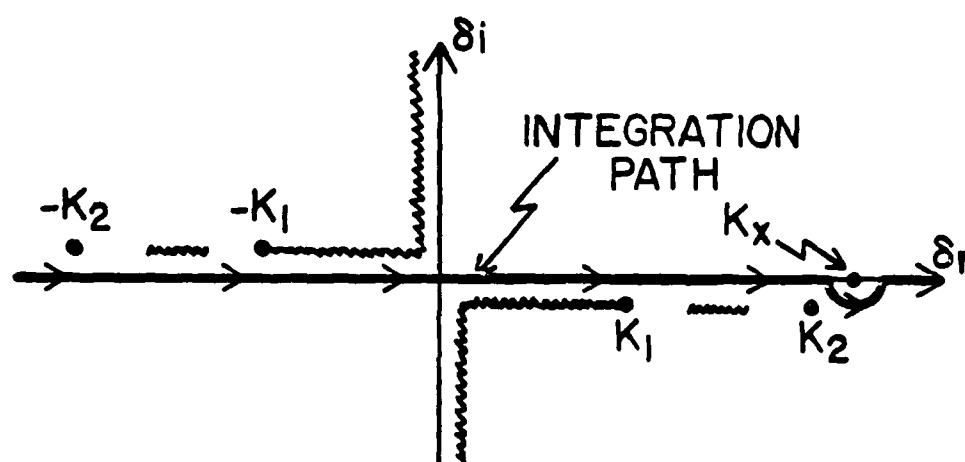
Figure 5.3.   Integration path for F_+.
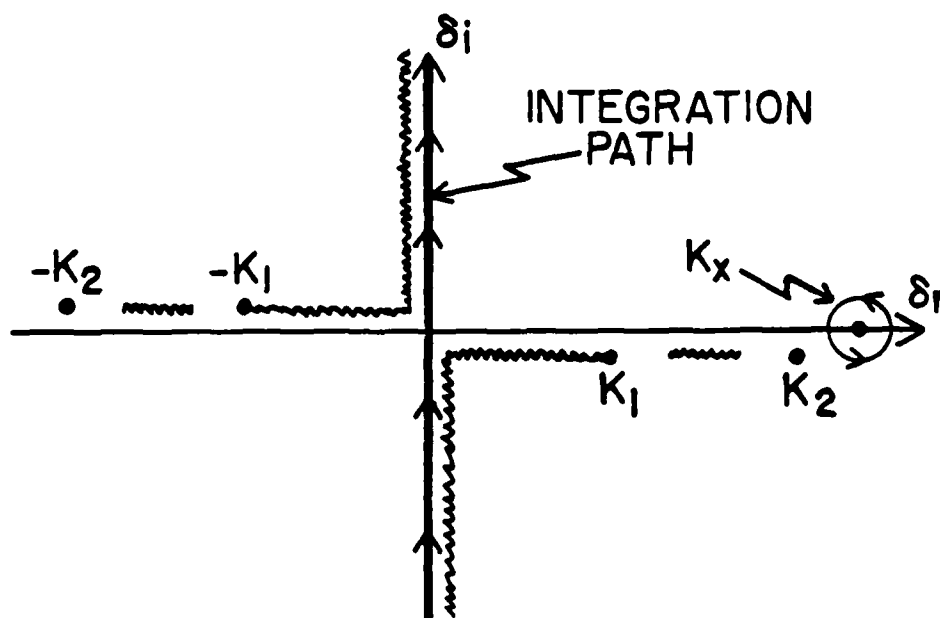
Figure 5.4. Deformed integration path for F_+.

any singularities of the integrand (as long as k_x is off of the imaginary δ axis), it is seen that

$$\left|\frac{\ln F}{\delta^2 - k_x^2}\right| \leq M/\left|\delta^2 - k_x^2\right|$$

for a suitably chosen constant M. Now the right hand side of (5.3.4) can be partitioned as

$$\int_0^{j[2\text{Im}(k_x)]} + \int_{j[2\text{Im}(k_x)]}^{j\infty}.$$

The first integral is clearly convergent for any k_x and for the second,

$$\frac{M}{\left|\delta^2 - k_x^2\right|} \leq \frac{M}{\left|\delta - k_x\right| \cdot \left|\delta\right|} \leq \frac{M}{\left|\frac{\delta}{2}\right| \cdot \left|\delta\right|}.$$

Therefore (5.3.4) is uniformly convergent and is a regular function for k_x off of the imaginary δ axis (see Mittra and Lee(1971), section 3.3). Hence if k_x is any point in the complex plane, then (5.3.2) applies and is the analytic continuation of the exponential factor of $F_+(k_x)$. Also (5.3.3) is the valid expression for the factorization of F for all points in the k_x plane.

Observe that with the expression given in (5.3.3), it is unnecessary to be concerned with the detailed behavior of the roots and poles of the function $F(k_x)$ in evaluating the integral $H(k_x)$. It is a straightforward operation to parameterize (5.3.4) using $\delta = j\cot(\pi t/2)$, for t on the interval (0, 1), to arrive at

$$2k_x \int_{\delta=0}^{j\infty} \frac{\ln\{F[\delta]\}}{\delta^2 - k_x^2} \, d\delta = 2k_x \int_{t=1}^{0} \frac{\ln\{F[\delta(t)]\}}{-\cot^2\left(\frac{\pi t}{2}\right) - k_x^2} \left[-j\,\frac{\pi}{2}\frac{dt}{\sin^2\left(\frac{\pi t}{2}\right)}\right]$$

$$= -j\pi k_x \int_{t=0}^{1} \frac{\ln F}{\cos^2\left(\frac{\pi t}{2}\right) + \left[k_x \sin\left(\frac{\pi t}{2}\right)\right]^2} \, dt \, . \quad (5.3.5)$$

Observe that (5.3.5) is an odd function of k_x implying that

$\exp\{(5.3.5)\} = 1$ for $k_x = 0$.

Some interesting observations can be made concerning the factorization process and how it works. In electromagnetics problems one often encounters a function $G(\varepsilon)$ which must be factorized and satisfies the following conditions:

1. G is an even function of ε.

2. The Wiener-Hopf strip includes the real ε axis.

3. G meets the conditions of the integral factorization theorem.

Then

$$G_+(\varepsilon) = \exp\left\{\frac{1}{2\pi j} \int_{\delta=-\infty}^{\infty} \frac{\ln G(\delta)}{\delta-\varepsilon} \, d\delta\right\} \qquad (5.3.6)$$

for ε in the Wiener-Hopf strip and $\text{Im}(\varepsilon) > 0$. When ε is extended into the rest of the complex plane, we have

$$G_+(\varepsilon) = \begin{cases} \exp\left[\dfrac{1}{2\pi j} \displaystyle\int_{-\infty}^{\infty} \dfrac{\ln G(\delta)}{\delta-\varepsilon}\right], & \text{Im}(\varepsilon) > 0 \\[3em] G(\varepsilon) \cdot \exp\left[\dfrac{1}{2\pi j} \displaystyle\int_{-\infty}^{\infty} \dfrac{\ln G(\delta)}{\delta-\varepsilon}\right], & \text{Im}(\varepsilon) < 0 \end{cases} \qquad (5.3.7)$$

If we consider only the integral in the exponential, then we observe that it must be an odd function of ε .

$$H(-\varepsilon) = \frac{1}{2\pi j} \int_{\delta=-\infty}^{\infty} \frac{\ln G(\delta)}{\delta-(-\varepsilon)} \, d\delta = \frac{1}{2\pi j} \int_{(-\delta)=\infty}^{-\infty} \frac{\ln[G(-(-\delta))]}{-[(-\delta)-\varepsilon]}[-d(-\varepsilon)]$$

$$= -\frac{1}{2\pi j} \int_{\gamma=-\infty}^{\infty} \frac{\ln G(-\gamma)}{\gamma-\varepsilon} \, d\gamma = -H(\varepsilon)$$

$$H(-\varepsilon) = -H(\varepsilon) \tag{5.3.8}$$

Therefore if we consider an ε such that $\text{Im}(\varepsilon) > 0$, then we have

$$G_+(-\varepsilon) = G(-\varepsilon) \cdot \exp[H(-\varepsilon)] = G(\varepsilon) \cdot \exp[-H(\varepsilon)] = G(\varepsilon)/G_+(\varepsilon). \tag{5.3.9}$$

Therefore if we accept $G_-(\varepsilon) = G_+(-\varepsilon)$ (as can be seen directly from the formula for the function G_-), then

$$G_+(\varepsilon) \cdot G_-(\varepsilon) = G(\varepsilon)$$

where G_+ is analytic in the upper half-plane and G_- is analytic in the lower half-plane. Since $H(\varepsilon)$ is analytic and therefore bounded, G_+ and G_- will be non-zero in their respective half-planes of analyticity.

We collect below the results for the factorization of the slab problem:

$$G_+(k_x) = F_+(k_x)/\sqrt{k_1 - k_x}$$

$$G_-(k_x) = F_-(k_x)/\sqrt{k_1 + k_x} \tag{5.3.10}$$

where the square root functions are interpreted as in section 2.2 and

$$F_+(k_x) = \begin{cases} F(k_x) \cdot \exp[H(k_x)], & \text{Re}(k_x) > 0 \\ \\ \exp[H(k_x)] & , \text{Re}(k_x) < 0 \end{cases} \qquad (5.3.10.a)$$

where

$$H(k_x) = -\frac{k_x}{2} \int_{t=0}^{1} \frac{\ln\{F[\delta(t)]\}}{\cos^2\left(\frac{\pi t}{2}\right) + [k_x \sin\left(\frac{\pi t}{2}\right)]^2} \, dt \quad , \qquad (5.3.10.b)$$

$$\delta(t) = j \cot\left(\frac{\pi t}{2}\right) ,$$

and $F(k_x) = (5.2.7.b)$ with $(k_x', t') \to (k_x, t)$,

$$F_-(k_x) = F_+(-k_x).$$

To complete the factorization analysis, it is necessary to determine the asymptotic behavior of $G_+(k_x)$ as $|k_x| \to \infty$. We consider first $H(k_x)$ as $|k_x| \to \infty$ along a ray, then

$$H(k_x) = -\frac{k_x}{2} \int_{t=0}^{1} \frac{\ln F}{\cos^2\left(\frac{\pi t}{2}\right) + [k_x \sin\left(\frac{\pi t}{2}\right)]^2} \, dt \sim -\frac{k_x}{2} \int_{t=0}^{1} \frac{\ln F}{k_x^2 \sin^2\left(\frac{\pi t}{2}\right)} \, dt$$

$$= \frac{M}{2k_x} \qquad (5.3.11)$$

since $\ln(F) \to 0$ as $t \to 0$. Therefore

$$F_+(k_x) = F(k_x) \cdot \exp(H(k_x)) \to 1 \cdot 1 \qquad (5.3.12)$$

and so

$$G_+(k_x) \sim |k_x|^{-\frac{1}{2}} \qquad \text{as } |k_x| \to \infty . \qquad (5.3.13)$$

A similar result applies for $G_-(k_x)$.

5.4 Decomposition

Having performed the factorization of the function $G(k_x)$ in (5.3.10), we proceed to the decomposition of the function A_+/G_-. As in the interface problem, this step can be carried out by inspection. The resulting functions are

$$S_-(k_x) = \frac{\psi}{G_-(k_x) \cdot (k_x + k_1 \cos\theta)} - \frac{\psi}{G_-(-k_1 \cos\theta) \cdot (k_x + k_1 \cos\theta)} \qquad (5.4.1)$$

and

$$S_+(k_x) = \frac{\psi}{G_-(-k_1 \cos\theta)(k_x + k_1 \cos\theta)} \qquad (5.4.2)$$

where $\psi = jF_\theta \cdot E_0$, defined in (5.2.7) and (5.2.11). The formal steps to complete the Wiener-Hopf analysis are similar to those given in section 3.5. Therefore the Fourier transform of the current on the PEC screen is

$$J_z(k_0 k_x) = \frac{1}{\omega\mu_0'\sqrt{\frac{\pi}{2}}} \Phi_+(k_x) = \frac{1}{\omega\mu_0'\sqrt{\frac{\pi}{2}}} \left[\left(\frac{\psi}{G_-(-k_1 \cos\theta)} \right) \frac{1}{G_+(k_x) \cdot (k_x + k_1 \cos\theta)} \right] .$$
$$(5.4.3)$$

To establish the radiation integral for this problem, it is necessary to reconsider the initial formulation. The procedure was to partition the fields of the problem into two components: the fields due to diffraction of the incident plane wave from the slab inhomogeneity with no PEC screen present and the fields radiated by the induced electric currents on the screen. Therefore

$$e_z^{total} = e_z^{NP} + e_z^{Rad} \quad , \qquad (5.4.4)$$

where e_z^{NP} is the field structure due to the incident wave with no PEC screen present and e_z^{Rad} is the radiated field structure of the currents on the PEC.

The expression for e_z^{NP} is given in (5.2.8) and will not be considered further. The expression for e_z^{Rad} is given in (5.2.1) with the kernel given in (5.2.4) and (5.2.6) but with $y \neq 0$. In the sections which follow the asymptotic evaluation of the radiation integral is considered for the two half-spaces involving medium 1.

The asymptotic expansion of the field in the slab itself will consist of modal waves propagating in the positive and negative x directions. While these fields are certainly of interest, they are left for future work.

5.5 Asymptotic Evaluation of the Radiation Integral for the Reflection Region (y > 0)

The Fourier transform of the radiation integral for the reflection region is written as

$$E_z^{Rad}(k_x',y') = F\left\{e_z^{Rad}\right\} = F\left\{\int_{x_0'=0}^{\infty} j_z(x_0') \cdot g^{refl}(x',x_0',y')dx_0'\right\}$$

$$= J_z(k_x') \cdot [\sqrt{2\pi} \; G^{refl}(k_x',y')] \qquad (5.5.1)$$

$$= \phi_+^u(k_x') \cdot \frac{-\omega\mu_0'}{2} G(k_x')e^{-j\beta_1'y'} \quad \text{where } G(k_x') = \frac{F(k_x')}{\beta_1'} \; ,$$

When converted to normalized coordinates, we have

$$E_z^{Rad}(k_x,y) = \frac{-1}{\sqrt{2\pi}\,k_0}\ \Phi_+(k_x)\cdot G(k_x)e^{-j\beta_1 y} \quad \text{where } y = k_0 y'. \quad (5.5.2)$$

Now the radiation integral itself is the inverse Fourier transform of (5.5.1),

$$e^{Rad}(x',y') = F^{-1}\left\{E_z^{Rad}\right\} = \frac{1}{\sqrt{2\pi}}\int_{-\infty}^{\infty} E_z^{Rad}\cdot e^{-jk_x' x'}\,dk_x'\ . \quad (5.5.3)$$

Again reverting to normalized coordinates,

$$e_z^{Rad}(x,y) = \frac{-1}{2\pi}\int_{-\infty}^{\infty}\Phi_+(k_x)\cdot G(k_x)e^{-j(\beta_1 y + k_x x)}\,dk_x$$

$$= \frac{-1}{2\pi}\int_{\infty}^{\infty}\left\{\left[\frac{\psi}{G_-(-k_1\cos\theta)}\right]\frac{1}{(k_x + k_1\cos\theta)\cdot G_+(k_x)}\right\}G(k_x)e^{-j(\beta_1 y + k_x x)}\,dk_x. \quad (5.5.4)$$

Substituting for ψ from the definition following (5.4.2), we arrive at

$$e_z^{Rad}(x,y) = \xi\int_{-\infty}^{\infty}\frac{G_-(k_x)}{(k_x + k_1\cos\theta)}\,e^{-j(\beta_1 y + k_x x)}\,dk_x, \quad (5.5.5)$$

where

$$\xi = \frac{-j\ E_0 k_1\sin\theta\ G_+(-k_1\cos\theta)}{2\pi}$$

and $(G_+,\ G_-)$ are the factorizations discussed in section 5.3.

The integral in (5.5.5) can now be transformed into one in the angular spectral domain using the substitution, $k_x = k_1\sin(\alpha)$, to give

$$e_z^{Rad}(\rho,\phi) = \int_\Gamma \frac{\cos(\alpha) \cdot G_-(k_1\sin\alpha)}{(\sin\alpha + \cos\theta)} e^{-jk_1\rho\sin(\alpha+\phi)} \qquad (5.5.6)$$

where ϕ is the angle of observation $(0 < \phi < \pi)$. The saddle point for (5.5.6) is given by $\alpha_s = (\pi/2)-\phi$ and the equation for the SDP is given by (A.5.2) with ϕ replaced by $-\phi$ and $k_i = 0$; that is,

$$\cos(u-u_s)\cosh(v) = 1 \qquad (5.5.7)$$

where u_s is the saddle point location and $\alpha = u+jv$. The integrand of (5.5.6) contains no branch cuts since the mapping removes the β_1 branch cuts and β_2 has none. Therefore the singularities are as follows:

1. <u>Geometrical Optics Pole</u> – Root of $(\sin\alpha + \cos\theta)$. It is clear that this pole lies on the real α axis between $-(\pi/2)$ and $+(\pi/2)$.

2. <u>Poles of G_-</u> – Lie on the line $u = -(\pi/2)$, $v < 0$ between $\alpha = -(\pi/2)$ and the mapping of $-k_2$.

Forming the asymptotic form of the steepest descent integral for (5.5.6) through the saddle point proceeds as in the foregoing analysis and is given by

$$(e_z^{Rad})_{SDP} \sim \left[-j\sqrt{\frac{k_1}{2\pi}} \frac{\sin\theta\sin\phi\, G_-(k_1\cos\theta)\, G_-(k_1\cos\phi)}{(\cos\theta + \cos\phi)} E_0 e^{j\pi/4} \right] \frac{e^{-jk_1\rho}}{\sqrt{\rho}} .$$
$$(5.5.8)$$

Similarly the analysis leading to the residue contribution of the geometrical optics pole is straightforward and results in

$$(e_z^{Rad})_{g.o.} = -j2\pi\,\xi\,G_-(-k_1\cos\theta)e^{jk_1\rho\cos(\theta+\phi)} . \qquad (5.5.9)$$

Observe that the geometrical optics contribution suffers no decay as ρ increases and will therefore dominate the saddle point contribution if it is present. As in the classical Sommerfeld half-plane diffraction problem, the diffraction term is only important in the shadow region of the problem.

To formulate the residue contribution for the poles of $G_-(k_1 \sin\alpha)$, it is necessary to determine

$$\lim_{\alpha \to \alpha_p} \{(\alpha - \alpha_p) \, G_-(k_1 \sin\alpha)\} = H(\alpha_p). \qquad (5.5.10)$$

To evaluate (5.5.10), G_- is reconstructed as G/G_+ and it is recognized that G_+ is analytic and well-behaved at α_p.

$$H(\alpha_p) = \lim_{\alpha \to \alpha_p} \left\{ (\alpha - \alpha_p) \, \frac{G(k_1 \sin\alpha)}{G_+(k_1 \sin\alpha)} \right\}$$

$$= \frac{1}{G_+(k_1 \sin\alpha_p)} \lim_{\alpha \to \alpha_p} \{(\alpha - \alpha_p) \, G(k_1 \sin\alpha)\} \qquad (5.5.11)$$

Using (5.2.7.b) for $G = F/\beta_1$, we have

$$H(\alpha_p) = \left[\frac{2(j\beta_1(\alpha_p) + \beta_2(\alpha_p) \cdot \cot(\beta_2(\alpha_p) \cdot t)}{G_+(k_1 \sin\alpha_p)} \right]$$

$$\times \lim_{\alpha \to \alpha_p} \left\{ \frac{\alpha - \alpha_p}{j[\beta_1^2(\alpha) + \beta_2^2(\alpha)] + 2 \cdot \beta_1(\alpha) \cdot \beta_2(\alpha) \cdot \cot(\beta_2(\alpha) \cdot t)} \right\}.$$

$$(5.5.12)$$

Applying L'Hospital's rule to (5.5.12) and recognizing that the denominator in the braces in (5.5.12) is zero for $\alpha = \alpha_p$, we arrive at

$$\lim_{\alpha \to \alpha_p} \left\{ \frac{\alpha - \alpha_p}{[\ ]} \right\} = \frac{-j2\beta_{1p}(2+j\beta_{1p}t)\sin\alpha_p}{\sin^2(\beta_{2p}t)} , \qquad (5.5.13)$$

where $\beta_{1p} = \beta_1(\alpha_p)$ and $\beta_{2p} = \beta_2(\alpha_p)$. Using (5.5.12) and (5.5.13), the residue contribution for the surface wave poles is

$$(e_z^{Rad})_{G_-} = j2\pi\xi \frac{\cos(\alpha_p) \cdot H(\alpha_p)}{[\sin(\alpha_p)+\cos\theta]} e^{-jk_1\rho\sin(\alpha_p+\phi)}$$

$$= -2\pi\xi \frac{\sin^2(\beta_{2p}t)[j\beta_{1p}+\beta_{2p}\cot(\beta_{2p}t)] e^{-jk_1\rho\sin(\alpha_p+\phi)}}{k_1\beta_{1p}(2+j\beta_{1p}t) \ G_+(k_1\sin\alpha_p) \cdot \tan(\alpha_p) \cdot (\sin(\alpha_p)+\cos\theta)}$$

$$(5.5.14)$$

Note that (5.5.14) exhibits the exponential decay factor,

$$e^{-k_1\rho \sin\phi \sinh |v_p|} ,$$

where $\alpha_p = -(\pi/2)+jv_p$. Therefore at large ρ the surface wave contributions are dominated by both of the other two components. This is not surprising since large ρ implies an observation point far from the slab while the surface waves are confined to the region near the slab's surface.

Since the geometrical optics pole is present in every problem and lies on the real α axis between $-(\pi/2)$ and $(\pi/2)$, it is necessary to formulate a uniform asymptotic expansion for the SDP contribution to the radiated field when the saddle point is near the geometrical optics pole. This result is given below:

$$(e_z^{Rad})_{SDP \atop unif} \sim \sqrt{\pi} \; \xi \; e^{-jk_1\rho}$$

$$\times \left\{ \text{sgn}(\theta+\phi-\pi)G_-(-k_1\cos\theta)e^{j2k_1\rho\cos^2\left(\frac{\theta+\phi}{2}\right)} \right.$$

$$\times \; Q\left[\sqrt{2k_1\rho}\left|\cos\left(\frac{\theta+\phi}{2}\right)\right|e^{j\pi/4}\right]$$

$$\left. + \frac{e^{j\pi/4}}{\sqrt{k_1\rho}}\left[\frac{\sqrt{2}\;\sin\phi\;G_-(k_1\cos\phi)}{(\cos\phi+\cos\theta)} - \frac{G_-(-k_1\cos\theta)}{\sqrt{2}\;\cos\left(\frac{\theta+\phi}{2}\right)}\right]\right\} \quad , \qquad (5.5.15)$$

where $Q(y)$ is given in (4.1.17.a).

Before moving on to the fields for the transmitted region $(y < -t)$, the following observation can be made. Recall from (5.4.4) the partitioning of the fields in the problem. For $y > 0$ the fields, which arise from the diffraction of the incident plane wave off of the slab with the PEC screen removed, can be written as

$$e_z^{NP} = e_z^{inc} + e_z^{refl} = E_0 \; e^{jk_1(x\cos\theta + y\sin\theta)} \qquad (5.5.16.a)$$

$$+ E_0(F_\theta - 1)e^{jk_1(x\cos\theta - y\sin\theta)}$$

where $F_\theta = F(k_1\cos\theta)$ with F defined in (5.2.7) or can be written as

$$e_z^{NP} = E_0 \, e^{jk_1 \rho \cos\theta \cos\phi} \, [j2\sin(k_1 \rho \sin\theta \sin\phi)]$$
$$+ E_0 k_1 \sin\theta \cdot G(k_1 \cos\theta) \, e^{jk_1 \rho \cos(\theta+\phi)} \quad . \qquad (5.5.16.b)$$

Observe that the second term of (5.5.16.b) is canceled by the geometrical optics contribution (5.5.9) in the shadow region for observation angles such that the geometrical optics pole is crossed, $\phi > (\pi - \theta)$. See Figure 5.5. The term in (5.5.16.b) which is canceled is the reflection which would be seen from a PEC screen covering the entire upper interface of the slab. Since the actual screen is only a half-plane, this geometrical optics field is forced to zero in the shadow region, but the correction term (compensating between the slab and a PEC sheet) represented by F_θ remains.

5.6 Asymptotic Evaluation of the Radiation Integral for the Transmission Region ($y < -t$)

To begin the asymptotic evaluation of the radiation integral, it is necessary to form the Fourier transform of the Green's function for the transmission region. This is done using (5.2.4) and (5.2.6) to arrive at

$$G^{tran}(k_x, y) = \sqrt{\frac{2}{\pi}} \, \eta_0 \, e^{j\beta_1 t} \left\{ \frac{\beta_2}{(\beta_1 - \beta_2)^2 e^{-j\beta_2 t} - (\beta_1 + \beta_2)^2 e^{j\beta_2 t}} \right\} e^{j\beta_1 y} \qquad (5.6.1)$$

where normalized coordinates are used and $\eta_0 = \sqrt{\mu_0/\epsilon_0}$. Now the radiated field is given by the inverse Fourier transform (in normalized coordinates),
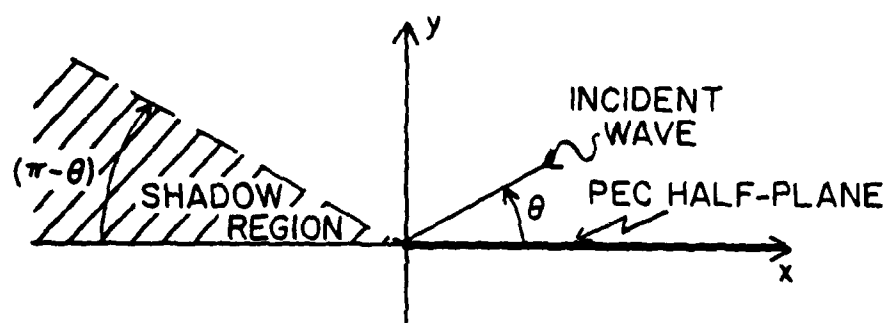
Figure 5.5. Geometrical optics field structure in
the reflection region.

$$e_z^{Rad}(x,y) = F^{-1}\{J(k_x') \cdot [\sqrt{2\pi}\ G^{tran}(k_{x,y})]\}$$

$$= k_0 \int_{-\infty}^{\infty} \left[\frac{\Phi_+(k_x)}{\omega\mu_0'\sqrt{\frac{\pi}{2}}}\right] \cdot \left[G^{tran}(k_{x,y})\right]\ e^{-j\,k_x x}\ dk_x$$

$$= -2\ \xi \cdot \int_{-\infty}^{\infty} \frac{G_-(k_x)\ \beta_2\ e^{j\beta_1 t}}{(k_x+k_1\cos\theta)[(\beta_1-\beta_2)e^{-j\beta_2 t} - (\beta_1+\beta_2)e^{j\beta_2 t}]}$$

$$\times\ e^{j(\beta_1 y - k_x x)}dk_x \quad . \tag{5.6.2}$$

where ξ is given in (5.5.5).

Before proceeding we note the singularities of the integrand of (5.6.2). As in the radiation integral for the reflection region, this integral has a geometrical optics pole at the root of $(k_x+k_1\cos\theta)$. For values of k_x with $\tau = \text{Im}(k_x) < 0$ (or if $\tau = 0$, then $\sigma = \text{Re}(k_x) > 0$), $G_-(k_x)$ is analytic and non-zero. Therefore the roots of the bracketed expression in the denominator of (5.6.2) with $\sigma > 0$ (which lie on the positive real k_x axis between k_1 and k_2) are poles of the integrand. While the symmetric roots with $\sigma < 0$ are canceled by the corresponding roots of G_-. However for $\sigma < 0$, $G_-(k_x)$ has poles of its own. Therefore exclusive of the geometrical optics pole, the integrand has poles at the poles of $G_-(k_x)$ which lie between $-k_2$ and $-k_1$ and poles at the roots of the

denominator factor which lie between k_1 and k_2. These poles correspond
to the surface waves for the slab problem.

It is interesting to note that for $\sigma < 0$ the pole locations corre-
spond to the surface waves for a slab of thickness t and must propagate
in the negative x direction. Clearly the field, which is launched by
the presence of the PEC screen, that propagates in the negative x direc-
tion from the edge of the PEC screen, must be a surface wave for the
slab. On the other hand the waves moving in the positive x direction
must characterize the surface waves for a slab of thickness (2t) due to
the imaging of the slab through the PEC screen. In fact, the pole reso-
nances for $\sigma > 0$, which characterize the waves propagating in positive x
direction, show just this behavior since they are roots of G_- and hence
roots of the numerator of G. These details are discussed in Appendix D.

To conveniently evaluate the poles of (5.6.2) exclusive of the
geometrical optics pole, two alternative forms can be used.

$$e_z^{Rad}(x,y) = -2\,\xi \int_{-\infty}^{\infty} \frac{\beta_2\, e^{j\beta_1 t}}{(k_x + k_1\cos\theta)}\, B(k_x)\, e^{j(\beta_1 y - k_x x)}\, dk_x \qquad (5.6.3.a)$$

with

$$B(k_x) = \begin{cases} \dfrac{G_-(k_x)}{[(\beta_1-\beta_2)e^{-j\beta_2 t} - (\beta_1+\beta_2)e^{j\beta_2 t}]} & ,\ \sigma > 0 \\[4em] \dfrac{2}{G_+(k_x)[(\beta_1-\beta_2)^2 e^{-j\beta_2 t} - (\beta_1+\beta_2)^2 e^{j\beta_2 t}]} & ,\ \sigma < 0 \end{cases} \qquad \bullet\ (5.6.3.b)$$

Moving to the spectral domain using the mapping, $k_x = k_1 \sin \alpha$, the radiation integral becomes

$$e_z^{Rad}(\rho,\phi) = -2\,\xi \int_\Gamma \frac{\beta_2 \cdot \cos\alpha \cdot e^{jk_1 t \cos\alpha}}{(\sin\alpha + \cos\theta)} B(k_1 \sin\alpha)$$

$$\times e^{-jk_1\rho\sin(\alpha-\phi)}\, d\alpha \qquad (5.6.4)$$

where ϕ is the observation angle with respect to the PEC half-plane $(-\pi < \phi < 0)$. The integration in the α plane is shown in Figure 5.6 (where the integration path is offset for clarity).

The asymptotic form of the saddle point integration is

$$(e_z^{Rad})_{SDP} \sim 2\,\xi \sqrt{\frac{2\pi}{k_1\rho}} \left[\frac{\beta_2(k_1\cos\phi) \cdot \sin\phi \cdot e^{(-jk_1 t\sin\phi + j\frac{\pi}{4})}}{(\cos\phi + \cos\theta)} B(k_1\cos\phi) \right] e^{-jk_1\rho}\,. \qquad (5.6.5)$$

The residue contribution for the geometrical optics pole is

$$(e_z^{Rad})_{\substack{g.o. \\ pole}} = j(4\pi\xi)[\beta_2(-k_1\cos\theta) \cdot B(-k_1\cos\theta)e^{jk_1 t\cos\theta}]$$

$$\times e^{jk_1\rho\cos(\theta-\phi)}\,. \qquad (5.6.6)$$

The geometrical optics pole is captured in the deformation of the integration path for $\phi > (\theta-\pi)$.

Finally the residue contribution for the surface wave poles must be given. Clearly the integration path must indent to the right of the poles when $Re(\alpha_p) < 0$ and to the left of the poles when $Re(\alpha_p) > 0$. When the residue is formed, the result is
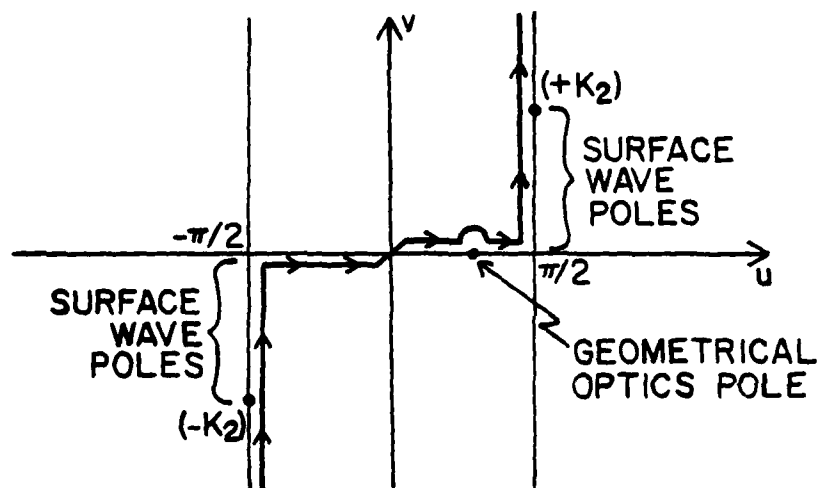
Figure 5.6.   Integration path for the radiation integral.

$$(e_z^{Rad})_{pole} = (SIGN) \cdot (j4\pi\xi) \left\{ \frac{\beta_2(\alpha_p) \cdot \cos \alpha_p \, e^{jk_1 t \cos(\alpha_p)}}{[\sin(\alpha_p) + \cos\theta]} \, e^{-jk_1 \rho \sin(\alpha_p - \phi)} \right\}$$

$$\times \lim_{\alpha \to \alpha_p} \, [(\alpha - \alpha_p) \cdot B(k_1 \sin\alpha)] \qquad (5.6.7)$$

where

$$SIGN \equiv 1 \quad \text{for } Re(\alpha_p) = \pm \frac{\pi}{2} \quad .$$

The limit in (5.6.7) must now be evaluated. Consider the case when $Re(\alpha_p) = -(\pi/2)$, then

$$\lim_{\alpha \to \alpha_p} [(\alpha - \alpha_p) \cdot B(k_1 \sin\alpha)] = \frac{2}{G_+(k_1 \sin \alpha_p)} \lim_{\alpha \to \alpha_p} \left[\frac{\alpha - \alpha_p}{[(\beta_1 - \beta_2)^2 e^{-j\beta_2 t} - (\beta_1 + \beta_2)^2 e^{j\beta_2 t}]} \right]$$

$$(5.6.8)$$

Applying L'Hospital's rule to the limit expression and simplifying,

$$(e_z^{Rad})_{pole} = \left[\frac{j4\pi\xi\beta_{2p}^2 \cot \alpha_p \, e^{j(\beta_{1p} - \beta_{2p})t}}{k_1(\sin \alpha_p + \cos\theta)} \, e^{-jk_1 \rho \sin(\alpha_p - \phi)} \right]$$

$$\times \left[\frac{-1}{(2 + j\beta_{1p} t)(\beta_{1p} + \beta_{2p})^2 G_+(k_1 \sin \alpha_p)} \right] e^{-jk_1 \rho} \qquad (5.6.9)$$

for $Re(\alpha_p) = -(\pi/2)$, where $\beta_{1p} = \beta_1(\alpha_p)$ and $\beta_{2p} = \beta_2(\alpha_p)$. A similar analysis to that used in (5.6.8) and (5.6.9) but using the other expansion for $B(k_1 \sin(\alpha))$, given following (5.6.3), results in

$$
(e_z^{Rad})_{pole} = \left[\frac{j4\pi\xi\beta_{2p}^2 \cot \alpha_p \; e^{j(\beta_{1p}-\beta_{2p})t}}{k_1(\sin \alpha_p + \cos\theta)} \; e^{-jk_1\rho\sin(\alpha_p-\phi)} \right]
$$

$$
\times \left[\frac{G_-(k_1\sin \alpha_p)}{2(\beta_{1p}+\beta_{2p})(1+j\beta_{1p}t)} \right] \qquad (5.6.10)
$$

for $Re(\alpha_p) = +(\pi/2)$.

As in the asymptotic analysis for the reflection region, it is necessary to give the uniform asymptotic expansion for the saddle point contribution since the geometric optics pole will approach the saddle point as ϕ approaches $(-\pi+\theta)$. The result is as follows:

$$(e_z^{Rad})_{\substack{SDP \\ unif.}} \sim + 2\xi\, e^{-jk_1\rho}$$

$$\times \left\{ \operatorname{sgn}(\theta-\phi-\pi)\, j2\sqrt{\pi}\beta_{2g}\, e^{jk_1 t\sin\theta}\, B(-k_1\cos\theta)e^{j2k_1\rho\cos^2(\frac{\theta-\phi}{2})} \right.$$

$$\times\, Q[\sqrt{2k_1\rho}|\cos(\tfrac{\theta-\phi}{2})|\quad e^{j\pi/4}]$$

$$+ \sqrt{\frac{\pi}{k_1\rho}}\, e^{j\pi/4} \left[\sqrt{2}\left(\frac{\beta_{2s}\cdot\sin\phi\cdot B(k_1\cos\phi)\, e^{-jk_1 t\sin\phi}}{\cos\phi + \cos\theta}\right)\right.$$

$$\left.\left. + \frac{\beta_{2g}\, B(-k_1\cos\theta)\, e^{jk_1 t\sin\theta}}{\sqrt{2}\,\cos(\frac{\theta-\phi}{2})}\right]\right\} \quad , \tag{5.6.11}$$

where $Q(y)$ is given in (4.2.17a), $\beta_{2g} = \beta_2(\alpha_{go})$ and $\beta_{2s} = \beta_2(\alpha_s)$.

Finally for convenience, the portion of the total field in the transmitted region due to the incident plane wave with the PEC screen

removed is

$$e_z^{NP}(\rho,\phi) = \frac{-4E_0\beta_1\beta_2 \, e^{j\beta_1 t}}{[(\beta_1-\beta_2)^2 e^{-j\beta_2 t} - (\beta_1+\beta_2)^2 e^{j\beta_2 t}]} \, e^{jk_1\rho\cos(\theta-\phi)} \qquad (5.6.12)$$

where $\beta_1 = k_1\sin(\theta)$, $\beta_2 = k_2\sin(\theta_2) = \sqrt{k_2^2 - k_1^2 \cos^2(\theta)}$.

CHAPTER VI

CONCLUSIONS

The objective of this study is the solution for the scattering of an electromagnetic plane wave from a PEC half-plane in the presence of planar media discontinuities. Two specific geometries are addressed. The interface problem represents a basic canonical configuration in this class of problems while the slab problem is one of practical interest. The case of TM incident polarization was chosen as manifesting all the primary characteristics of interest. It is the author's belief that the TE polarization will not manifest any new phenomena. In particular, the functions to be factorized in the interface problem are very similar to that of the case considered in Chapter III. Based on this it is asserted that the analysis presented here can be generalized to the other polarization.

In the interface problem the analysis leading to the radiation integral for the TM polarized wave is given along with an efficient form of the integral factorization. The asymptotic formulation of the various far field contributors is given. Numerical data is presented at the end of Chapter IV to demonstrate the behavior of the various field contributors as parameters are changed. It is seen that a diffracted cylindrical wave is launched from the edge of the half-plane which is similar to the wave described by the Keller diffraction coefficient as the media

149

contrast is eliminated. An interesting feature of the diffracted wave for the interface problem is the decrease in the radiation field as the observation angle approaches the interface. This condition is seen to be necessary for the total solution to provide a continuous tangential electric field across the interface.

The typical geometrical optics field for the interface problem is seen to reflect and refract according to the theory of geometrical optics. A peculiar feature of the interface problem is the launching of a lateral wave which is seen to have its peak amplitude in the more dense medium (which is defined as the medium having the greater real part of its wave-number). Finally, the theory indicates the possibility of a pole term which appears to be similar to the Zenneck pole. An example of this pole has not been found which contributes significantly to the asymptotic field.

The analysis of the slab problem is presented in Chapter V. In this case no lateral wave is present but surface waves are launched instead. The asymptotic analysis has been performed for the media surrounding the slab but is not presented for the slab itself as a self-consistent expansion has not yet been found. No data is presented for this case.

While this investigation has laid the foundations for study of the interface and slab geometries, it has by no means exhausted even the theoretical topics of interest. In the interface problem the issue remains concerning the possibility of a Zenneck-like pole contribution. While this pole occurs in the TM case only if the media have dissimiliar permeabilities, it may occur in the TE case for media which have

differing permittivities and is therefore of importance in the TE case.

Another area of future work would be the development of the uniform

asymptotic expansion of the saddle point integral in the presence of a

branch point. The data given in Chapter IV seems to imply that the local

disturbance in the diffracted cylindrical wave due to the lateral wave

is representative of the field structure at small observation radii even

though the formal mathematics of asymptotic theory breaks down. It

would be useful to confirm this conjecture. Clearly, another avenue of

possible work would be to perform the analysis for the TE case. In the

slab problem numerical implementation remains to be performed. The a-

symptotic expansion of the field structure in the slab also must be per-

formed and the work completed indicates that an explicit modal field

will result.

The form of the solutions is structured to generate the ray-type

diffraction coefficients needed for GTD analysis. While the diffracted

cylindrical wave and the geometrical optics field behave as simple homo-

geneous waves, the lateral wave and Zenneck-type pole wave are inhomogen-

eous plane waves and will require an extension of the GTD to include

scattering of complex rays in order to be utilized. It is hoped that

this work provides a clear demonstration that the numerical evaluation

of the formal Wiener-Hopf factorization integrals is a feasible process

for generating ray-optic solutions to complex scattering geometries.

The application of the GTD to model lap junctions between metallic and

composite dielectric sheets is a relatively straightforward result of

this work.

APPENDIX A

CHARACTERISTIC EQUATIONS OF THE
MAPPING $k_x = k \sin \alpha$

A.1 Introduction

The purpose of this appendix is to establish the principal results which determine the mapping of significant curves in the complex k_x plane onto the α plane. In the mapping we take $k = k_r - jk_i$ as the complex wave number of the medium of observation and define $\alpha = u + jv$. The mapping is written as follows:

$$\sigma + j\tau = (k_r - jk_i)\sin(u+jv) = (k_r - jk_i)(\sin u \cosh v + j \cos u \sinh v)$$

$$\sigma = k_r \sin u \cosh v + k_i \cos u \sinh v \; ; \; \tau = k_r \cos u \sinh v - k_i \sin u \cosh v .$$

$$(A.1.1)$$

Note that (A.1.1) maps the entire k_x plane into a finite-width strip in the α plane and that the α plane is periodic in its real part with period 2π. These results are based on the assumption that both media are lossy in the problem treated.

It is also of interest to provide an inverse mapping from the top sheet of the k_x plane onto the α plane. This is given by

153

$$\alpha_{\substack{\text{top} \\ \text{sheet}}} = -j \; \ell n \left[j\left(\frac{k_x}{k}\right) + \frac{\beta}{k} \right] \qquad \text{(A.1.2)}$$

where ℓn is the principal value of the logarithm, i.e. if $Arg(\ell n) = \theta$ then $-\pi < \theta < \pi$ and $\beta = \sqrt{k^2 - k_x^2}$ as defined in Section 2.2.

A.2 Real and Imaginary k_x Axes

By setting the real and imaginary parts of (A.1.1) to zero, we arrive at mappings of the axes in the k_x plane onto the α plane. The real axis is mapped into the contour defined by

$$\tanh(v) = (k_i/k_r)\tan(u). \qquad \text{(A.2.1)}$$

From this formula it is clear that the mapping of the real k_x axis (about $\alpha = 0$) lies in the regions of the α plane characterized by $(u,v) > 0$ and $(u,v) < 0$ for any media to be considered. Also the origin in the k_x plane corresponds to the origin in the α plane.

The imaginary k_x axis maps into

$$\tanh(v) = -(k_r/k_i) \tan(u) \qquad \text{(A.2.2)}$$

Therefore the imaginary k_x axis maps into the two regions in the α plane which do not contain the real axis mapping.

A.3 Hyperbolic Branch Cuts for k

The branch cuts for $\pm k$ in the k_x plane can be shown to "open up" so that no branch cuts for β are required in the α plane. The multiplicity of function values for β as k_x migrates between the two sheets of the k_x

plane is manifested in the periodicity in $\text{Re}(\alpha)$ under the mapping. However the mappings of the branch cuts on the α plane delimit the boundaries of the top sheet of the function $\sqrt{k^2 - k_x^2}$.

The branch of $\beta = \sqrt{k^2 - k_x^2}$ is given by $\text{Im}(\beta) < 0$. Therefore the branch cut lies on $\text{Im}(\beta) = 0$.

$$\text{Im}(\beta) = \text{Im}(\sqrt{k^2(1 - \sin^2(\alpha))}) \qquad (A.3.1)$$

$$= -k_r \sin(u)\sinh(v) - k_i \cos(u)\cosh(v) = 0$$

Hence

$$-(k_i/k_r) = \tan(u)\tanh(v) \qquad (A.3.2)$$

After some simple manipulation we find that the curves in the α plane which correspond to the branch cuts from $\pm k$ in the k_x plane are given by

$$\tanh(v) = (k_i/k_r) \tan(u \pm \pi/2). \qquad (A.3.3)$$

These lines correspond to the mapping of the real k_x axis onto the α plane but offset by $\pm(\pi/2)$ along the u axis. This region corresponds to the top sheet of the functions involving β. Therefore these lines together with the mappings of the real and imaginary k_x axes divide the top sheet region of the α plane into the mappings of the four quadrants in the k_x plane.

A.4 Hyperbolic Branch Cut for $(-k_{op})$

The integrands in the field integrals arising in the interface problem will involve the factorization function $G_-(k_x)$ which contains

functions with the original hyperbolic branch cut for β_{op} extending from $k_x = -k_{op}$. (We have chosen to use k as the wave number of the observation medium, therefore k_{op} is the wave number for the opposing medium). Hence it is necessary to determine the position of the mapping of this branch cut.

As in the case of the branch cuts for β, the β_{op} branch cuts lie along the curve $\text{Im}(\beta_{op}) = \text{Im}(\sqrt{k_{op}^2 - k_x^2}) = 0$. So β_{op}^2 must be positive and real for points on the cut. Therefore

$$\text{Im}(\beta_{op}^2) = \text{Im}(k_{op}^2 - k^2 \sin^2(\alpha)) = 0$$

yields the defining equation for the locus of points on the β_{op} branch cut,

$$(k_{op,r})(k_{op,i}) + (k_r^2 - k_i^2)(\sin u \cos u \sinh v \cosh v) =$$

$$(k_r k_i)(\sin^2 u \cosh^2 v - \cos^2 u \sinh^2 v) \qquad (A.4.1)$$

where $k_{op} = k_{op,r} - jk_{op,i}$ and $k = k_r - jk_i$.

After algebraic manipulations, we arrive at

$$a^2 - 2ab \sin(2u)\sinh(2v) + b^2 \sin^2(2u)\sinh^2(2v) = \cos^2(2u)\cosh^2(2v)$$

$$[b^2\sin^2(2u) - \cos^2(2u)]\sinh^2(2v) - [2ab \sin(2u)]\sinh(2v) + [a^2 - \cos^2(2u)] = 0$$

$$(A.4.2)$$

where $a = 1 - 2(k_{op,r} \cdot k_{op,i})/(k_r \cdot k_i)$,

and $b = (k_r^2 - k_i^2)/(2 \cdot k_r \cdot k_i)$.

Applying the quadratic formula and simplifying:

$$\sinh(2v) = \frac{1}{[(b\sin(2u))^2 - \cos^2(2u)]} \left[ab\ \sin(2u) \right.$$

$$\left. \pm |\cos(2u)|\ \sqrt{(a^2-1) + (b^2+1)\sin^2(2u)} \right] \quad , \qquad (A.4.3)$$

where the correct sign for the square root must be chosen. The analysis for choosing the appropriate sign of (A.4.3) is straightforward and the results are given below.

For $|a| > 1$,

$$\sinh(2v) = \frac{1}{[(b\sin(2u))^2 - \cos^2(2u)]} \times$$

$$\left[ab\ \sin(2u) - \text{sgn}\left(\frac{\pi}{4} + u\right) \cdot \text{sgn}\left(\frac{3\pi}{4} + u\right) \right.$$

$$\left. \times |\cos(2u)|\sqrt{(a^2-1) + (b^2+1)\sin^2(2u)} \right] \qquad (A.4.4)$$

for $(-\pi + \tan^{-1}(k_i/k_r)) < u < u_{(k_x = -k_{op})}$ and $v < 0$.

where sgn is the signum function.

For $|a| < 1$,

$$\cos(2u) = \frac{a - b\ \sin(2u)\sinh(2v)}{\cosh(2v)} \qquad (A.4.5.a)$$

for $v \geq v_{(k_x = -k_{op})}$ and $-(\pi/2) < u < 0$,

where

$$\sin(2u) = \frac{1}{[\cosh^2(2v) + b^2\sinh^2(2v)]} \times$$

$$\left[ab\,\sinh(2v) - \cosh(2v)\,\sqrt{-(a^2+b^2) + (b^2+1)\cosh^2(2v)} \right],$$

$$(A.4.5.b)$$

For $|a| = 1$ there are two cases: $a = \pm 1$. If $a = -1$, then $(k_{op,r}\ k_{op,i}) = (k_r\ k_i)$ and the branch cut for β_{op} will coincide with at least a portion of the locus of points on the β cut in the α plane from $\alpha = -(\pi/2)$. In fact, either (A.4.4) or (A.4.5.a) may be used recognizing that (A.4.4) gives the portion of the β_{op} branch cut for $v < 0$ and (A.4.5.a) will give the portion for v going to $+\infty$. On the other hand if $a = 1$, then $k_{op,i} = 0$ and the β_{op} cut must run along the projection of the positive imaginary k_x axis, hence we must use (A.4.5.a).

A.5 Steepest Descent Path

The characteristic curves discussed in previous sections of this appendix are fixed for a given problem once the media are specified. As stated in Section 4.1.2, the saddle point for the field integral is found as a root of the derivative of the exponent in the integrand and is found to be given as $\alpha_s = \phi + \pi/2$. At the saddle point the exponent is

$$-jk\rho\,\sin(\alpha_s-\phi) = -jk\rho\,\sin(\tfrac{\pi}{2}) = -jk\rho. \qquad (A.5.1)$$

Now the steepest descent path is determined such that the imaginary part of the exponential for all points on the path is equal to the saddle

point value, i.e.

$$Im(-jk \sin(\alpha-\phi)) = -(k_r \sin(u-\phi)\cosh(v)+k_i \cos(u-\phi)\sinh(v)) = -k_r$$

or equivalently

$$1 - \sin(u-\phi)\cosh(v) = (k_i/k_r)\cos(u-\phi)\sinh(v). \qquad (A.5.2)$$

This expression may be reduced to an explicit formula for the steepest descent path.

By manipulating (A.5.2) and using the quadratic formula, one arrives at

$$\tanh(v) = (-B\pm\sqrt{B^2-AD})/A , \quad \text{for } v \gtrless 0, \qquad (A.5.3)$$

$$\text{where } A = 1 + (k_i\cos(u-\phi)/k_r)^2,$$

$$B = \gamma \sin(2(u-\phi))/2,$$

$$D = - \cos^2(u-\phi),$$

$$\gamma = k_i/k_r ,$$

We observe here that as $v \rightarrow + \infty$, the asymptotic form for the original expression is:

$$- \tan(u-\phi) \sim (k_i/k_r)\tanh(v) \sim (k_i/k_r). \qquad (A.5.4)$$

Using the trigonometric identity $\tan(u-u_s+\pi/2) = -1/\tan(u-u_s)$ where u_s is the position of the saddle point ($u_s = \phi+ \pi/2$), we arrive at the following:

$$\tan(u-u_s) = 1/(k_i/k_r) \rightarrow u-u_s = \pi/2-\tan^{-1}(k_i/k_r). \qquad (A.5.5)$$

So as $v \to +\infty$ we see that $u \to u_s + (\pi/2 - \tan^{-1}(k_i/k_r))$. Similarly as $v \to -\infty$, $u \to u_s - (\pi/2 - \tan^{-1}(k_i/k_r))$. Using these values it can be seen that when the saddle point lies at $u = \pm\pi/2$, the asymptotes of the steepest descent path are the same as the asymptotes of the respective boundaries of the top sheet (mappings of the hyperbolic branch cuts from the points $k_x = \pm k$).

One final point of interest, which is important in the evaluation of the steepest descent integral through the saddle point, is the value of the slope of the path at the saddle point. If we consider points in the vicinity of the saddle point ($\alpha = u_s + \rho e^{j\theta}$), then the exponent of the integrand of the field integral will be given by

(A.5.6)

$$g = -jk \sin(\alpha - \phi) \overset{\sim}{\sim} -jk + (jk/2!)(\alpha - \alpha_s)^2 + \ldots$$
$$= -j(k_r - jk_i) + (j/2)(k_r - jk_i)\rho^2(\cos(2\theta) + j \sin(2\theta)) + \ldots$$
$$= (-k_i + (\rho^2/2)(k_i \cos(2\theta) - k_r \sin(2\theta)))$$
$$+ j(-k_r + (\rho^2/2)(k_r \cos(2\theta) + k_i \sin(2\theta)))$$

Now since $(Im(g))_{\substack{saddle \\ point}} = -k_r$, then we must require

$$(k_r \cos(2\theta) + k_i \sin(2\theta)) = 0. \tag{A.5.7}$$

Hence:

$$(\tan(2\theta))_{\substack{saddle \\ point}} = -(k_r/k_i) \tag{A.5.8}$$

which is the slope of the steepest descent path at the saddle point.

A.6 Path of Integration

The field integral involves an integration path which lies in the Wiener-Hopf strip. The path will lie in a region bounded by the singularity at $k_x = -k_1 \cos(\theta)$ which represents the incoming wave in the upper half space. Therefore we can take this path to lie along the real k_x axis for $0 < \theta < \pi/2$ using the aperture formulation. For $\pi/2 < \theta < \pi$, we can take the path to lie on a line with the imaginary value of k_x given by $\tau = \text{Im}(-k_1 \cos(\theta))$ and indented counterclockwise below the pole. For this case we can use the expression

$$\text{Im}(-k_1 \cos \theta) = k_{1i} \cos\theta = \text{Im}(k \sin \alpha)$$

$$= k_r \cos u \sinh v - k_i \sin u \cosh v. \qquad (A.6.1)$$

However this is not convenient. The main significance of this curve is the following observation. If we consider the integration path to be the real axis in the α plane for the sake of simplicity, then as the geometrical optics pole moves to the right of the real k_x mapping ($\theta > \pi/2$), it will only be crossed in the deformation of the original integration path when the steepest descent path is to the left of the geometrical optics pole. This point is made visually in Figure A.1. Put another way, the only possible singularity of the integrand which can lie between the true integration path and the real k_x axis mapping is the geometrical optics pole.

A.7 Locus of the Geometrical Optics Pole

A singularity whose residue contributes to the far field and is of
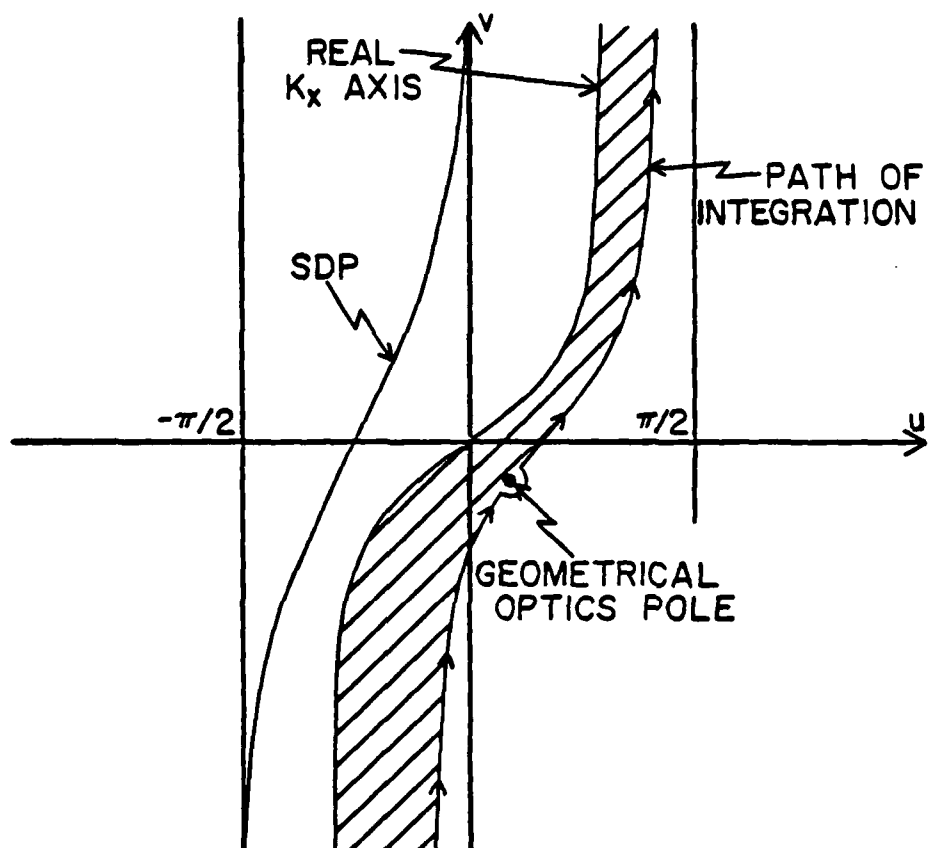
Region swept by deforming integration path
to coincide with the real k_x axis mapping

Figure A.1. Deformation of the integration path
to the real k_x axis mapping.

particular interest is the root of $(k \sin \alpha + k_1 \cos \theta)$, where k is the wave number of the observation medium, k_1 is the wave number of the upper medium and θ is the angle of the incident plane wave $(0 < \theta < \pi)$. This contribution constitutes the so-called geometrical optics field. Clearly, if $k = k_1$ (that is, the observation point is in the upper medium), then $\alpha_r = \theta - \pi/2$ and the locus of the geometrical optics pole (GOP) in the α plane is the real α axis between $u = -(\pi/2)$ and $u = +(\pi/2)$. If $k = k_2$ (lower medium wave number), then the locus of the GOP leaves the real α axis, crossing it at $\alpha = 0$.

To compute the locus of the GOP for $k = k_2$, we expand the root α_r in the α plane

$$k_2 \sin(\alpha_r) = -k_1 \cos(\theta). \tag{A.7.1}$$

Substitute $k_1 = k_{1r} - jk_{1i}$, $k_2 = k_{2r} - jk_{2i}$ and $\alpha = u + jv$ and after some algebraic manipulations arrive at

$$\tan(u) = \left[\frac{k_{1r}k_{2r} + k_{1i}k_{2i}}{k_{1r}k_{2i} - k_{1i}k_{2r}} \right] \tanh(v) \text{ for } k_{1r}k_{2i} \neq k_{1i}k_{2r}. \tag{A.7.2}$$

Note that if $k_{1r} \cdot k_{2i} = k_{1i} \cdot k_{2r}$, then k_1 lies on the line in the k_x plane which runs through both k_2 and the origin. In this case the GOP locus will run between $-\alpha_{(k_1)}$ and $+\alpha_{(k_1)}$ along the line segments shown in Figure A.2.

Clearly for a specific value θ we can use the standard mapping formula (A.1.2) to find the location of the GOP and it will lie on the curve
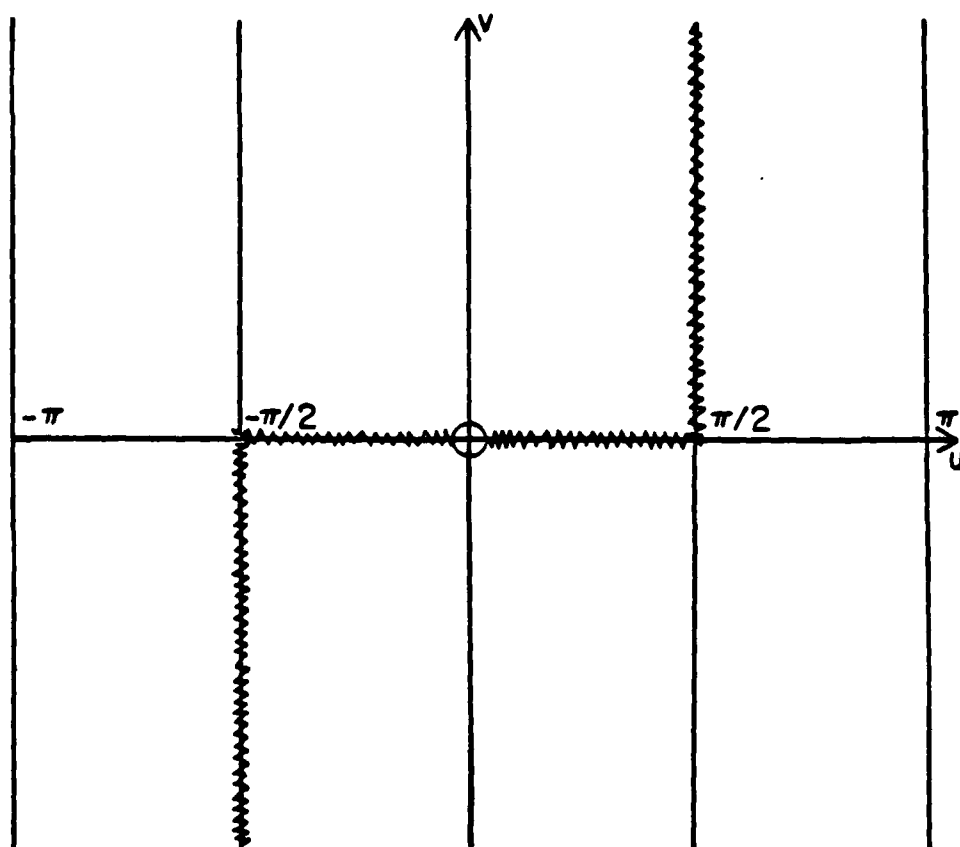
Figure A.2. Locus of the geometrical optics pole
when $k_{1r} \cdot k_{2i} = k_{1i} \cdot k_{2r}$.

specified by (A.7.2). We note in passing that it is possible for (A.7.2) to specify a curve which moves from $\alpha_{(-k_1)}$ onto the lower sheet of the α plane and running to $\alpha = -\pi$ rather than to $\alpha = 0$ as one might expect. This corresponds to the situation in the k_x plane where the locus of the GOP (a straight line from $-k_1$ to $+k_1$) crosses the β_2 branch cut. In effect, a pole moving from $k_x = -k_1$ to $k_x = 0$ is seen to move onto the lower sheet projection and simultaneously, the root from the lower sheet is seen to emerge onto the upper sheet projection.

It is useful to establish the slope and curvature characteristics of the GOP locus in the α plane (only the projection of the second quadrant of the k_x plane is of interest). Before proceeding it is necessary to consider a classification scheme for the second quadrant of the k_x plane (and its image in the α plane) which is based on the properties of the mapping $k_x = k_2 \sin\alpha$. The following equivalences hold in all cases:

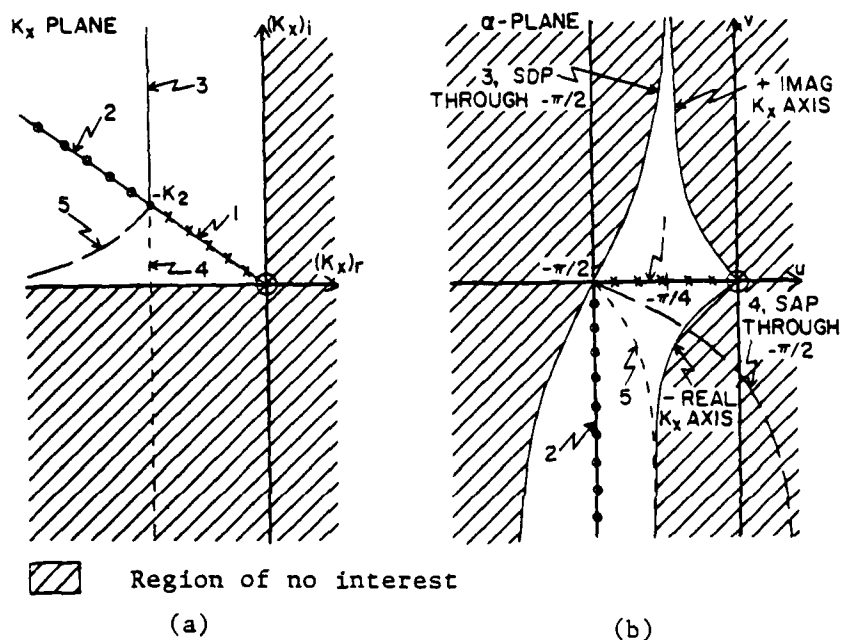| k_x plane	α plane
1. The straight line segment between $k_x = 0$ and $k_x = -k_2$.	1. The segment of the real axis between $u = 0$ and $u = -(\pi/2)$.
2. The extension of the above line segment from $k_x = -k_2$ to ∞.	2. The line segment for $u = -(\pi/2)$ and $v \leq 0$.

3. The straight line segment for $(k_x)_r = -k_{2r}$ and $(k_x)_i \geq k_{2i}$.

3. The SDP through $\alpha = -(\pi/2)$.

4. The extension of the line segment in 3 for $(k_x)_i < k_{2i}$.

4. The SAP through $\alpha = -(\pi/2)$ (only the portion on the top sheet is of interest).

5. The extension of the branch cut hyperbola from $k_x = -k_2$ (asymptotic to the negative real k_x axis).

5. The locus for $v \leq 0$ represented by the mapping of the imaginary k_x axis moved to intersect $u = -(\pi/2)$.

These images are shown in Figure A.3. As mentioned these particular loci will always map as indicated. Now we classify the second quadrant of the k_x plane and its image in the α plane as shown in Figure A.4. For the purposes of this discussion we will treat regions 2A and 2B as a combined domain, region 2.

First we form the derivative (dv/du) of the GOP locus equation (A.7.2) as

$$\left(\frac{dv}{du}\right)_{\substack{GOP \\ locus}} = \frac{\cosh^2(v)}{\kappa \cos^2(u)} \tag{A.7.3}$$

where $\kappa = \left|\frac{k_{1r}k_{2r} + k_{1i}k_{2i}}{k_{1r}k_{2i} - k_{1i}k_{2r}}\right| = \dfrac{[\quad]}{\left[(-\frac{k_{1i}}{k_{1r}}) - (-\frac{k_{2i}}{k_{2r}})\right]}$

Region of no interest

(a)   (b)

Figure A.3. Prominent lines in the k_x plane and their projections in the α plane.

a. Lines in the k_x plane.

b. Curves in the α plane.

(a)

(b)
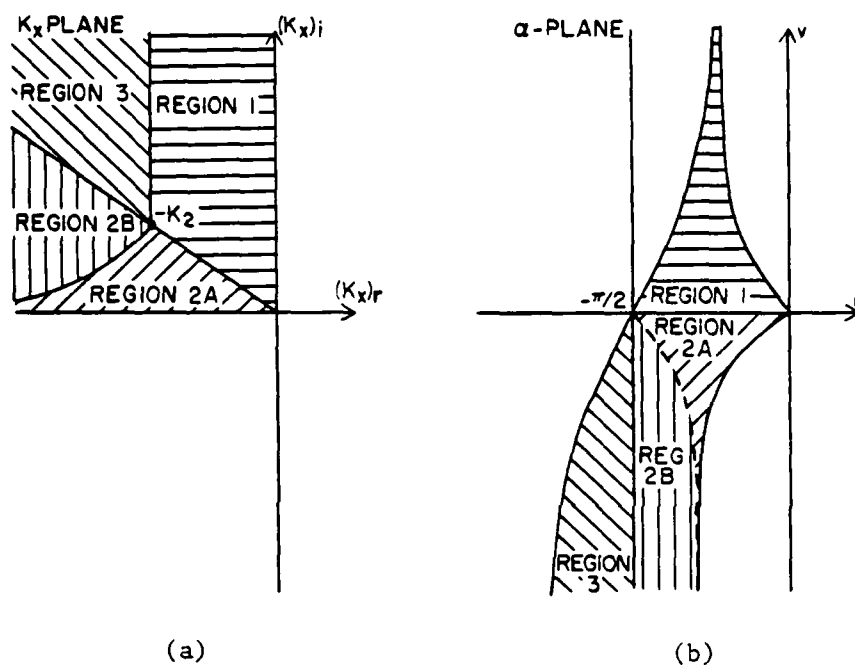
Figure A.4. Regions in the k_x plane and their projections in the α plane.

    a.   Regions in the k_x plane.

    b.   Regions in the α plane.

Clearly $\kappa > 0$ if the line in the k_x plane from $-k_{2r}$ to the origin lies above the GOP locus (that is, $(-k_1)$ in region 2); otherwise $\kappa < 0$. Forming the second derivative,

$$\left(\frac{d^2 v}{du^2}\right)^{GOP}_{locus} = \left[\frac{2(1+\kappa^2)\cosh^4(v)}{\kappa^2 \cos^4(u)}\right] \frac{\sin(u)\cos(u)}{\kappa} \quad . \quad (A.7.4)$$

For α_b in region 1, $\kappa < 0$ and $-(\pi/2) < u < 0$ so $(d^2 v/du^2) \geq 0$. For α_b in region 2, $\kappa > 0$ so $(d^2 v/du^2) \leq 0$. For α_b in region 3 we see from Figure A.4.a that the GOP line will cross the boundary between regions 1 and 3. Now since α_b is in region 3, $\kappa < 0$; but for the region 1 portion of the GOP locus, $-(\pi/2) < u < 0$ while for the region 3 portion of the GOP locus, $-\pi < u < -(\pi/2)$. These results are collected in table A.1 for the GOP locus in the α plane and shown in Figure A.5.

For α_b in	$\dfrac{dv}{du}$	$\dfrac{d^2 v}{du^2}$
Region 1	≤ 0	≥ 0
Region 2	≥ 0	≤ 0
Region 3 ($\alpha \epsilon$ Reg 1)	≤ 0	≥ 0
Region 3 ($\alpha \epsilon$ Reg 1)	≤ 0	≤ 0

Table A. 1. Curvature characteristics of the Locus of the Geometrical Optics Pole.
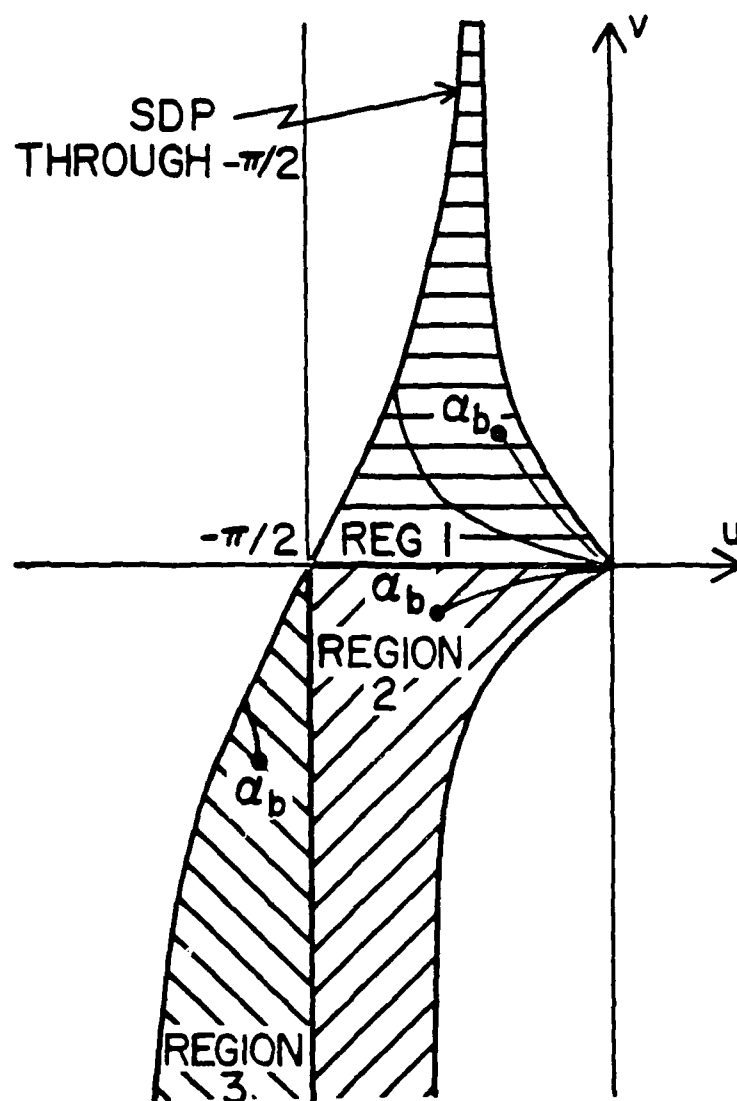
Figure A.5.   Examples of loci of the geometrical optics pole in the α plane.

A.8 Locus of the Connection from $-k_1$ to $-k_2$

In Section 3.4, which deals with the factorization of the function G_2, we saw that the branch cuts for β_1 and β_2 can be deformed along the connection lines between the branch points and will cancel on the semi-infinite portion of the cuts resulting in finite cuts between the branch points. (See Figure 3.3). It is also demonstrated in Section 3.4 that the function G_2 (and hence G) will not have roots on the top sheet using these finite branch cuts. It is important to the discussion in Appendix C, which examines the exposure of these roots in the process of deforming the β_1 branch cut, that the locus of the connection between $-k_1$ and $-k_2$ in the α plane be established.

In this section the formula for the connection locus from $-k_1$ to $-k_2$ in the α plane is given for observation angles in the lower medium, k_2. A similar analysis can be performed when the observation angle lies in k_1. We start with the parametric description of the connection in the k_x plane:

$$k_x^2 = k_2^2 + (k_1^2 - k_2^2)t, \quad \text{for } t \in [0,1]. \tag{A.8.1}$$

Substituting $k_x = k_2 \sin(\alpha)$ into (A.8.1), the expression can be reduced to the equality of the real and imaginary parts.

$$1 + \cos(2u)\cosh(2v) = -(\phi-2)t \tag{A.8.2}$$

$$-\sin(2u)\sinh(2v) = -\Psi t \tag{A.8.3}$$

where $\alpha = u+jv$ and ϕ, ψ are given by

$$(k_1 \cdot k_2^*) = (k_{1r}k_{2r} + k_{1i}k_{2i}) + j(k_{1r}k_{2i} - k_{1i}k_{2r}) = A + jB \quad (A.8.4)$$

$$\frac{2(k_1 \cdot k_2^*)^2}{|k_2|^4} = \left[\frac{2(A^2-B^2)}{|k_2|^4}\right] + j\left[\frac{4AB}{|k_2|^4}\right] = \phi + j\Psi \quad (A.8.5)$$

After manipulations the quadratic formula can be applied to arrive at

$$\sinh(2v) = \frac{1}{c^2-s^2}\left[s \pm c\sqrt{1-(c^2-s^2)}\right] \quad (A.8.6)$$

where $c = \cos(2u)$ and $s = \dfrac{\phi-2}{\Psi}\sin(2u)$.

It is necessary to establish which sign is appropriate and in the process the behavior of (A.8.6) must be examined. The result of this analysis for the path between $k_x = -k_1$ and $-k_2$ is

$$\sinh(2v) = \frac{s}{c^2-s^2} \pm \frac{\text{sgn}\left(\frac{\pi}{4} - |u+\frac{\pi}{2}|\right)}{c^2-s^2}\left|c\sqrt{1-(c^2-s^2)}\right| \quad (A.8.7)$$

$$\text{for} \quad v_{(-k_1)} \gtrless 0$$

$$\text{and either} \quad -\frac{\pi}{2} \le u \le u_{(-k_1)}$$

$$\text{or} \quad u_{(-k_1)} \le u \le -\frac{\pi}{2}$$

where

$$c = \cos(2u)$$

$$s = \left(\frac{\phi-2}{\Psi}\right)\sin(2u)$$

ϕ, Ψ: Defined by (A.8.4) and (A.8.5).

An exceptional case for (A.8.7) occurs if $v = 0$, then $s \rightarrow \infty$. This will occur if

$$k_{1r}k_{2i} = k_{1i}k_{2r}$$

$$\frac{k_{1i}}{k_{1r}} = \frac{k_{2i}}{k_{2r}}$$

(A.8.8)

Hence when this case occurs, $-k_1$ and $-k_2$ lie on the same ray from the origin in the k_x plane. If $k_{1r} < k_{2r}$ then we have that $v = 0$ on the connection path in the α plane and the locus lies on the real α axis. If $k_{2r} < k_{1r}$ then the connection must lie on the line $u = -(\pi/2)$, $v \leq 0$.

We now examine the slope and curvature characteristics of the connection line in the α plane using the same classification system as in Section A.7. By forming the derivatives of the locus equation for the connection line between $-k_1$ and $-k_2$ and manipulating the results, it can be shown that the curvature of the locus is as given in table A.2.

For α in	$\frac{du}{dv}$	$\frac{d^2u}{dv^2}$
Region 1	≥ 0	> 0
Region 2	≤ 0	< 0
Region 3	≥ 0	< 0

Table A. 2. Curvature Characteristics of Connection from $-k_1$ to $-k_2$.

These results imply that if α_b ($k_x = -k_1$) is in region 1 or 2, then the entire locus is in that region. It is possible for α_b to be in region 3 to have the locus cross the SDP boundary and its image appear in region 1. This case is considered in more detail in Section C.4.

In concluding this section on the connection line between $-k_1$ and $-k_2$, it is interesting to note that in the k_x plane the curve is actually a portion of a hyperbola which passes through $k_x = -k_1$ and $-k_2$ and has asymptotes which are perpendicular. This is due to the fact that the connection line lies on a straight line in the k_x^2 plane. This is a property of the mapping k_x^2 and accounts for the fact that the hyperbolas used to define the original branch cuts for β_1 and β_2 will map into parallel straight lines in the k_x^2 plane.

APPENDIX B

ASYMPTOTIC FAR FIELD RESULTS

FOR THE INTERFACE PROBLEM

B.1 Introduction

The purpose of this appendix is to present explicitly the asymptotic contributions to the far fields in the interface problem. The solution in the transmitted region ($y < 0$) is derived in this appendix. Similar steps can be followed in the reflected region and the generalized results are given in Chapter 4. Throughout this appendix we follow the approach of Felsen and Marcuvitz (1973a).

B.2 Asymptotic Far Field Constituents in the Transmission Region

The integral to be evaluated is shown below:

$$e_z(x,y) = \xi \int_\Gamma \frac{k_2 \cos\alpha}{G_-(k_2 \sin\alpha)(k_2 \sin\alpha + k_1 \cos\theta)} e^{jk_2\rho\sin(\alpha-\phi)} \, d\alpha \qquad (B.2.1)$$

for $y < 0$

where ξ = constant = $\dfrac{-jE_0 \sin\theta}{\pi\eta_1 G_+(-k_1\cos\theta)}$, E_0 = magnitude of incident field

θ = angle of propagation of incident plane wave

ϕ = observation angle ($-\pi < \phi < 0$)

G_+, G_- = factorizations

$$\rho = \text{radial distance from the edge of the PEC screen, normalized}$$

$$\eta_1, k_1, k_2 = \text{normalized values}$$

$$\Gamma = \text{path of integration in the } \alpha \text{ plane}$$

The singularities, which may be crossed (thereby contributing explicitly to the asymptotic field), are as follows:

1. Geometrical optics pole due to the root of

   $(k_2 \sin \alpha + k_1 \cos \theta)$.

2. A pole due to the root of G_- in the mapping of the second quadrant of the k_x plane (or on the adjacent lower sheet),

3. Branch point of $\beta_1 = \sqrt{k_1^2 - k_x^2}$ in the mapping of the second quadrant of the k_x plane. Due to $G_-(k_2 \sin \alpha)$.

Each of these contributors is considered below.

B.3 Steepest Descent Integral

After having deformed the integration path of the radiation integral (B.2.1) to the steepest descent path through the saddle point, $\alpha_s = \phi + \pi/2$, one is in the position to evaluate an asymptotic approximation to the saddle point integral.

The first two terms of the asymptotic expression for the steepest descent integral are known to be (Felsen and Marcuvitz (1973a))

$$(e_z)_{\substack{\text{saddle} \\ \text{point}}} \sim \sqrt{\frac{2\pi}{-j\,k_2}}^{\text{PV}} \left\{ \frac{f(\alpha_s)}{\rho^{\frac{1}{2}}} - \frac{1}{j\,2\,k_2\,\rho^{3/2}} \left[\frac{f(\alpha_s)}{4} + \frac{d^2 f(\alpha_s)}{d\alpha^2} \right] \times \right.$$

for $\phi < 0$,
where
$$\left. e^{-jk_2\rho} \right\} \qquad (B.3.1)$$

$$f(\alpha) = \frac{\xi\,k_2\,\cos\alpha}{G_-(k_2\,\sin\alpha)\,(k_2\,\sin\alpha + k_1\,\cos\theta)} \quad , \qquad (B.3.2)$$

$\alpha_s = \pi/2 + \phi$ and ρ is the normalized distance from the edge of the
PEC half-plane ($\rho = 2\pi$ distance in wavelengths in free space). As long
as ϕ is not in the neighborhood of $\phi = 0°$ or $-180°$, the lead term in the
series will dominate for observation distances greater than a wavelength
in free space from the edge of the PEC half-plane. As the observation
point approaches the interface between the media, however, the $(\cos\alpha)$
factor in (B.3.2) causes the lead term in (B.3.1) to vanish and the
second term dominates the expansion. In principle this evaluation can
be performed but this avenue of work has not been pursued since the ex-
pressions are tedious and of little practical value. Instead, the fol-
lowing observations are made concerning the significance of the second
term in the asymptotic expansion.

For observation radii exceeding one wavelength in free space, the
lead term dominates the first part of the second term in (B.3.1). It is
appropriate, therefore, to compare the behavior of the lead term with
the second part of the second term in (B.3.1). For $\phi \sim -180°$, the
second derivative of $f(\alpha_s)$ behaves as

$$f''(\alpha_s) \stackrel{\backsim}{} \frac{- 2 \cdot \mu_1 \cdot \xi \cdot k_2^2 \sin \alpha_s}{\mu_2 \cdot \beta_1 \cdot (k_2 \sin \alpha_s) \cdot G_-(k_2 \sin \alpha_s) \cdot (k_2 \sin \alpha_s + k_1 \cos \theta)} \tag{B.3.3}$$

If the modulus of the ratio of the lead term to the second term in (B.3.1) is evaluated in the vicinity of $\alpha_s = - \pi/2$ (that is, for $\phi = - 180°$) using (B.3.3), we see that

$$\left| \frac{\text{first term of (B.3.1)}}{\text{second term of (B.3.1)}} \right| = R \stackrel{\backsim}{} \frac{\rho}{\tan \alpha_s \cdot \sin \alpha_s} \left| \frac{\mu_2 \cdot \beta_1 (k_2 \sin \alpha_s)}{\mu_1} \right|$$

$$\tag{B.3.4}$$

As long as the contrast of the two media is substantial, we see that an estimate of the relative significance of the two terms is given by

$$R \stackrel{\backsim}{} \frac{\rho \tan \phi}{\cos \phi} \tag{B.3.5}$$

We observe that if ρ is taken as one wavelength in free space, then $R = 1$ for $\phi = 171°$ and if ρ is taken as five wavelengths, then $R = 1$ for $\phi = 178°$.

In effect, we assert that the "propagation field" (which behaves as $\rho^{-\frac{1}{2}}$) dominates the saddle point field contribution except in the vicinity of the interface plane where a lateral wave type of field exists and preserves the phase and amplitude propagation behavior of the total field across the interface aperture. The lead term in (B.3.1) is given by (4.1.8) when generalized to observation points in either medium.

B.4 Geometrical Optics Pole

This pole occurs at α_{gc} such that $k_2 \sin \alpha_{go} + k_1 \cos \theta = 0$.

Since the integration path Γ runs from $v = -\infty$ to $v = +\infty$ (where $\alpha = u+jv$), we see that the pole of the integrand at α_{go} will be encircled either positively or negatively when crossed depending on whether the geometrical optics pole lies to the left or right of the path of integration. All that remains is to evaluate the residue of the pole,

$$\text{Residue}(\alpha_{go}) = \left[(\alpha-\alpha_{go}) \frac{(\xi k_2 \cos\alpha\ e^{-jk_2\rho\sin(\alpha-\phi)})}{G_-(k_2\sin\alpha)(k_2\sin\alpha + k_1\cos\theta)} \right]_{\alpha=\alpha_{go}}$$

$$(e_z)_{go} = j2\pi\ \text{Res}(\alpha_{go}) = \frac{j2\pi\xi}{G_-(-k_1\cos\theta)}\ e^{-jk_2\rho\sin(\alpha-\phi)} \qquad (B.4.1)$$

$$(e_z)_{go} = \frac{2E_0\sin\vartheta}{\eta_1 G_-(-k_1\cos\theta)}\ e^{-jk_2\rho\sin(\alpha_{go}-\phi)} \qquad (B.4.2)$$

B.5 Root of $G_2(k_2\sin\alpha)$

It is noted in Section 3.4 that $G_+(\alpha) = G_-(-\alpha)$, $G(\alpha) = G_+(\alpha)\cdot G_-(\alpha)$ and that G_+ and G_- each have a single root which must be located at the same position as the roots of G. It was shown that G does not have roots on the top sheet of the analytic continuation of G_2 which has the finite branch cuts connecting the branch points. (Here we refer to the

partition G_2 of G given in (3.4.2)). However when the branch cut for β_1 is deformed in the process of evaluating the asymptotic contribution for the branch cut integral, this root may be brought up to the top sheet and be crossed as the integration path deforms to the SDP. In that case this pole contribution must be included and is discussed in this section. The question of when the root is exposed and crossed is discussed in Appendix C. The residue at the root of G_- is given as

$$\text{Residue } (\alpha_r) = \left[(\alpha-\alpha_r) \frac{\xi \, k_2 \cos\alpha \, e^{-jk_2\rho\sin(\alpha-\phi)}}{G_-(k_2\sin\alpha)(k_2\sin\alpha + k_1\cos\theta)} \right]_{\alpha=\alpha_r}$$

$$= \frac{\xi \, k_2 \cos\alpha_r \, e^{-jk_2\rho\sin(\alpha_r-\phi)}}{k_2\sin\alpha_r + k_1\cos\theta} \lim_{\alpha\to\alpha_r} \left[\frac{(\alpha-\alpha_r)}{G_-(k_2\sin\alpha)} \right]$$

$$= \gamma \cdot \lim_{\alpha\to\alpha_r} \left[\frac{(\alpha-\alpha_r)}{G_-(k_2\sin\alpha)} \right]$$

$$= \gamma \cdot G_+(k_2\sin\alpha_r) \lim_{\alpha\to\alpha_r} \left[\frac{(\alpha-\alpha_r)}{G(k_2\sin\alpha)} \right]$$

$$= \frac{\gamma \cdot G_+(k_2\sin\alpha_r)}{G'(k_2\sin\alpha_r)(k_2\cos\alpha_r)} \tag{B.5.1}$$

Now we observe

$$G' = \frac{d}{dk_x}\left[\frac{\beta_1}{\mu_1} + \frac{\beta_2}{\mu_2}\right] = -k_x\left[\frac{1}{\mu_1\beta_1} + \frac{1}{\mu_2\beta_2}\right] \quad . \tag{B.5.2}$$

However at $\alpha = \alpha_r$, $G(\alpha_r) = 0$ implies

$$\beta_1 = -(\beta_2\mu_1)/\mu_2 \quad \text{at} \quad \alpha=\alpha_r \quad . \tag{B.5.3}$$

Substituting this into (B.5.2) yields

$$G'(k_2\sin\alpha_r) = \left\{-k_x \cdot \left[\frac{1}{\mu_1\left(\frac{-\beta_2\mu_1}{\mu_2}\right)} + \frac{1}{\mu_2\beta_2}\right]\right\}_{k_x=k_2\sin\alpha_r}$$

$$= \left[\frac{\mu_2^2 - \mu_1^2}{\mu_1^2\mu_2}\right]\tan\alpha_r \tag{B.5.4}$$

B.6 Branch Cut of β_1 for $k_x = -k_1$

The last singularity contributor that we need to evaluate is the branch cut integral due to the presence of $G_-(k_x)$ in the integrand of (B.2.1). As we deform from the integration path Γ to the SDP, there will be a critical angle ϕ_{cr} such that the SDP will cross the branch point α_b for all ϕ such that $|\phi| \geq |\phi_{cr}|$. In order to deal with the contribution of the branch point in a systematic manner which will be amenable to asymptotic evaluation, we choose to follow an approach which is analogous to conventional steepest descent analysis.

The essential point in steepest descent analysis is to deform the integration contour to lie along a path of constant phase in the exponential factor. As a result, we are guaranteed that the magnitude of the exponential factor will change most rapidly along such a path. Because this path is chosen to pass through the saddle point of the exponential, there are, in fact, four possible paths along which we may proceed. Two of the paths are colinear at the saddle point and are referred to as the steepest descent path (SDP) while the remaining two colinear paths make up the steepest ascent path (SAP). However if we choose some other point in the complex plane and examine the contours of constant phase of the exponential, we find that there is only one set of colinear paths from the chosen point (see Figure B.1). One direction will follow a path which is asymptotic to the SDP while the other direction will cause one to move on a path which is asymptotic to the SAP.

Consider the following procedure. We specify a given observation angle ϕ such that $|\phi| \geq |\phi_{cr}|$ and therefore the integration path must capture the branch point which characterizes $-k_1$ as it deforms to the SDP. We deform the branch cut for β_1 to the steepest descent path through α_b (SDP_b) which is the portion of the constant phase contour that is asymptotic to the SDP. Then we deform the integration path to the SDP. In the process of this deformation we must enclose the entire β_1 branch cut and the integration paths for this branch cut integral will lie along the steepest descent path from x_b. The specifics of this deformation are considered in Appendix C. For our purposes here, we assume that such a deformation has occurred and the branch cut for β_1 lies along the SDP_b from α_b. We are now interested in evaluating the branch cut integral and fol-
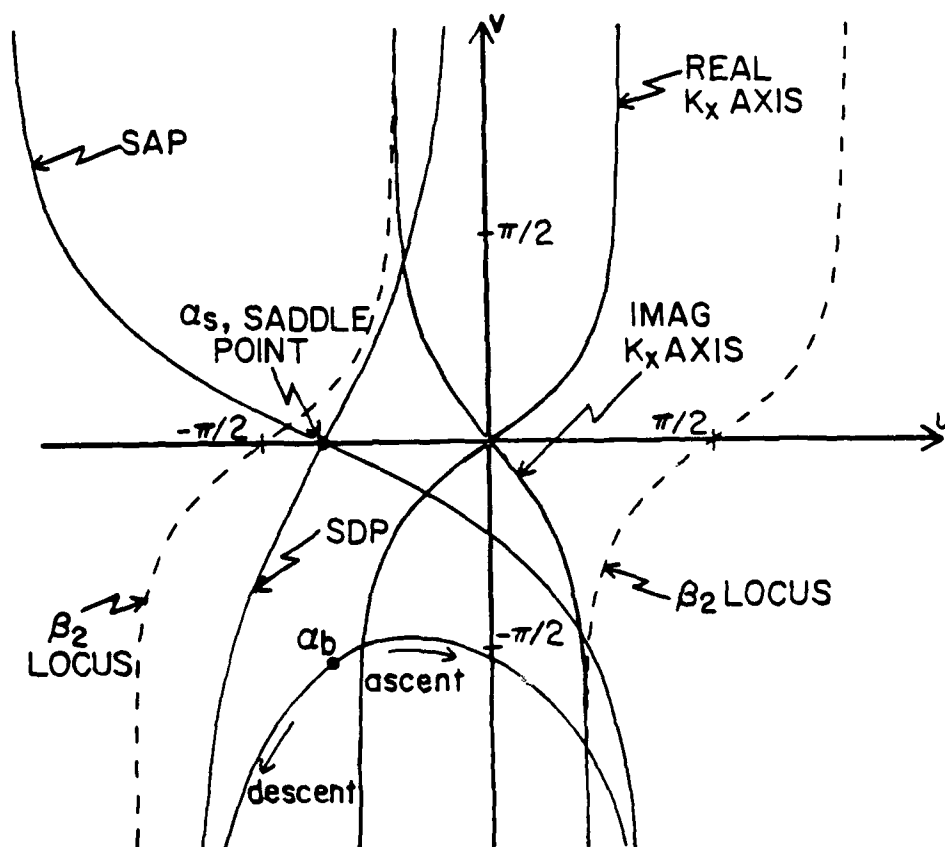
Figure B.1. An example of the steepest descent/ascent
loci for an arbitrary point α_b.
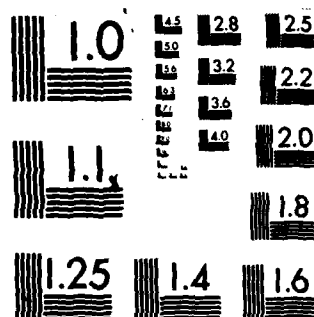
MICROCOPY RESOLUTION TEST CHART
NATIONAL BUREAU OF STANDARDS-1963-A

low the analysis discussed in Section 4.8 in Felsen and Marcuvitz (1973a). We want to characterize the portion of the integrand in (B.2.1) exclusive of the exponential in the vicinity of α_b. Hence,

$$
\begin{aligned}
f(\alpha) &= \frac{\xi \, k_2 \cos\alpha}{G_-(k_2\sin\alpha) \cdot (k_2\sin\alpha + k_1\cos\theta)} \\[2ex]
&= \left[\frac{\xi \cdot k_2 \cdot \cos\alpha \cdot G_+(k_2\sin\alpha)}{k_2\sin\alpha + k_1\cos\theta} \right] \frac{1}{G(k_2\sin\alpha)} \\[2ex]
&= \frac{u(\alpha)}{\left[\dfrac{k_2\cos\alpha}{\mu_2} + \left(\dfrac{\sqrt{k_1 - k_2\,\sin\alpha}}{\mu_1} \right) \sqrt{k_1 + k_2\sin\alpha} \right]} \\[2ex]
&= \left\{ \frac{u(\alpha)}{\left[\dfrac{k_2\cos\alpha}{\mu_2} \right]^2 - \left[\dfrac{k_1^2 - k_2^2\sin^2(\alpha)}{\mu_1^2} \right]} \left[\frac{k_2\cos\alpha}{\mu_2} - \left(\frac{\sqrt{k_1 - k_2\sin\alpha}}{\mu_1} \right) \sqrt{k_1 + k_2\sin\alpha} \right] \right\}
\end{aligned}
$$

$$\tag{B.6.1}$$

For α near α_b, we have

$$
[f(\alpha)]_{\substack{\text{near} \\ \alpha_b}} = \left[\frac{\xi\,\mu_2 G_+(-k_1)}{k_1(\cos\theta - 1)} \right] + \left[\frac{-\xi\,\sqrt{2}\,\mu_2^2\,G_+(-k_1)}{\sqrt{k_1}^{PV}\,\mu_1\,\sqrt{\beta_2(k_1)}^{PV}(\cos\theta - 1)} \right] \sqrt{(\alpha - \alpha_b)}^\theta
$$

$$\tag{B.6.2}$$

where $\sqrt{}^\theta$ refers to the analytic continuation of the original branch of $\sqrt{k_1 + k_2\sin\alpha}$ in the vicinity of α_b (discussed below). $\sqrt{}^{PV}$ is the principal value with the branch cut along the negative real axis.

Before proceeding we need to clarify the meaning of $\sqrt{\alpha - \alpha_b}^{\,\theta}$. To do this we begin with $\sqrt{k_1 + k_2 \sin \alpha}$. The original specification of this function is given in Section 2.2 (specifically (2.2.2) and Figure 2.3). We see there that the quantity $(k_1 + k_x) = k_x - (-k_1)$ can be considered as a vector from $(-k_1)$ to k_x. If this is done then the following equations hold for the branch definition:

If $(k_1 + k_x) = |k_1 + k_x| e^{j\theta}$, then $\sqrt{(k_1 + k_x)} = |k_1 + k_x|^{\frac{1}{2}} e^{j\theta/2}$. (B.6.3)

It is shown in Section C.3 that the SDP_b branch cut for β_1 never crosses the α plane locus of the straight line from $k_x = -k_1$ to $k_x = 0$ in the k_x plane (locus of the geometrical optics pole). Hence the function $\sqrt{k_1 + k_x}^{\,\theta}$ will retain its original value from the hyperbolic branch cut definition for all points on this line. If we examine points on this line (referred to as α_g) in the α plane near α_b, we find that

$$(-k_2)t = (k_1 + k_2 \sin \alpha_g) \quad \text{for} \quad t \in [0,1]$$
$$\sim -k_1 + \beta_2(k_1) \cdot (\alpha_g - \alpha_b)$$

(B.6.4)

$$[\beta_2(k_1)] \cdot (\alpha_g - \alpha_b) \sim (1-t)k_1 \quad .$$

We have:
$$\text{Arg } \beta_2(k_1) + \text{Arg } (\alpha_g - \alpha_b) = \text{Arg } k_1$$

and

$$\text{Arg}(\sqrt{k_1 + k_x}^{\,\theta}) = \tfrac{1}{2} \text{Arg } k_1 \sim \text{Arg}[\sqrt{\beta_2(k_1) \cdot (\alpha_g - \alpha_b)}]$$

Hence

$$\text{Arg}[\sqrt{\beta_2(k_1) \cdot (\alpha_g - \alpha_b)}^{\,\theta}] = \tfrac{1}{2} \text{Arg } \beta_2(k_1) + \tfrac{1}{2} \text{Arg } (\alpha_g - \alpha_b) = \tfrac{1}{2} \text{Arg } k_1$$

So
$$\text{Arg}(\alpha_g - \alpha_b) = \theta_g = \text{Arg } k_1 - \text{Arg } \beta_2(k_1)$$

and

$$\sqrt{\beta_2(k_1) \cdot (\alpha_g - \alpha_b)}^{\,\theta} = \sqrt{\beta_2(k_1)}^{\,PV} \cdot |\alpha_g - \alpha_b|^{\frac{1}{2}} e^{j\theta_g/2}$$

Having specified values on the branch of $\sqrt{}^{\,\theta}$ near α_b, we can analytically continue them. So,

$$\sqrt{\beta_2(k_1) \cdot (\alpha - \alpha_b)}^{\,\theta} = \sqrt{\beta_2(k_1)} \cdot |\alpha - \alpha_b|^{\frac{1}{2}} e^{j\theta/2} \cdot \qquad (B.6.6)$$

where α is near α_b and θ assumes a value by rotation from θ_g. Consider, in particular, the ray from α_b along the SDP_b which results from the counterclockwise rotation from θ_g and call the angle θ_+. Then

$$f(\alpha_+) = \gamma + m\sqrt{(\alpha - \alpha_b)}^{\,\theta} \; . \qquad (B.6.7)$$

where γ and m are given in (B.6.2) and $\sqrt{\alpha_+ - \alpha_b}^{\,\theta} = |\alpha_+ - \alpha_b|^{\frac{1}{2}} e^{j\theta_+/2}$ with $\theta_g < \theta_+ < \theta_g + 2\pi$ and θ_+ is the angle of the SDP_b from α_b. Turning to the analysis of Felsen and Marcuvitz, we see that the branch cut contribution for a branch integral, which has the integration path running counterclockwise around the branch point, is given by

$$I_b \sim \frac{m\sqrt{\pi} \;\; \exp(j3\theta+/2)}{|k_2\rho\cos(\alpha_b - \phi)|^{3/2}} \; e^{jk_2\rho\sin(\alpha_b - \phi)} \qquad (B.6.8)$$

Generalizing the result for the reflection half space gives (4.1.16).

APPENDIX C

DEFORMATION OF

THE β_1 BRANCH CUT

C.1 Introduction

The case to be considered in this appendix is that of the interface problem where the field integral is to be evaluated in the transmitted region, i.e. the same case as that in Appendix B (specifically (B.2.1)). As discussed in Section B.6, it is useful to deform the branch cut of β_1 from $k_x = -k_1$ arising in the factor $G_-(k_2 \sin \alpha)$ in (B.2.1). In particular, we deform to the steepest descent path (SDP$_b$) from the point α_b where $-k_1 = k_2 \sin \alpha_b$. Section C.2 examines the constant phase contours specifying SDP$_b$ for a given saddle point location (α_s) and develops the relevant equations. In Section C.3, we examine the effect of the deforming branch cut integral on the various singularity contributors. Finally, in Section C.4 we consider the exposure of the root of $G_-(k_2 \sin \alpha)$.

C.2 Constant Phase Contours

The steepest descent path (and steepest ascent path) from the saddle point α_s is actually a path in the α plane along which the phase of the exponential in (B.2.1) is constant. Therefore

$$\text{Im}[-jk_2 \sin(\alpha-\phi)] = \text{Im}[-jk_2 \cos(\alpha-\alpha_s)] \ . \qquad \text{(C.2.1)}$$

where $\alpha = u + j\,v$, $k_2 = k_{2r} - j\,k_{2i}$; k_{2r}, $k_{2i} \geq 0$.

So the phase is given by

$$\gamma = k_{2i}\sin(u-u_s)\sinh(v) - k_{2r}\cos(u-u_s)\cosh(v).$$

Along the SDP (with respect to α_s), $\gamma = -k_{2r}$. It is clear from the discussion in Section 4.1.3 (and Figure 4.4), that if $\alpha_s = 0$, then the region between the two shifted mappings of the imaginary k_x axis (the zero phase lines) will have $\gamma < 0$. It is useful to consider the contours of constant phase which lie to the right of the SDP (and hence characterize points which will be crossed by the SDP for $-\pi < \phi < -\pi/2$). See Figure C.1. Observe that for $-k_{2r} < \gamma \leq 0$, the contours run more or less vertically and lie between the SDP/SAP and the right zero phase line. For $\gamma < -k_{2r}$ the contours curve downward and lie between the SDP and SAP. We observe another point: namely it is clear that the portion of the contour which is asymptotic to the SDP is the SDP_b from the point α_b. Hence if $\gamma > -k_{2r}$, the SDP_b runs up and to $v = +\infty$ while if $\gamma < -k_{2r}$, the SDP_b curves to the left and down to $v = -\infty$. Therefore as the saddle point moves to $-\pi/2$, the SDP_b deforms continuously as shown in Figure C.2. We notice in particular that when α_b lies on the SAP, the SDP_b may be taken as running to either $v = -\infty$ or $v = +\infty$. We can view the phase contour plot of Figure C.1 as fixed to α_s and visualize α_b as moving to the right on the phase plot as α_s moves from 0 to $-\pi/2$.

We have seen in the above discussion that the SDP_b alters radically as α_s moves to $-\pi/2$. However, note that the SDP_b will always lie to the left of the SDP through α_s which passes through α_b. This can be seen by
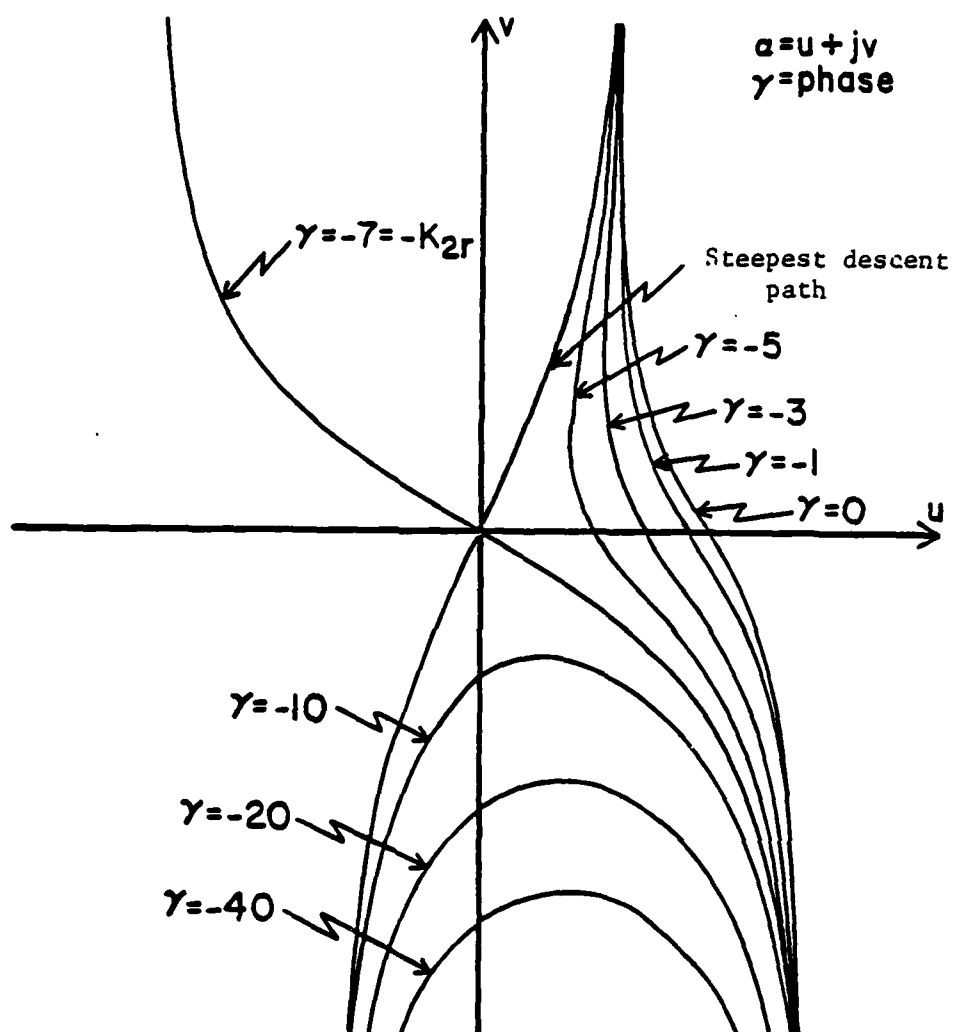
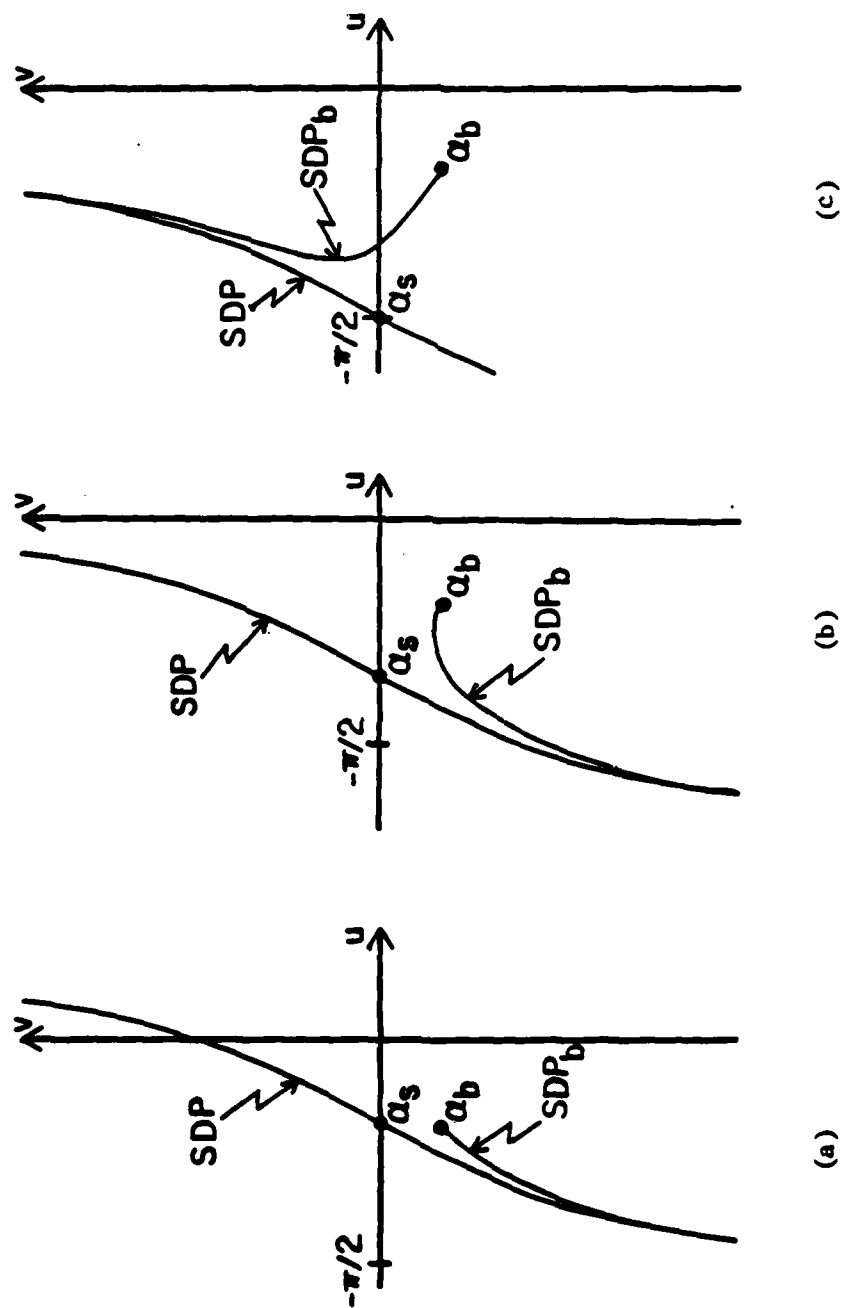Figure C.1. Contours of constant phase in the α plane about the saddle point location.

Figure C.2. Deformation of the branch cut for β_1 to the SDP_b.

observing that if the derivative (dv/du) is formed from (C.2.1), then in all cases the SDP_b will have a tangent from α_b which moves into the region to the left of the SDP through α_b and remains in that region. Also we know that the SDP_b is bounded on the left by the SDP through α_s. So for any α_b and α_s we have a band between the two SDP loci in which a root of $G_-(k_2\sin\alpha)$ may be exposed (and obviously crossed by the SDP through α_s). Viewed the other way if the root of G_- lies outside this band then it cannot lie on the top sheet and be crossed by the SDP so it can be ignored. To use this information it is helpful to know the value of α_s (referred to as α_{sb}) such that the SDP runs through α_b. To determine this we set $\gamma = -k_{2r}$ and $\alpha = \alpha_b$ in (C.2.1) and solve for α_{sb}. The result is

$$\cos(u_{sb}) = \frac{1}{A^2+B^2} [k_{2r} A \pm \sqrt{B^2(A^2+B^2-k_{2r}^2)}] \quad \text{for } v \lessgtr 0 \quad . \quad (C.2.2)$$

where $\alpha = u+jv$,

$$A = \text{Re}[\beta_2(\alpha_b)] = k_{2r}\cos(u_b)\cosh(v_b) - k_{2i}\sin(u_b)\sinh(v_b)$$

$$B = \text{Re}[k_x(\alpha_b)] = k_{2r}\sin(u_b)\cosh(v_b) + k_{2i}\cos(u_b)\sinh(v_b)$$

and $-\frac{\pi}{2} < u_{sb} < 0$.

Now consider an arbitrary point α_b (which must lie in the second quadrant of the k_x plane) and an arbitrary saddle point α_s (between $-\pi/2$ and 0). We wish to derive an explicit equation for points on the SDP_b. To begin we solve (C.2.1) for α. Then we invert (C.2.1) for to arrive

at the following expressions:

If $\gamma \geq -k_{2r}$:

$$\sin(u-u_s) = \frac{1}{A^2+B^2} \left[-B + A\sqrt{A^2+B^2-1} \right] \quad \text{for } (u-u_s) > 0, \text{ all } v, \quad (C.2.3)$$

where

$$\alpha = u + j\, v \quad \text{and} \quad A = \frac{k_{2r}\cosh(v)}{|\gamma|} \,,$$

$$B = \frac{k_{2i}\sinh(v)}{|\gamma|} \quad .$$

If $\gamma \leq -k_{2r}$:

$$\sinh(v) = \frac{1}{A^2+B^2} \left[B - \text{sgn}\!\left(\frac{\pi}{2} - u + u_s\right) \sqrt{A^2(B^2-A^2+1)} \right]$$
$$\text{for } -\theta_1 < (u-u_s) < \theta_1, \ v < 0, \quad (C.2.4)$$

where

$$A = \frac{k_{2r} \cdot \cos(u)}{|\gamma|} \qquad (C.2.4.a)$$

$$B = \frac{k_{2i} \cdot \sin(u)}{|\gamma|} \qquad (C.2.4.b)$$

$$\theta_1 = \tan^{-1}\left|\frac{k_{2r}}{k_{2i}}\right| \qquad (C.2.4.c)$$

Note that in the limit of $\gamma = -k_{2r}$, these equations describe points on the SDP and SAP which define the bounds of their respective regions $(\gamma \gtrless -k_{2r})$. However we recognize the following limitations for the application of (C.2.3) and (C.2.4) when $\gamma = -k_{2r}$:

(C.2.3) gives u as a function of v for: a. SDP for $v > 0$
                                        b. SAP for $v < 0$

(C.2.4) gives v as a function of u for: a. SAP for $u > u_s$
b. SDP for $u < u_s$.

These results can easily be extended by recognizing that the SDP and SAP are symmetric with respect to the saddle point α_s.

C.3 Effect of Deformation on the Contributing Singularities

As discussed in Section B.6, it is desirable to deform the β_1 branch cut from $k_x = -k_1$, which arises from $G_-(k_x)$ in the denominator of the field integral, to lie along the SDP_b in preparation for the deformation of the path of integration to the SDP through the saddle point. This permits a formulation of the branch cut contribution which is amenable to asymptotic analysis. As is recognized in Sections B.5 and B.6, this deformation of the β_1 branch cut has two effects on the integrand resulting from the fact that the steepest descent analysis is performed on an analytic continuation of the integrand. First, the question arises concerning value of β_1(that is, + or - the original hyperbolic definition of β_1). Since we only evaluate the integrand at the positions of the singularities in the complex α plane, the question reduces to determining if the specific singularity is crossed in the process of deforming the β_1 branch cut. The second issue arising from the deformation is the determination of whether a root of G_- is brought onto the top sheet of the integrand (and is crossed by the integration path as we move to the SDP of integration). This question is rather involved and is considered in Section C.4.

We begin by recalling the field integral to be evaluated

$$I = \int\limits_{-\infty+jc}^{\infty+jc} \frac{1}{G_-(k_x) \cdot (k_x + k_1 \cos\theta)} \, e^{j(\beta_2 y - k_x x)} \, dk_x$$

$$= \int\limits_{-\infty+jc}^{\infty+jc} \frac{G_+(k_x)}{G(k_x) \cdot (k_x + k_1 \cos\theta)} \, e^{j(\beta_2 y - k_x x)} \, dk_x \quad \text{for } y < 0 , \quad (C.3.1)$$

We note that the second form displays explici · the β_1 and β_2 branch cuts in the second quadrant of the k_x plane t ⁄ ‚h the function $G(k_x)$. The branch cut for β_1 affects only the portion of the integrand outside of the exponential, hence deformation of the β_1 branch cut does not affect convergence of (C.3.1). In the second form given in (C.3.1) the value of $G_+(k_x)$ is unaffected by the deformation of the branch cut from $k_x = -k_1$ and can be evaluated using the factorization integral without alteration.

We utilize the classification scheme of the α plane given in Section A.7 and add a level of refinement. We now break region 2 into 2A and 2B as shown in Figure A.4.

Having stated this classification, we begin by considering the saddle point contribution. Consider α_b in region 1. It is clear from the phase contour plots (Figure C.1) that the SDP_b will have $v \geq 0$. However it is also clear from Figure A.4.a that the original hyperbolic branch cut for α_b in region 1 will lie in region 1 and not cross the connection from $-k_1$ to the origin. Therefore we have demonstrated that

if the branch point α_b is in region 1 then the deforming branch cut β_1 will not cross the real α axis and so the saddle point contribution will use the original β_1 definition. Now consider α_b in region 3. Similar arguments to those for α_b in region 1 apply and the conclusion is that, again, for α_b in region 3 the original value of β_1 is correct for the saddle point contribution.

We now consider α_b in region 2 and must consider regions 2A and 2B separately. Consider first α_b in region 2B. When we examine Figure A.4.a, it is clear that the original hyperbola will cross the ray from the origin through $-k_1$ at some point beyond $-k_2$. Therefore in the α plane it must cross the line $u = -(\pi/2)$ for some point $v < 0$ and curve down into region 3. At this point we consider the SDP_b for α_b in region 2B. Referring back to Section C.2, if we consider the derivative (dv/du) of (C.2.1) and set it to zero, we have

$$\left(\frac{dv}{du}\right)_{\substack{\text{const} \\ \text{phase} \\ \text{contour}}} = \frac{k_{2r}\tan(u-u_s) + k_{2i}\tanh(v)}{k_{2r}\tanh(v) - k_{2i}\tan(u-u_s)} = 0 \qquad \text{(C.3.2a)}$$

which gives

$$k_{2r}\tan(u-u_s) = -k_{2i}\tanh(v) \qquad \text{(C.3.2b)}$$

We note that this equation is identical to (A.2.2) with the exception that the intersection with the real α axis occurs at $u = u_s$. Hence the locus of zero tangent lines to the constant phase contours lies on the image of the imaginary k_x axis mapping shifted to $u = u_s$ and when $u_s = -(\pi/2)$ this locus can be shown to map back into the k_x plane as the

extension of the hyperbolic branch cut through $-k_2$ which is asymptotic to the negative real k_x axis. This implies that the boundary between regions 2A and 2B in the α plane (which is the extension of the hyperbola going through $-k_2$ in the k_x plane) is the locus of zero slope for all the phase contours with $\gamma < -k_{2r}$ and $u_s = -(\pi/2)$. Hence we are guaranteed that the SDP_b will go into region 3 and that in the course of deforming to it we will not cross the saddle point. So for α_b in region 2B we also have that the original β_1 definition is correct.

Finally we must consider α_b in region 2A, a more difficult case. We note that the original hyperbolic branch cut will now cross the saddle point locus (Figure A.4.a) in all cases. Specifically we will assume that the original β_1 hyperbola crosses the real α axis at $\alpha = u_{cr}$ where $-(\pi/2) < u_{cr} \leq 0$. Consider the behavior of the SDP_b as u_s moves from $u = 0$ to $u = -(\pi/2)$. We recognize that given α_b there is a unique value $u = u_{sb}$ specified by (C.2.2) for the saddle point at which the SDP through the saddle point u_{sb} crosses the branch point α_b. It is clear that for $u_s > \max(u_{cr}, u_{sb})$, the saddle point moves on the original top sheet of β_1. Now, if $u_s = u_{sb}$, the SDP_b must lie on the SDP through u_{sb} and run to $v = -\infty$. For simplicity, we will deform the β_1 cut to this locus initially, recognizing that in the process all values of $u < u_{cr}$ on the real α axis enforce the lower sheet value of the original hyperbolic definition of β_1. Now as u_s proceeds from $u = 0$ to $u = -(\pi/2)$, it will run into either u_{cr} or u_{sb}. If it encounters u_{sb} first there is no effect on β_1 since the SDP_b must curve below the real α axis until the SAP crosses α_b. Therefore only top sheet values of β_1 will be achieved until

u_s reaches either u_{cr} or the value of u_s at which the SAP crosses α_b, referred to as u_{sap}. Assume that $u_{sap} < u_{cr}$, then for $u_{sap} < u_s < u_{cr}$, the lower sheet value of β_1 is correct. Since for all $u_s < u_{sap}$ the SDP_b must lie to the right of the saddle point, we must use the top sheet value of as the deformation from the original β_1 branch cut to the SDP_b will not cross the saddle point. Therefore for the case where $u_{sap} < u_{cr}$, we have the following:

$$\beta_1 = \begin{cases} +(\beta_1)_{orig} & , \ u_{cr} \leq u_s \\ \\ -(\beta_1)_{orig} & , \ u_{SAP} \leq u_s < u_{cr} \quad \text{where } -\frac{\pi}{2} \leq u_s < 0 \\ \\ +(\beta_1)_{orig} & , \ u_s < u_{SAP} \end{cases} \quad (C.3.3)$$

Now we assert that $u_{sap} < u_{cr}$ for all cases. This can be seen from a somewhat heuristic argument based on Figure A.3. Clearly the possible exceptional points must occur in the triangle in Figure A.3.a bounded by the lines 1, 4 and the real k_x axis, since branch points outside this region (but in region 2A) will not have $u_{sap} > -(\pi/2)$. But observe that the SAP in A.3.b maintains a constant acute angle from the saddle point with respect to line 1. Since the mapping $(k_x = k_2 \sin \alpha)$ is conformal except at $\alpha = -(\pi/2)$, this angle is maintained in the k_x plane with respect to line 1. However the β_1 hyperbola clearly has a tangent line at the intersection with line 1 which maintains a greater angle (usually obtuse) with respect to line 1. This angle must be maintained in the α plane. But both the original β_1 hyperbola and the SDP_b must originate

at α_b, so clearly $u_{sap} < u_{cr}$.

Summarizing the results for the value of β_1 to be used for the saddle point contribution, when the effect of the deformation of the β_1 branch cut to the SDP_b is included, we have:

For α_b in regions 1,2B and 3: Use $\beta_1 = +(\beta_1)_{original}$.

$$(C.3.4)$$

For α_b in region 2A: Use $\beta_1 =$ (C.3.3).

Now we consider the effect of the β_1 deformation on the geometrical optics pole (GOP). We recognize that the locus of the pole is a straight line in the k_x plane connecting $-k_1$ with the origin. Consider the case where α_b is in region 1. Examining Figure A.4.a, we see that the hyperbolic branch cut and the GOP locus intersect only at the branch point, $-k_1$. Considering Section A.7 and examining Figure A.5 (which depicts the curvature of the locus of the geometrical optics pole in the α plane), we see that the same will be true for the SDP_b , which must run up from α_b to $v = +\infty$. Therefore the GOP locus will not be crossed during the deformation of the β_1 branch cut to the SDP_b when α_b is in region 1 and hence the original top sheet definition of β_1 is correct. A similar analysis is seen to apply for α_b in region 2. Finally we consider α_b in region 3. As mentioned above all GOP locus lines will cross the boundary line between regions 1 and 3. Also we know that for α_b in region 3 the deformed SDP_b cut must stay in region 3. Regarding the original hyperbolic branch cut for β_1, we see from Figure A.4.a that it does not cross the GOP locus and in deforming to the SDP_b (which lies totally in region

3) that it will not cross the locus. Therefore for α_b in region 3, the original top sheet value of is correct. Collecting these results for the GOP contribution, we see that the original value for β_1 will always apply.

Having established these rules for choosing the value of β_1 when evaluating the asymptotic contribution of each singularity, we see that they are amenable to implimentation during numerical evaluation of the far fields in a problem.

C.4 Effect of the β_1 Branch Cut Deformation on the Root of $G_-(k_x)$

We begin by determining under what situations the root of $G_-(k_x)$, is exposed in the deformation of the β_1 branch cut to the SDP_b and is crossed by the deformation of the integration path to the SDP through the saddle point. We utilize the same division of the α plane as presented in Section A.7 (that is, into regions 1,2 and 3). In addition we need the following terminology:

$\alpha = u + jv$

$\alpha_b = u_b + jv_b$ is the branch point in the α plane such that $-k_1 = k_2 \sin\alpha_b$.

α_s or u_s is the value of the saddle point $(-(\pi/2) \leq u_s \leq 0)$.

$\alpha_0 = u_0 + jv_0$ is the root of $G_-(k_x)$.

α_{sb} or u_{sb} is the value of the saddle point such that the SDP intersects α_b.

α_{s0} or u_{s0} is the value of the saddle point such that the SDP intersects α_0.

$\alpha_{conn} = u_{conn} + jv_{conn}$ refers to points on the connecting line between $k_x = -k_1$ and $-k_2$ (discussed in Section A.8).

$\gamma(\alpha, u_s)$ refers to the value of the phase function (C.2.1)

We recognize that the branch cut for β_2 in the second quadrant of the k_x plane exists in both the exponential factor of the integrand of the field integral and in the denominator factor $G_-(k_x)$, while the β_1 branch cut exists only in $G_-(k_x)$. Therefore we can view the β_1 branch cut as deforming from the original hyperbolic locus to overlay the hyperbola as depicted in Figure C.3.a. In the α plane the configuration will appear as in Figure C.3.b (shown for α_b in region 3). We will take this as our initial β_1 branch cut configuration since we are guaranteed by the analysis of Section 3.4 that no roots of G_- will occur on the top sheet. For all values of the saddle point such that $u_{sb} < u_s$, there will be no roots crossed in deforming to the SDP. We know that the root of G_- lies somewhere in the region $\text{Re}(k_x) \geq 0$ and the point at issue is whether it is exposed on the top sheet and crossed in deforming the integration path. We also know that for a root to be crossed by the integration path, $-(\pi/2) < u_s < u_{s0}$.

Consider α_b in region 1. When $u_s < u_{sb}$, then the SDP_b must run up to $v = +\infty$. Since the initial branch cut for β_1 also runs to $v = +\infty$ along the SDP through $\alpha = -(\pi/2)$, it is clear that any root α_0 with $v_0 \leq 0$ will never be brought to the top sheet and can therefore be ignored. We assume now that $v_0 > 0$. We now observe that the root α_0 must lie to the left of the SDP through α_{sb} and α_b. Since all SDP_b contours lie to the left of this boundary line, any root which may be exposed in the branch cut deformation must lie to the left of this curve. Hence we
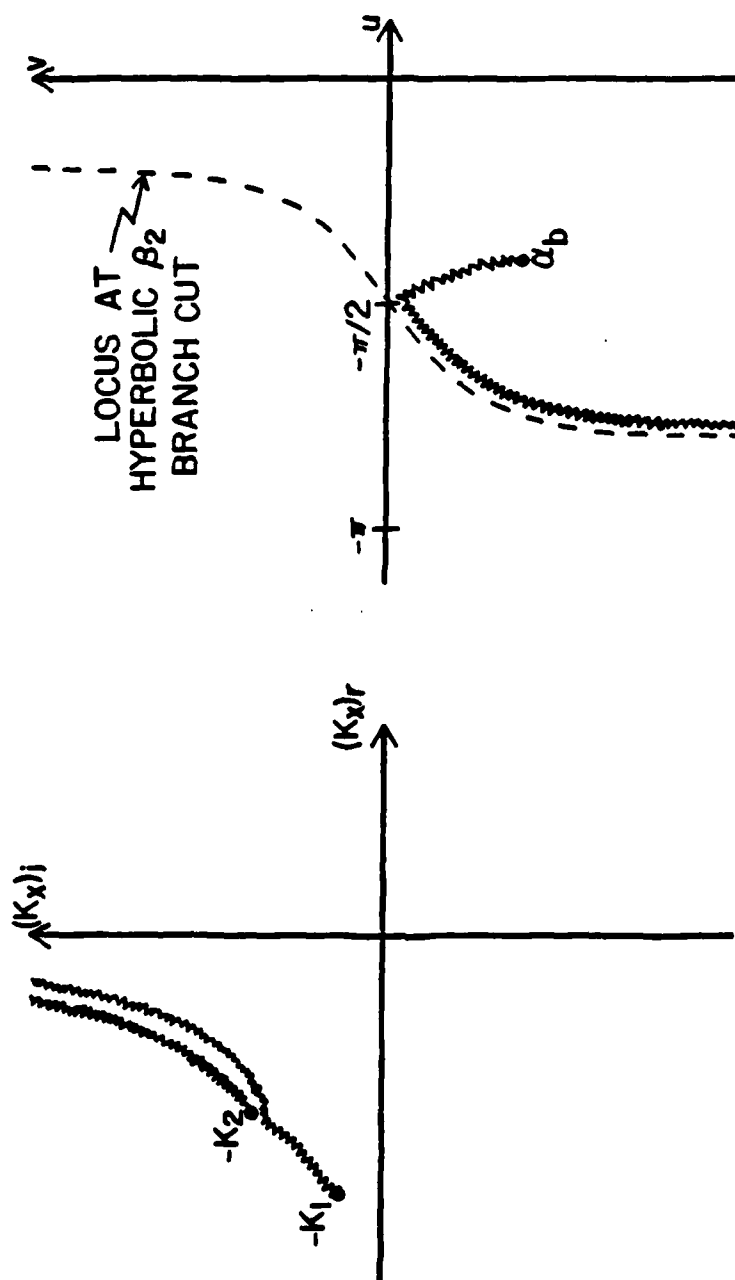
(a)

(b)

Figure C.3. Initial deformation of the branch cut for β_1 from $k_x = -k_1$.

a. Branch cut locus in the k_x plane.

b. Branch cut locus in the α plane.

have that $u_{s0} < u_{sb}$ in order for α_0 to be exposed at all. The one exception to this is if the connection line from $-k_1$ to $-k_2$ of the initial, root-free top sheet configuration is indented below the SDP through α_{sb} and the root α_0 lies in this indention. (Note that the connection line has positive curvature and positive slope). If this is the case then for all $u_s < u_{s0}$ the root will be both exposed and crossed by the SDP through u_s. See Figure C.4. This is due to the fact that for $u_s < u_{s0}$, the branch cut for β_1 which initially coincides with the connection line must deform to coincide with the SDP (which goes through α_0). Further movement of u_s toward $u = -(\pi/2)$ will force the branch cut to expose the root which is clearly crossed by the integration path deforming to the SDP through u_s since $u_s < u_{s0}$. Once $u_s < u_{sb}$, the SDP_b deforms up toward $v = +\infty$ and the root will continue to be exposed as u_s progresses to $-(\pi/2)$.

Continuing the analysis for α_b in region 1, we consider that $u_{s0} < u_{sb}$ so that the root may be exposed. If α_0 lies to the left of the curve defined by the connection from $-k_1$ to $-k_2$ and the SDP_b running from α_b to $v = +\infty$ (See Figure C.5), then the root has been exposed on the top sheet (and crossed by the integration path since $u_s < u_{s0}$). Otherwise the root is not exposed and does not contribute.

Consider α_b in region 2. We again note that unless $u_{s0} < u_{sb}$ the root cannot be exposed and there is no exception this time as the connection line has positive curvature and negative slope. See Figure C.6. Now for α_b in region 2 it is possible for the SDP_b to go to $v = \pm\infty$ depending on whether $\gamma_b = \gamma(\alpha_b)$, the phase function for the phase
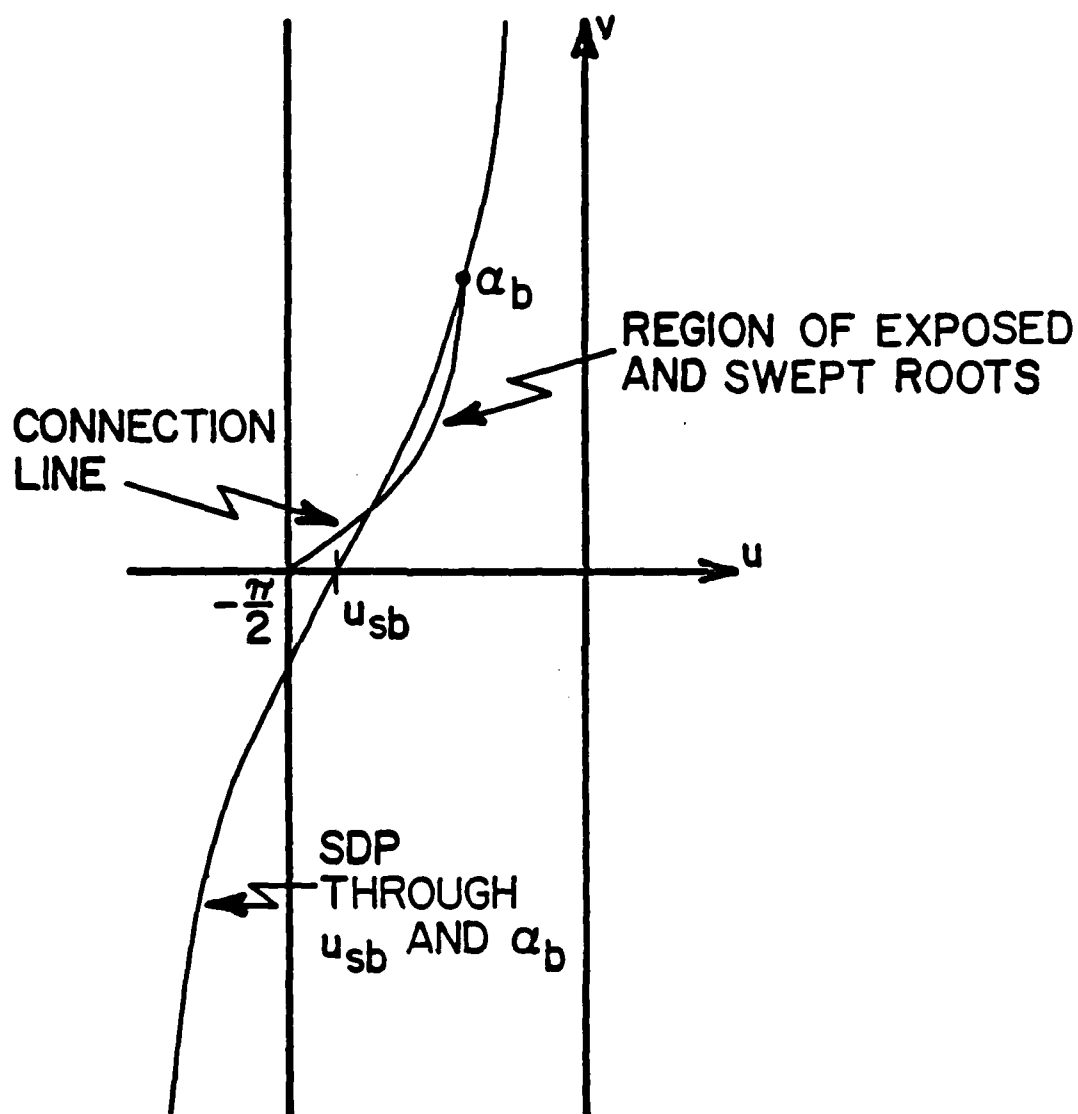
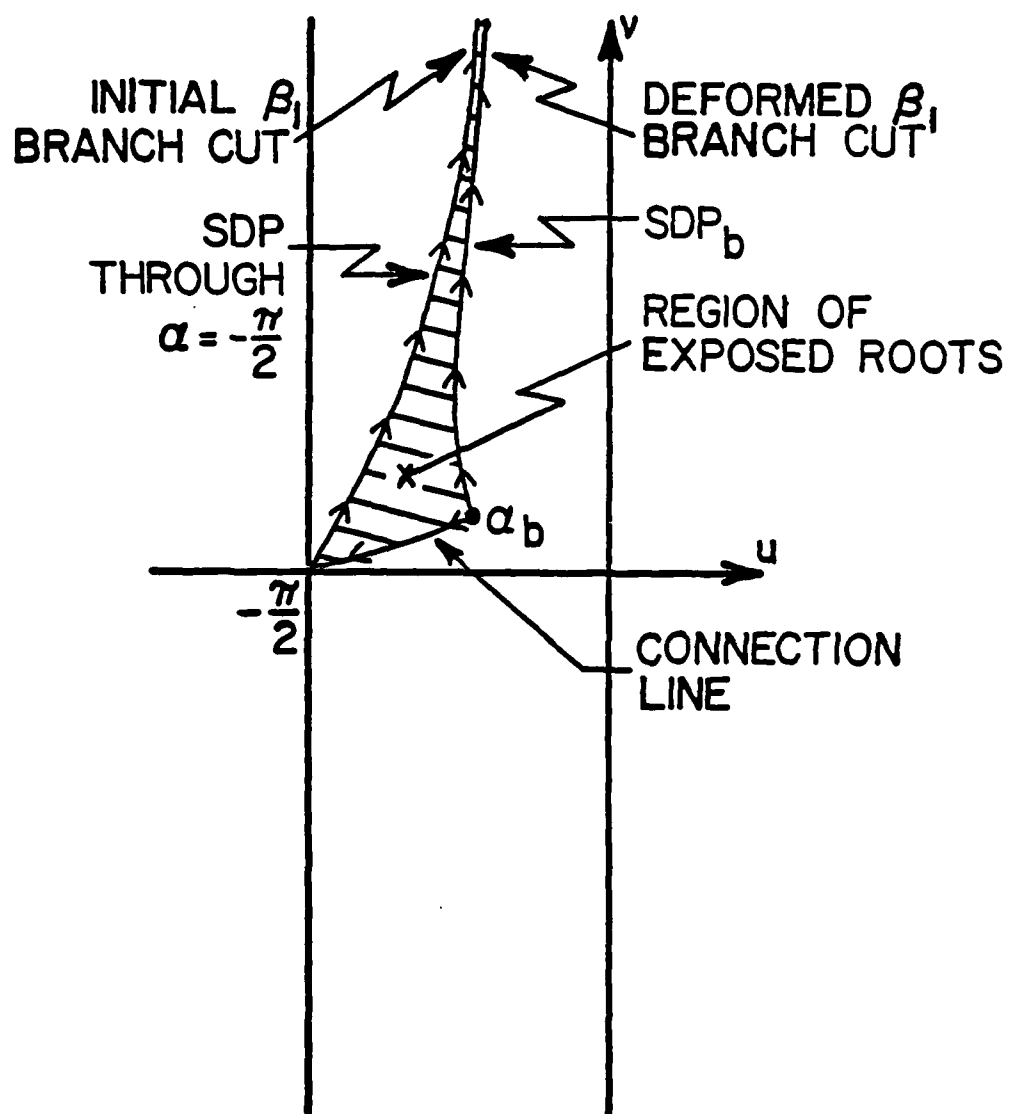Figure C.4. Possible region of exposed roots of G_- in the α plane.

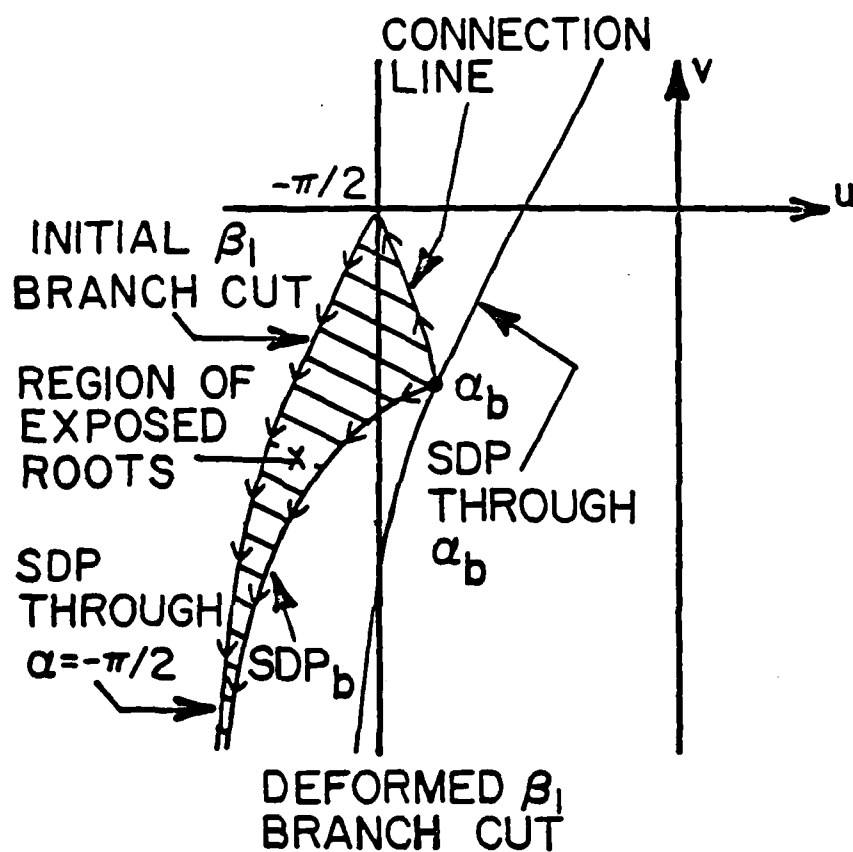Figure C.5. Possible region of exposed roots of G_- in the α plane.

Figure C.6.   Possible region of exposed roots of G_
in the α plane.

contour through α_b, is $\gtrless -k_{2r}$. Assume first that $\gamma_b < -k_{2r}$ so that the SDP$_b$ curves down to $v = -\infty$. Clearly if $v_0 \geq 0$, then the root is never exposed. Assume $v_0 < 0$. Then a possible situation is shown in Figure C.7. If α_0 lies between the curves defined by the lower leg of the SDP through $\alpha = -(\pi/2)$, the connection line from $-(\pi/2)$ to α_b and the SDP$_b$, then α_0 is exposed (and crossed since $u_s < u_{s0}$).

Consider the same situation as that discussed in the paragraph above but with $-k_{2r} < \gamma_b < 0$, so that the SDP$_b$ runs up to $v = +\infty$. Then we may encounter into the situation shown in Figure C.8. As for the case when $\gamma_b < -k_{2r}$, we find that if α_0 lies between the upper leg of the SDP through $\alpha = -(\pi/2)$, the connection line and the SDP$_b$, then α_0 is exposed.

Finally we consider α_0 in region 3. We saw in Section A.8 that the slope and curvature of the connection line was given by Table A.2. If we consider sets of these curves we arrive at Figure C.9. We observe, in particular, that it is possible for α_b to lie in region 3 and have its connection line appear in region 1. This is of particular significance since the SDP$_b$ loci must lie completely in region 3. Therefore if a root appears in region 1 between the connection line and the SDP through $-(\pi/2)$, it is exposed and crossed for $u_s < u_{s0}$. Otherwise, if $v_0 \geq 0$, the root is never exposed. Now assume that the root has $v_0 < 0$. Assuming that $u_s < u_{sb}$ so that the branch cut has deformed from the initial position to the SDP$_b$ and exposed a portion of the lower sheet of G_-, then any root in the region bounded by the lower portion of the SDP through $-(\pi/2)$, the connection between $-(\pi/2)$ and α_b, and the SDP$_b$ will
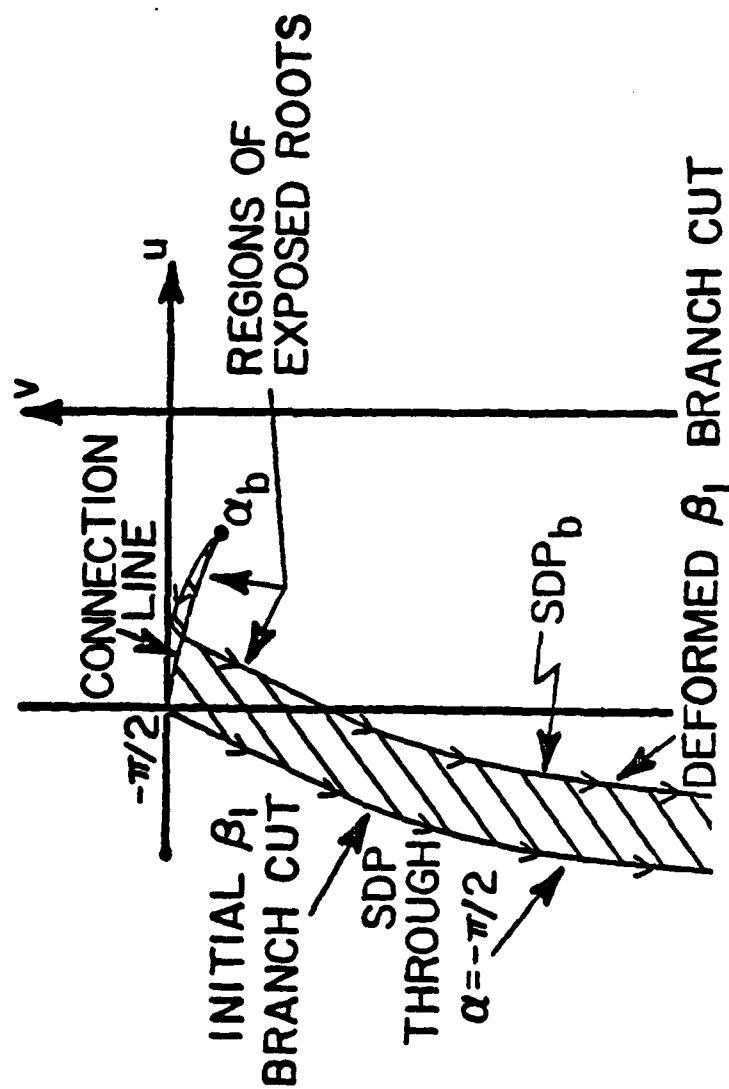
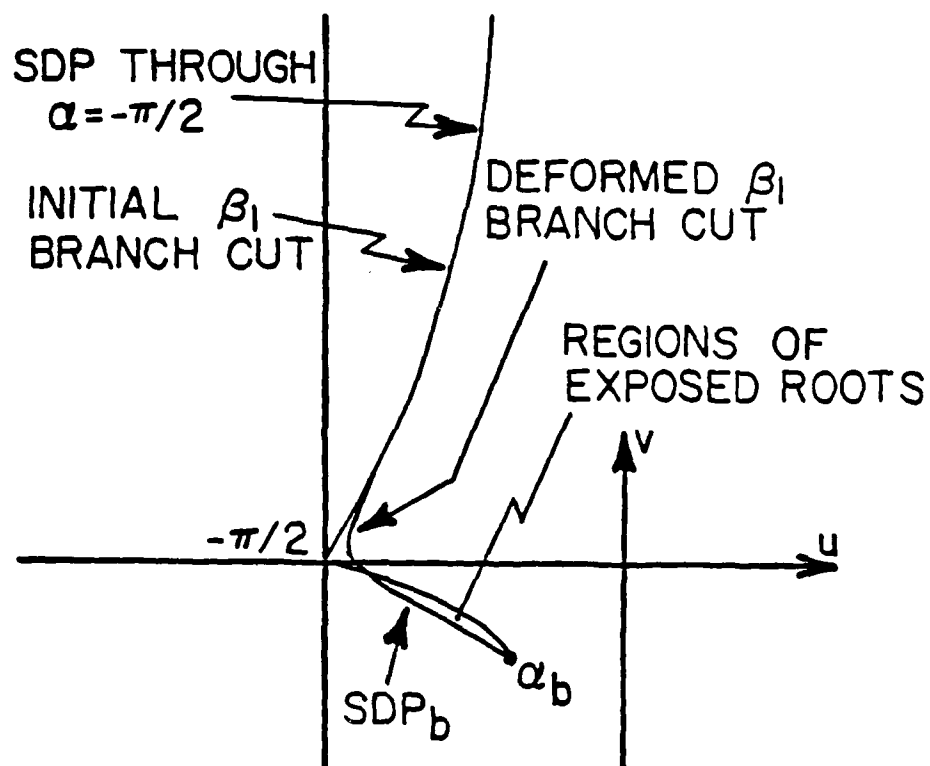Figure C.7. Possible region of exposed roots of G_-
in the α plane.

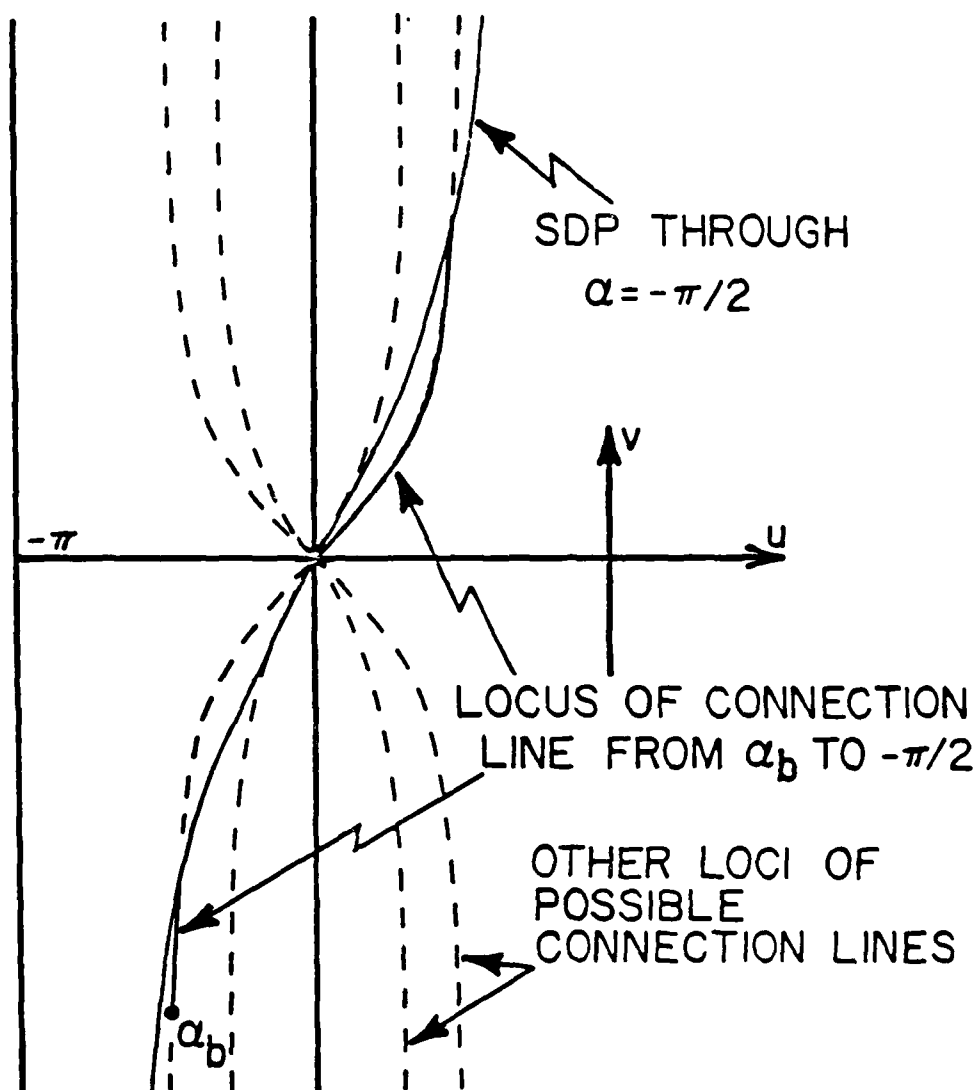Figure C.8. Possible region of exposed roots of G_- in the α plane.

Figure C.9. Loci of connection lines from $-k_1$ to $-k_2$ in the α plane.

be exposed and crossed (since $u_s < u_{s0}$).

We can summarize the results of this analysis in a manner amenable to implementation on a computer. We accept the following definitions:

u_s is the given saddle point value

u_{s0} is the saddle point value for which the SDP runs through α_0, the root of interest.

(u_b, v_b): $\alpha_b = u_b + jv_b$, α_b is the branch point for $k_x = -k_1$.

(u_0, v_0): $\alpha_0 = u_0 + jv_0$, α_0 is the root of interest.

u_{sb} is the saddle point value for the SDP running through α_b.

γ_b is the value of the phase function for α_b and u_s.

$$
v_{con}(u_0) \equiv
\begin{cases}
[\text{if } u_b > -(\pi/2)] =
\begin{cases}
v_{SDP}, \text{ SDP through } u = -\frac{\pi}{2} \text{ ; for } u_0 \le -\frac{\pi}{2} \\[2em]
v_{conn}, \text{ value on connection curve; for } -\frac{\pi}{2} < u_0 < u_b \\ \left(-\frac{\pi}{2}\right) \text{ to } \alpha_b \\[2em]
v_{SDP}, \text{ SDP through } \alpha_b; \text{ for } u_b \le u_0
\end{cases} \\[6em]
[\text{if } u_b \le -(\pi/2)] =
\begin{cases}
v_{SDP}, \text{ SDP through } u = -\frac{\pi}{2}; \text{ for } -\frac{\pi}{2} < u_0 \\[2em]
v_{conn}; \text{ for } u_b < u_0 < -\frac{\pi}{2} \\[2em]
v_{SDP}, \text{ SDP through } \alpha_b; \text{ for } u_0 \le u_b
\end{cases}
\end{cases}
$$

$$u_{SDP_b}(v_0) \equiv \begin{cases} u_{SDP_b} \text{, on } SDP_b \text{; for } v_b \leq v_0 \\ \\ \\ u_b \text{, fixed; for } v_0 < v_b \end{cases}$$

$$v_{SDP_b}(u_0) \equiv \begin{cases} v_{SDP} \text{, SDP through } \alpha_b \text{; } u_b \leq u_0 \\ \\ v_{SDP_b} \text{, on } SDP_b \text{; for } \left(u_{sb} - \frac{\pi}{2}\right) < u_0 < u_b \\ \\ -\infty \text{ ; for } u_0 < \left(u_{sb} - \frac{\pi}{2}\right) \end{cases}$$

$$v_{con}^{im}(u_0) = -v_{con}(-\pi - u_0) .$$

$$v_{test}(u_0) \equiv \begin{cases} v_{con}(u_0) \text{ ; for } u_b \leq u_0 \\ \\ \\ v_{SDP_b} \text{, on } SDP_b \text{ ; for } u_0 < u_b \end{cases}$$

We enumerate the following inequalities which will be use in the logical constructions of the flowchart derived from the earlier analysis:

a. $-\frac{\pi}{2} < u_s$

b. $u_s < u_{s0}$

c. $v_b \geq 0$

d. $u_b \leq -\frac{\pi}{2}$

e. $v_0 \geq 0$

f. $u_{s0} \geq u_{sb}$

g. $v_0 > v_{con}$

h. $u_0 < u_{SDP_b}$

i. $\gamma_b > k_{2r}$

j. $v_{con} < v_0 < v_{SDP_b}$

k. $v_{SDP_b} < v_0 < v_{con}$

l. $u_0 > u_{SDP_b}$

m. $v_0 > v_{con}^{im}$

n. $u_s < u_{sb}$

o. $v_0 > v_{test}$

We can then organize the logic of this section into the flowchart shown in Figure C.10. The question concerning the value of β_1 to be used in the residue contribution of the root of G_- does not arise because the form of the contribution (Section B.5) implicitly includes the correct value of β_1 due to (B.5.3).

213
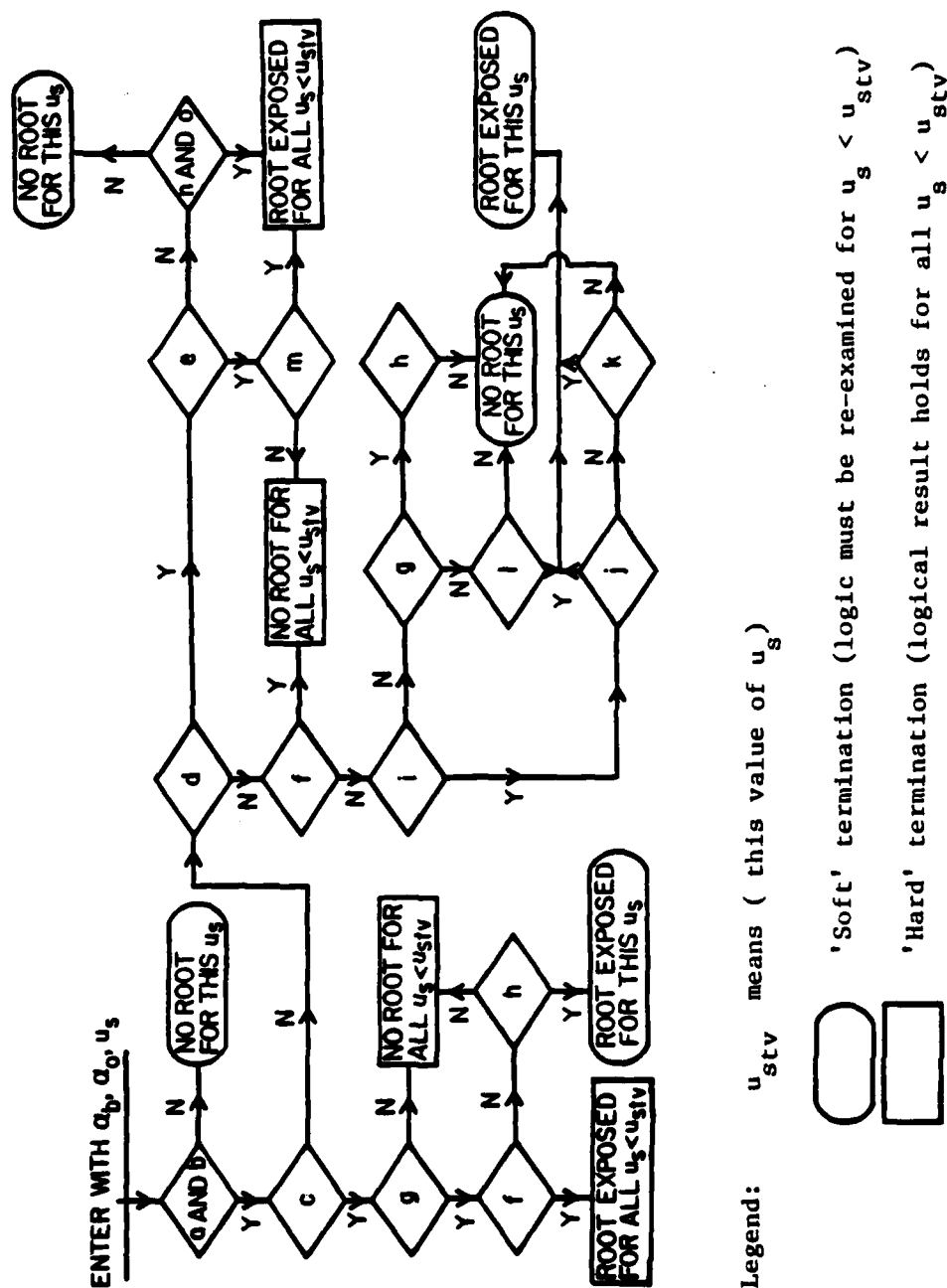

Figure C.10. Logic for the determination of the exposure and capture of the root of G_- by the steepest descent path.

Legend: u_{stv} means (this value of u_s)

'Soft' termination (logic must be re-examined for $u_s < u_{stv}$)

'Hard' termination (logical result holds for all $u_s < u_{stv}$)

APPENDIX D

BEHAVIOR OF THE GREEN'S FUNCTION IN THE SLAB PROBLEM

In this appendix the behavior of the Green's function for the slab problem is considered when the media are lossless, have the same permeability μ_0' and the slab has a greater permittivity than the surrounding medium ($\epsilon_2' > \epsilon_1'$). The Green's function is given in (5.2.6) and we consider here the functional form, $F(k_x')$, given in (5.2.7). In normalized coordinates, we have

$$F(k_x') = \left\{ 2\beta_1' \left[\frac{(\beta_1'-\beta_2')e^{-j\beta_2't'} - (\beta_1'+\beta_2')e^{j\beta_2't'}}{(\beta_1'-\beta_2')^2 e^{-j\beta_2't'} - (\beta_1'+\beta_2')^2 e^{j\beta_2't'}} \right] \right\} \qquad (D.1)$$

$$F(k_x') = \left\{ 2\beta_1't' \left[\frac{j\beta_1't' + \beta_2't'\cot(\beta_2't')}{j[(\beta_1't')^2 + (\beta_2't')^2] + 2(\beta_1't')(\beta_2't')\cot(\beta_2't')} \right] \right\}$$

$$(D.2)$$

The slab is taken to have thickness t' (expressed in normalized coordinates, $t = t' \cdot k_0$). Also the normalized permeability is equal to 1, so $k_1^2 = \epsilon_1$. Only the roots and poles of the expression in brackets need be

215

discussed in detail, so the factor β_1 will be ignored. We follow the analysis of Barone (1956) and give the results for our formulation in the present notation.

Consider the roots of the numerator of (D.2),

$$j\beta_1 t + \beta_2 t \cot\beta_2 t = 0 \quad . \tag{D.3}$$

Letting $\beta_1 t = w = \mu + jv$ and $\beta_2 t = z = x + jy$, then (D.3) becomes

$$\omega = jz \cot z \quad . \tag{D.4}$$

We recognize that

$$z^2 - \omega^2 = (k_2^2 - k_1^2)t^2 = (\epsilon_2 - \epsilon_1)t^2 = a^2 \tag{D.5}$$

where $a \geq 0$. Analyzing (D.4) and (D.5) together allows for the locus of the roots as a function of (a) to be determined. It can be shown that all the roots reside on the lower sheet except for a finite number which must lie between k_1 and k_2 on the real k_x axis (and their images which lie between $-k_2$ and $-k_1$ on the negative real axis). Determining the location of the roots requires solving the equations,

$$x^2 + v^2 = a^2 \tag{D.6}$$

and

$$v = \pm a \cos(x) \quad \text{such that } v < 0, \text{ simultaneously.} \tag{D.7}$$

This can be thought of graphically as shown in Figure D.1, where the locus defined by (D.6) is shown as a circle of radius a and (D.7) is
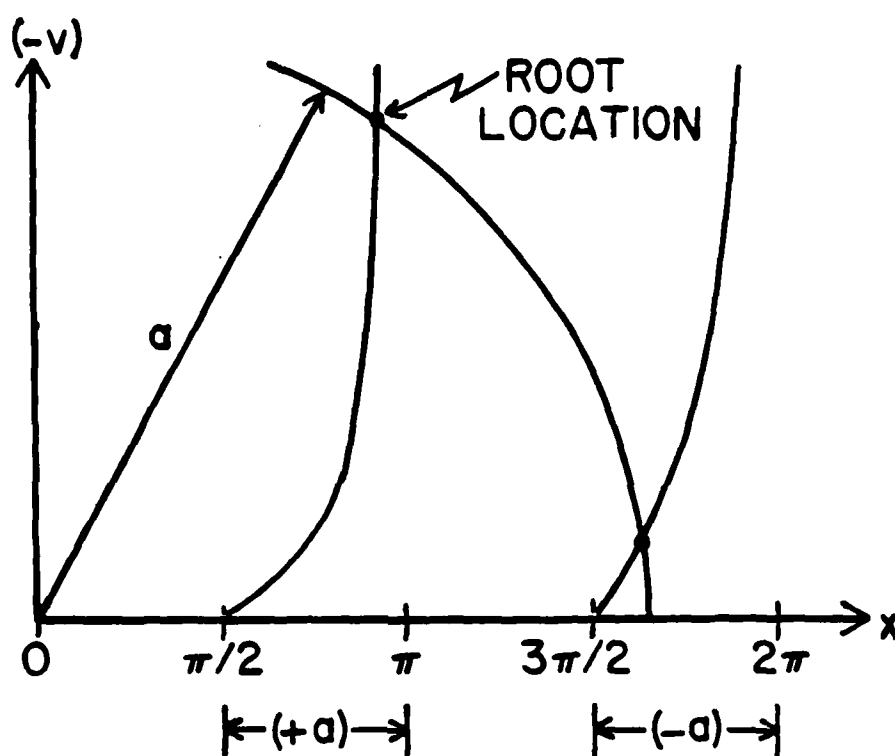
Figure D.1. Graphic determination of the roots
of the numerator of the function F
in the slab problem. Roots of
$x = \pm a \sin x$

shown for $v < 0$. Alternatively, the roots of

$$x = \pm\, a \, \sin(x) \qquad\qquad\qquad (D.8)$$

can be determined (clearly $|x| \leq a$) and then (D.7) gives v. It is evident from Figure D.1 that no roots occur until $a \geq (\pi/2)$. This being the case, there will be n roots on the interval (k_1, k_2), where n is the integer portion of $(a/\pi + 1/2)$.

The roots of (D.3) are seen to correspond to the surface waves of a dielectric slab waveguide of thickness t with one surface covered by a PEC screen (that is, the so-called short circuit bisection problem). It is shown in the asymptotic analysis for the transmitted region $(y < -t)$ that the roots give rise to surface waves propagating in the positive x direction from the edge of the PEC screen. It is no surprise that these surface wave roots are the same as the surface wave roots of the slab structure since for $x > 0$, the configuration is coincident with that of the short circuit bisection problem.

Consider now the roots of the denominator of $F(k_x)$,

$$(\beta_1 - \beta_2)^2 e^{-j\beta_2 t} - (\beta_1 + \beta_2)^2 e^{j\beta_2 t} = 0 \qquad , \qquad (D.9)$$

After some manipulation this reduces to two families of roots,

$$\frac{\beta_1 t}{2} = j\,\frac{\beta_2 t}{2}\,\cot\!\left(\frac{\beta_2 t}{2}\right) \qquad\qquad (D.10.a)$$

and

$$\frac{\beta_1 t}{2} = -j\,\frac{\beta_2 t}{2}\,\tan\!\left(\frac{\beta_2 t}{2}\right) \qquad . \qquad (D.10.b)$$

Comparing (D.10.a) with (D.3), it is clear that an identical analysis applies using (t/2) rather than t. In particular, from (D.5) we see that a becomes $b = (a/2)$. Therefore we have no roots until $a = \pi$ and then n roots such that n is the integer portion of $(b/\pi + 1/2)$. These roots solve (D.6) and (D.7) or (D.8) with the appropriate adjustment in t and a. From the earlier discussion, it is clear that these poles correspond to the short circuit bisection problem for a slab of thickness (t/2). Thus these waves have an odd functional behavior with respect to the center of the slab.

Examining (D.10.b), it can be shown that using $(\beta_1 t/2) = w$ and $(\beta_2 t/2) = z$, the equation can be reduced to

$$\omega = -jz \tan(z) \qquad \text{(D.11.a)}$$

and

$$z^2 - \omega^2 = b^2 = (\varepsilon_2 - \varepsilon_1)\left(\frac{t}{2}\right)^2 . \qquad \text{(D.11.b)}$$

Hence the respective real and imaginary parts of the roots satisfy

$$x^2 + v^2 = b^2 \qquad \text{(D.12.a)}$$

and

$$v = \pm b \sin(x) , \qquad \text{(D.12.b)}$$

or

$$x = \mp b \cos(x) . \qquad \text{(D.13)}$$

The graphical depiction of (D.12) is shown in Figure D.2. Observe that this pole does not suffer a cutoff for b < (π/2) unlike the short circuit waves discussed previously. These waves represent the even functional waves characterized by the surface waves of a dielectric slab of thickness t/2 with one surface covered by a perfectly magnetically conducting screen (the open circuit bisection problem for a slab of thickness t/2).

By combining the functions shown in Figures D.1 and D.2, it can be shown that as a (which equals $\sqrt{\epsilon_2 - \epsilon_1}$ t) increases from zero, the following sequence of roots and poles appears on the interval (k_1, k_2) of the real k_x axis (and by symmetry, on the interval $(-k_2, -k_1)$). First, a pole emerges from k_1 and moves toward k_2 as a increases to (π/2). For a > (π/2), a root then emerges and follows the preceding pole toward k_2. Then when a reaches π, a second pole emerges from k_1 and moves toward k_2. This alternation between poles and zeros is seen to continue as a increases. This progression of roots is shown in Figure 5.2 which describes the behavior of the logarithm of the Green's function of the slab problem.
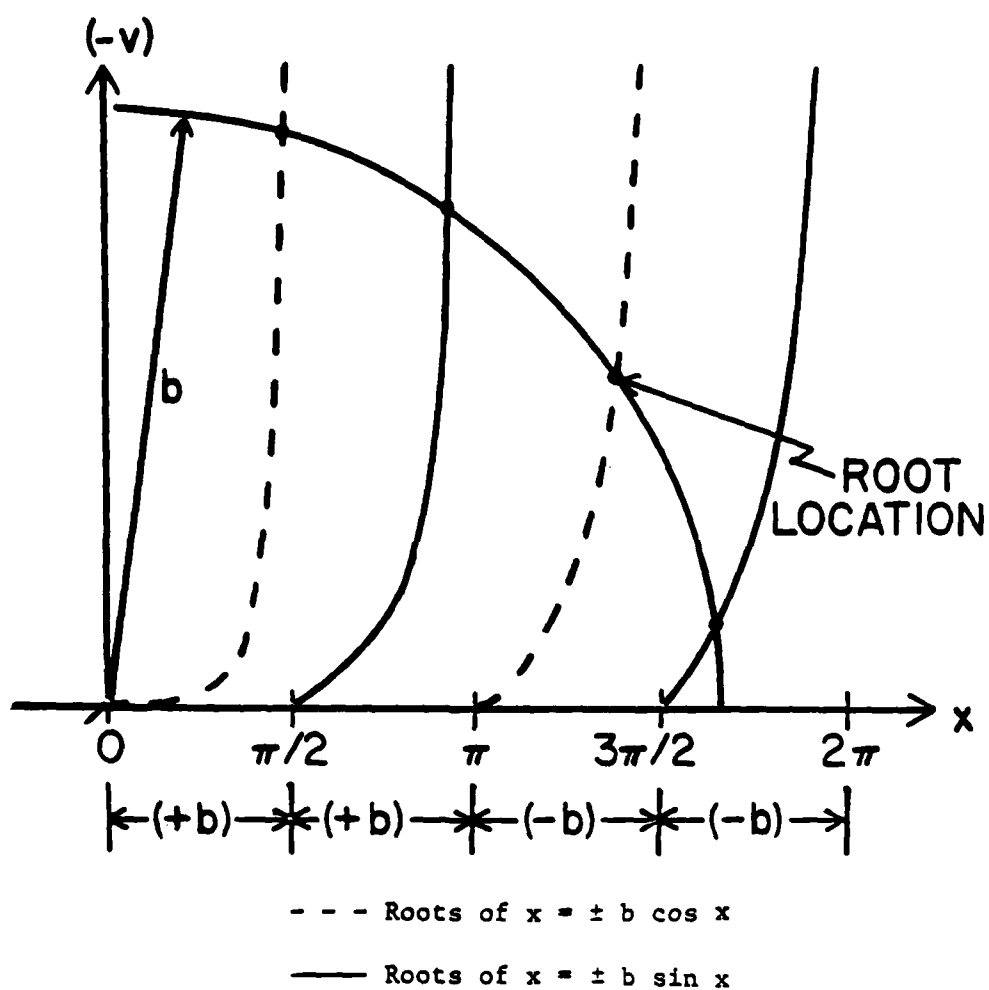
Figure D.2. Graphic determination of the roots of the denominator of the function F in the slab problem.

BIBLIOGRAPHY

Ament, W.S. (1954), "Application of a Wiener-Hopf technique to certain diffraction problems", U.S. Naval Res. Lab Report No. 4334, Washington, D.C., pp. 19-22.

Baños, A., Jr. (1966), <u>Dipole Radiation in the Presence of a Conducting Half-Space</u>, New York:Pergamon Press.

Barone, S. (1956), "Leaky wave contributions to the field of a line source above a dielectric slab", Microwave Res. Inst., Polytechnic Inst. of Brooklyn, Report R-532-56, PIB-462, Nov. 1956.

Barone, S. and A. Hessel (1958), "Leaky wave contributions to the field of a line source above a dielectric slab, part II", Microwave Res. Inst., Polytechnic Inst. of Brooklyn, Report R-698-58,PIB-626, Dec. 1958.

Bazar, J. and S.N. Karp (1962), "Propagation of plane electromagnetic waves past a shoreline", J. Res. (Natl. Bur. Std.), D66, pp. 319-334.

Brekhovskikh, L.M. (1980), <u>Waves in Layered Media</u>, 2nd ed., trans. by R.T. Beyer, New York:Academic Press.

Butler, C.M. and K.R. Umashankar (1976), "Electromagnetic penetration through an aperture in an infinite, planar screen separating two half spaces of different electromagnetic properties", Radio Sci., 11(7), pp. 611-619.

Carrier, G.F., M. Krook, and C.E. Pearson (1966), <u>Functions of a Complex Variable</u>, New York:Mcgraw-Hill, pp. 376-424.

Clemmow, P.C. (1953), "Radio propagation over a flat earth across a boundary separating two different media", Phil. Trans. Roy. Soc. London Ser. A, vol. 246, pp. 1-55.

Clemmow, P.C. (1966), <u>The Plane Wave Spectrum Representation of Electromagnetic Fields</u>, New York:Pergamon Press.

Collin, R.E. (1960), <u>Field Theory of Guided Waves</u>, New York:McGraw-Hill, pp. 454-506.

Collin, R.E. and F.J. Zucker (1969), <u>Antenna Theory</u>, Part 1, New York:McGraw-Hill, pp. 62-74.

Copson, E.T. (1946), "On an integral equation arising in the theory of diffraction", Quart. J. Math, 17, pp. 19-34.

Copson, E.T. (1978), An Introduction to the Theory of Functions of a Complex Variable, Oxford:Oxford University Press.

Felsen, L.B. and N. Marcuvitz (1973a), Radiation and Scattering of Waves, Englewood Cliffs, N.J.:Prentice-Hall, pp. 370-431.

Felsen, L.B. and N. Marcuvitz (1973b), op. cit., pp. 144-153.

Felsen, L.B. and N. Marcuvitz (1973c), op. cit., pp. 459-476.

Felsen, L.B. and N. Marcuvitz (1973d), op. cit., pp. 506-554.

Felsen, L.B. (1982), Private communication.

Gakhov, F.D. (1966), Boundary Value Problems, 2nd ed., edited by I.N Sneddon, New York:Pergamon Press, pp. 1-37.

Hansen, R.C. (1981), Geometrical Theory of Diffraction, New York:IEEE Press.

Harrington, R.F. (1961), Time-Harmonic Fields, New York:McGraw-Hill.

Heins, A.E. and H. Feshbach (1954), "On the coupling of two half planes", Proc. Symp. Appl. Math. V, New York:McGraw-Hill, pp. 75-87.

Heitman, W.G. and P.M. van den Berg (1975), "Diffraction of electromagnetic waves by a semi-infinite screen in a layered medium", Can. J. Phys., 53(14), pp. 1305-1317.

Jeffreys, H. and B. Jeffreys (1956), Methods of Mathematical Physics, Cambridge:University Press.

Jones, D.S. (1964), The Theory of Electromagnetism, New York:MacMillan, pp. 581-590.

Keller, J.B. (1957), "Diffraction by an aperture", J. Appl. Phys., 28, pp. 426-444. Also in Hansen (1981).

Keller, J.B. (1962), "Geometrical theory of diffraction", J. Opt. Soc. Am., 52(2), pp. 116-130. Also in Hansen (1981).

Markushevich, A.I. (1977), Theory of Functions of a Complex Variable, 2nd ed., trans by R.A. Silverman, New York:Chelsea, vol. 1, pp. 293-316.

Meixner, J. (1954), "The behavior of electromagnetic fields at edges", Inst. Math. Sci. Res. Rept EM-73, New York University, New York, N.Y., Dec. 1954.

Miles, J.W. (1949), "On the diffraction of an electromagnetic wave through a plane screen", J. Appl. Phys. 20, pp. 760-771.

Mittra, R. and S.W. Lee (1971a), Analytical Techniques in the Theory of Guided Waves, New York:Macmillan, pp. 73-153.

Mittra, R. and S.W. Lee (1971b), op. cit., pp. 1-29.

Nevels, R.D. and C.M. Butler (1982), "Electromagnetic diffraction by a slot in a ground screen covered by a dielectric slab", IEEE Trans. Antennas Propagat., AP-30, pp. 390-395.

Noble, B. (1958), Methods Based on the Wiener-Hopf Technique, New York:Pergamon Press.

Schwinger, J.S. (1944), Seminar on the theory of guided waves, MIT Radiation Lab. Notes available from the MIT Radiation Lab. Mentioned in Miles (1949).

Sommerfeld, A. (1896), "Mathematische Theorie der Diffraktion". Math. Ann. 47, pp. 317

Stratton, J.A. (1941a), Electromagnetic Theory, New York:McGraw-Hill, pp. 490-520.

Stratton, J.A. (1941b), op. cit., pp. 573-587.

Sunahara, Y. and T. Sekiguchi (1981), "Ray theory of diffraction by a half-sheet parallel to a flat earth", Radio Sci., 16(1),pp. pp. 141-155.

Tamir, T. and A.A. Oliner (1963), "Guided complex waves", Proc. IEE, 110(2), pp. 310-324.

Tamir, T. and L.B. Felsen (1965), "On lateral waves in slab configurations and their relation to other wave types", IEEE Trans. Antennas Propagat., AP-13, pp. 410-422.

Tyras, G. (1969a), Radiation and Propagation of Electromagnetic Waves, New York:Academic Press, pp. 28-38.

Tyras, G. (1969b), op. cit., pp. 100-129.

Tyras, G. (1969c), op. cit., pp. 316-327.

Weinstein, L.A. (1969), The Theory of Diffraction and the Factorization Method, Boulder, CO:Golem Press.

Whitmer, R.M. (1948), "Fields in nonmetallic waveguides", Proc. IRE, 36, pp. 1105-1109.

Whitmer, R.M. (1952), "Radiation from a dielectric wave guide", J. Appl. Phys., 23(9), pp.949-953.

Wiener, N. and E. Hopf (1931), "Uber eine klasse singularer integral gleichungen", S.B. Preuss. Akad. Wiss., 1931, pp.696-706.